X-731-67-159

NASA TM X-63219

POSITION LOCATION AND AIRCRAFT COMMUNICATION EQUIPMENT (PLACE)

APRIL 1967

GSFC

GODDARD SPACE FLIGHT CENTER

GREENBELT, MARYLAND

X-731-67-159

PLACE

POSITION LOCATION AND AIRCRAFT COMMUNICATION EQUIPMENT

by

Charles R. Laughlin
Roger C. Hollenbaugh
Erwin Hirschmann
Walter K. Allen

April 1967

Goddard Space Flight Center
Greenbelt, Maryland

CONTENTS

APPENDICES

CONTENTS—Continued

LIST OF FIGURES

Section 2

LIST OF FIGURES–Continued

Section 3

PLACE

POSITION LOCATION AND AIRCRAFT COMMUNICATION EQUIPMENT

1. INTRODUCTION

The large variety of commercial aircraft types, the wide range in their performance characteristics, and the ever increasing density of air traffic, particularly over the North Atlantic area, has spurred an intense search for improved air traffic control techniques. A necessary first step in this direction has recently been achieved through successful communications with aircraft in flight by relay through the ATS-1 satellite. These tests have vividly demonstrated the potential contributions that synchronous satellites can provide in the future. However, an essential feature of a complete air traffic control system which is yet to be demonstrated is an ability to continually determine the location of all aircraft in the system and to monitor their positions relative to each other. An overall system concept for the Position Location and Aircraft Communication Equipment (PLACE) is described herein. This system would provide two-way voice and digital data communications between all cooperating aircraft and their associated ground control facilities by means of a transponder aboard a single geosynchronous satellite. Real-time surveillance, within the area of coverage of the satellite, would be provided through continuous position tracking and automatic reporting from telemetry sensors on-board the aircraft. The PLACE system would accomodate all types of commercial aircraft and could be expanded into a future world-wide air traffic control network by launching additional satellites to provide global coverage.

The PLACE communications would consist of two duplex radio links. Each ground station would be equipped with a high-gain antenna transmitting to and receiving from the satellite in the 5 GHz frequency range. Up to ten independent ground stations could operate simultaneously in the communication mode. Any of the ground stations could function as a master control by providing it with timing, tracking, and computing equipments necessary for position location. The satellite would transmit to and receive from the aircraft in the 1.5 GHz (L-Band) frequency range. All satellite equipment requirements are within the present capabilities of the Applications Technology Satellite (ATS) program so that no advancements in present technology are required. Participating aircraft equipped with a high-gain L-Band antenna could receive any of the ground control voice and data transmissions. Any of the aircraft could transmit voice and data to all ground facilities, and more than 200 aircraft could be accommodated on an operational basis with a single satellite.

The position-location scheme can be divided into two areas: (1) ranging by satellite alone, and (2) satellite augmented ranging from VLF ground transmitters. The two-way range from the ground station-to-satellite-to-aircraft and return is measured at the same time as the two-way range from the ground station-to-satellite and return by means of standard side-tone ranging techniques. From these two measurements, and the known aircraft altitude, the range from the sub-satellite point to the aircraft can be determined. A circular line of position (LOP) is thereby defined which contains the aircraft position and which is centered at the sub-satellite point.

A second LOP is defined by the range of the aircraft from a VLF ground transmitter. This range measurement is also made at the ground station from signals relayed from the aircraft by means of the same satellite transponder. If the Omega navigation network becomes operational, the Omega VLF transmitters will be used, but in the event that they are not, any suitable VLF transmission standard emitting a single tone in the 10-14 KHz frequency range can be used. Single frequency transmitters will produce a set of LOP's so that the resulting ambiguity must be resolved by other means. The proposed primary method of doing this in the PLACE system is by continuous tracking from a known starting position.

A second and completely independent method of position-location has also been incorporated into the PLACE design for the purpose of increasing the overall reliability of aircraft surveillance and to provide a secondary method of ambiguity resolution. This subsystem, designated SIND, for Satellite Inertial Navigation Determination, makes use of the measured range and range-rate between the aircraft and the satellite along with the telemetered aircraft velocity vector derived from on-board accelerometers. These measurements alone will define the position of the aircraft to an accuracy sufficient for ambiguity resolution and will also permit ground observation of on-board navigation equipment performance.

A preliminary experiment based on the PLACE system concept could utilize a single synchronous altitude satellite transponder, a single ground control facility of minimum size, and a maximum of four cooperating aircraft. The ground control facility could be instrumented to demonstrate the feasibility of the PLACE system, including both two-way voice and digital communications along with simultaneous tracking of four aircraft. However, the experimental system could be expanded into a complete operational PLACE system simply by upgrading and expanding the ground communications and position-location processing equipments.

2. PLACE SYSTEM DESCRIPTION

The movement of modern commercial aircraft requires that a traffic routing or control agency know the location and identity of all aircraft in a given area of responsibility and that a reliable means of communicating with the aircraft exists. Thus, both navigation and communication must be embodied in a practical air traffic control system. Communication includes the two-way transfer of information whether voice, digital, or analog between a ground control station and an aircraft. Navigation as herein used means the process of position determination and safe movement of aircraft from one point to another. The PLACE concepts described in this section provide both of these essential capabilities in a single system design.

2.1 Communication System

The principle elements of the PLACE communication system are shown in Figure 2-1. These are: (1) a Primary Control Center; (2) one or more Alternate Control Centers; (3) Synchronous Satellite; and (4) the cooperating Aircraft in the area of coverage. The operational capacity of the communication system is limited by the satellite-to-aircraft transmission link; which in PLACE has been configured to conform with the capabilities of presently programmed Applications Technology Satellites (ATS). Specifically, the available satellite transmitter output power has been assumed to be 40 watts operating into an antenna which provides nearly earth disc coverage in the 1500 MHz aeronautical band. It is shown in a following section that ten voice-quality communication channels can be supported over this link. The bandwidth of each of these voice channels is taken to be nominally 3 KHz while the design goal for the received signal-to-noise ratio at the aircraft is taken to be 25 db. These channels can be utilized for either voice transmissions, digital data transmissions or some combination thereof as operational requirements dictate. The PLACE design concepts will accommodate any such desired arrangement and based on this flexibility, it has been assumed that up to 200 aircraft can operationally share the ten ground-to-aircraft communication links. Accordingly, PLACE has been configured to operate simultaneously with 200 aircraft utilizing a transponder within the ATS capabilities.

Figure 2-2 summarizes the important constraining parameters and design choices on which the PLACE system is based. This figure is laid out with the Control Center on the left, the Satellite with its dual transponder in the middle, and the Aircraft on the right. For purposes of clarity in the discussion which follows, the closed loops formed in the system, which are not apparent in Figures 2-1 or 2-2, should be identified. A forward path exists from the Primary Control Center transmitter through the Satellite to the Aircraft receiver

along with a return path from the Aircraft transmitter through the same Satellite to the Primary Control Center. The only independent oscillator in this loop is a frequency standard located at the Primary Control Center. Both the Satellite transponder and the Aircraft transceiver contain frequency synthesizers of similar design. The frequency synthesizer in the Satellite is locked in frequency and phase to the carrier component of the signal transmitted from the Primary Control Center and this synthesizer generates all frequencies required in the Satellite transponder for both directions of transmission. The frequency synthesizer contained in the Aircraft transceiver is locked in turn to the frequency and phase of the carrier component of the signal received from the Satellite. This synthesizer also generates all frequencies required within the Aircraft transceiver including those necessary for selecting the appropriate channel in which the Aircraft is operating and for providing a gross doppler correction in the transmission paths.

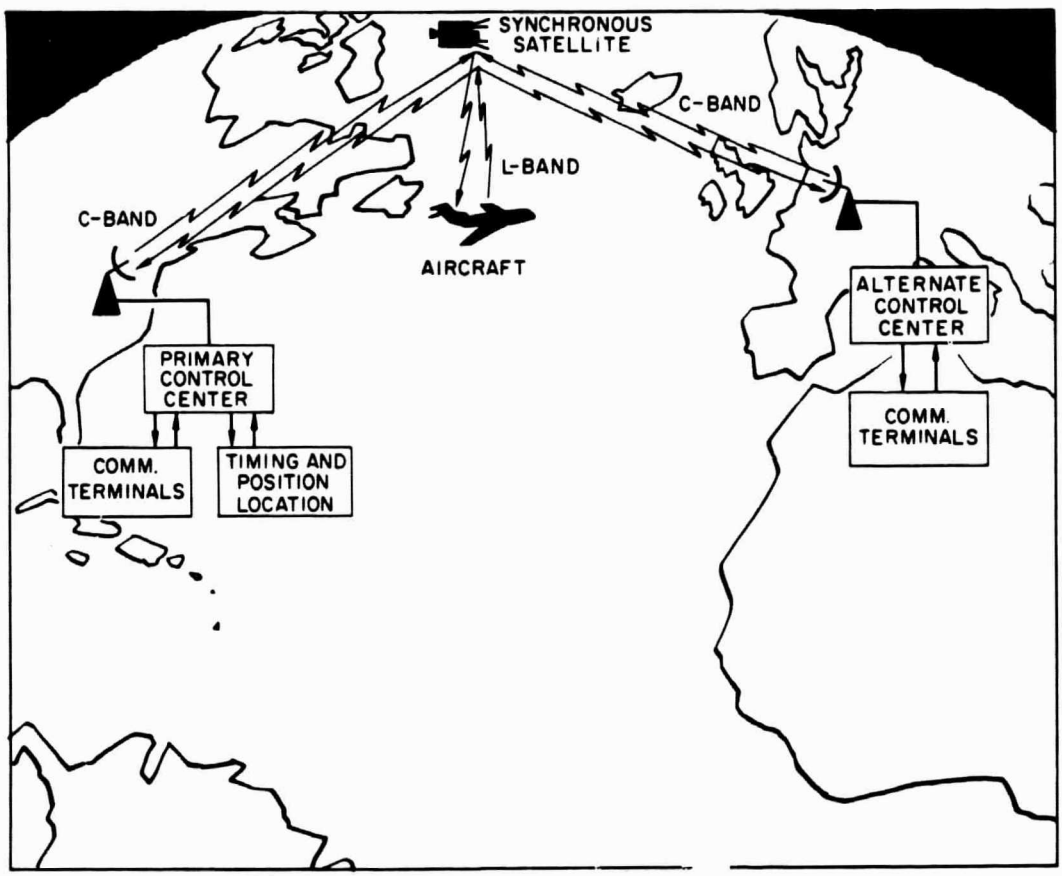

Figure 2-1–Diagram Illustrating the PLACE System

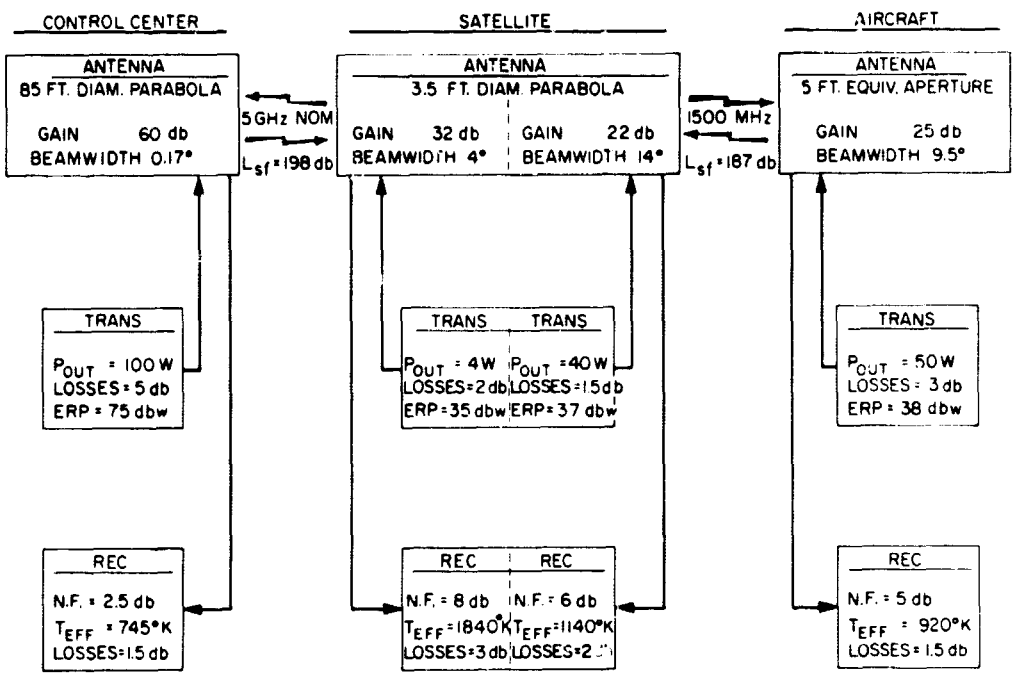

Figure 2-2.-Summary of PLACE Communication Parameters

All of the ground stations operating in the system will receive both the satellite-to-ground and the satellite-to-aircraft transmissions in the 5 GHz and 1500 MHz bands, respectively. Reception of the 5 GHZ transmission is necessary to complete the aircraft-to-ground station communication path, whereas reception of the 1500 MHz transmission is required for channel monitoring and power control functions. The Primary Control Center will receive the 1500 MHz satellite-to-aircraft transmission to provide range and range-rate measurements between the Primary Control Center and the satellite. The Primary Control Center will also receive the 5 GHz transmission to derive the positional information necessary to locate all the aircraft in the system. All other ground stations in the system will use the received 5 GHz signal to individually control the frequency and phase of their transmissions with respect to the Primary Control Center. In this way, the composite signal in the satellite, as received from all of the ground stations, will be made to look essentially as though it originated from a single ground station.

2.1.1 Ground Station Transmitters

For purposes of describing the system design, a particular operational configuration will now be hypothesized. This configuration is selected only to clarify the discussion which follows and it is in no way implied that an operational PLACE system is limited to this particular configuration. Assume that nine of the available ground-to-aircraft voice-quality channels are being utilized for voice transmissions while the tenth channel is being utilized for digital data transmission. If each of the nine voice channels is assigned to a separate control center, then there could be as many as nine independent ground stations (more than nine would be possible with the addition of time-sharing features). On the other hand, some or all of the control centers could be co-located at one ground station so as to share a common antenna, receiver and transmitter. Assume that this is not the case, but that instead, there are nine separate control centers and ground stations so that these two terms can be used interchangeably in what follows without confusion. Then, referring again to Figure 2-1, one of the ground stations will function as the Primary Control Center or master station which will perform all position location operations, while the remaining eight will function as Alternate Control Centers. (One or more of eight could of course, be equipped to assume primary control.)

In the hypothetical arrangement established above, it is tacitly assumed that inter-communications between the control centers will be by other means external to the PLACE system. Such communications would undoubtedly be by a variety of methods including hard-wire, radio relay, dispatch, etc. However, for emergency use, or for initial implementation, it would be possible to reduce the PLACE capacity and to reserve a portion of the communication system for inter-station communication (particularly trans-oceanic). Either a time-shared high speed data link or multiple frequency-division, low speed data links for inter-station could thereby be provided and a relatively small part of the PLACE system capacity should be required. Further, it will become apparent later that considerably greater channel capacity between ground stations can be provided for a given portion of the satellite transmitter power because of the high ground station antenna gain compared with the aircraft antenna gain. Because of the many-faceted operational implications involved, inter-station communications will not be considered further here.

The discussion will now return to the hypothetical arrangement established above. The Primary Control Center station will transmit at its assigned carrier frequency in the 5 GHz region in accordance with available frequency assignments for this type of service. Referring to Figure 2-3, this carrier will be modulated by a baseband signal consisting of: (1) a timing/control (digital) signal; (2) a pattern of ranging tones; (3) a digital data signal in channel 1;

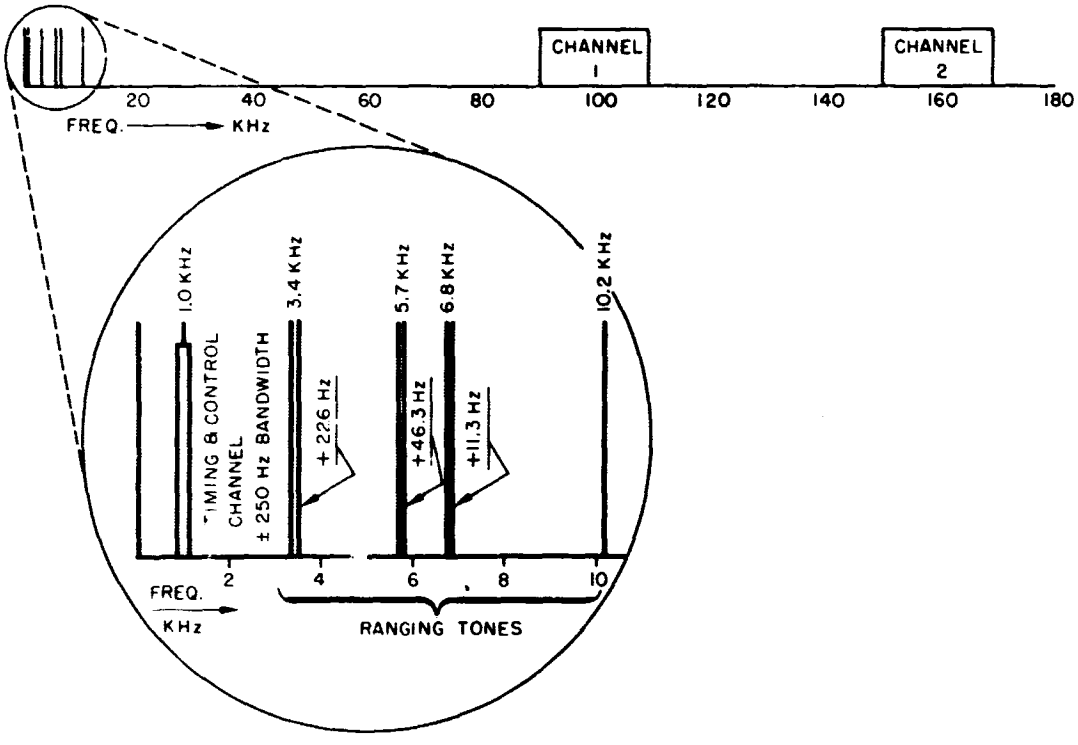

Figure 2-3–Primary Control Center Baseband Spectral Diagram

and (4) a voice signal in channel 2. The timing/control signal will occupy a total bandwidth of about 500 Hz, while each of the ranging tones is at a single discrete frequency. These signals properly belong to the position-location portions of the PLACE and their function will be described later. The voice channels occupy approximately 18 KHz of bandwidth each and consist of nominal 3 KHz wide baseband signals; frequency modulated onto carriers with an rms deviation ratio of 2:1. Each of the ground stations will transmit a similar frequency modulated voice signal on a carrier which is displaced from the Primary Ground Station carrier by 40 (1 + 3N/2) KHz, where N is an integer representing the channel number with $1 \leq N \leq 10$.

2.1.2 Satellite Transponder – Ground to Aircraft

A great deal of flexibility has been afforded in the PLACE communication system design by providing for access to the satellite transponder from a multiplicity of both ground stations and aircraft. The power spectrum of the combined signal received from all of the ground stations is shown in Figure 2-4, as it appears in the receiver portion of the Ground-to-Aircraft (GA) transponder. This

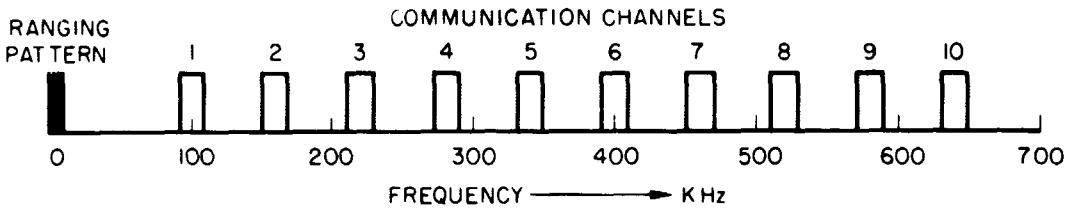

Figure 2-4–Composite Spectral Diagram at the Satellite

signal can be translated to baseband in the satellite through synchronous detection since the satellite frequency synthesizer is phase locked to the Primary Control Center carrier component. The resulting baseband signal can then be used to directly phase modulate the GA transmitter carrier which is also derived from the same frequency synthesizer. The constant amplitude signal transmitted by the GA transponder will be angle-modulated with an rms phase deviation of one radian. Therefore, there are no particular amplitude linearity requirements on the transmitter final amplifiers and there will be no undue loss in efficiency of operation.

Figure 2-5 shows a simplified block diagram of the GA transponder. This transponder will receive the nominal 5 GHz transmissions from the ground

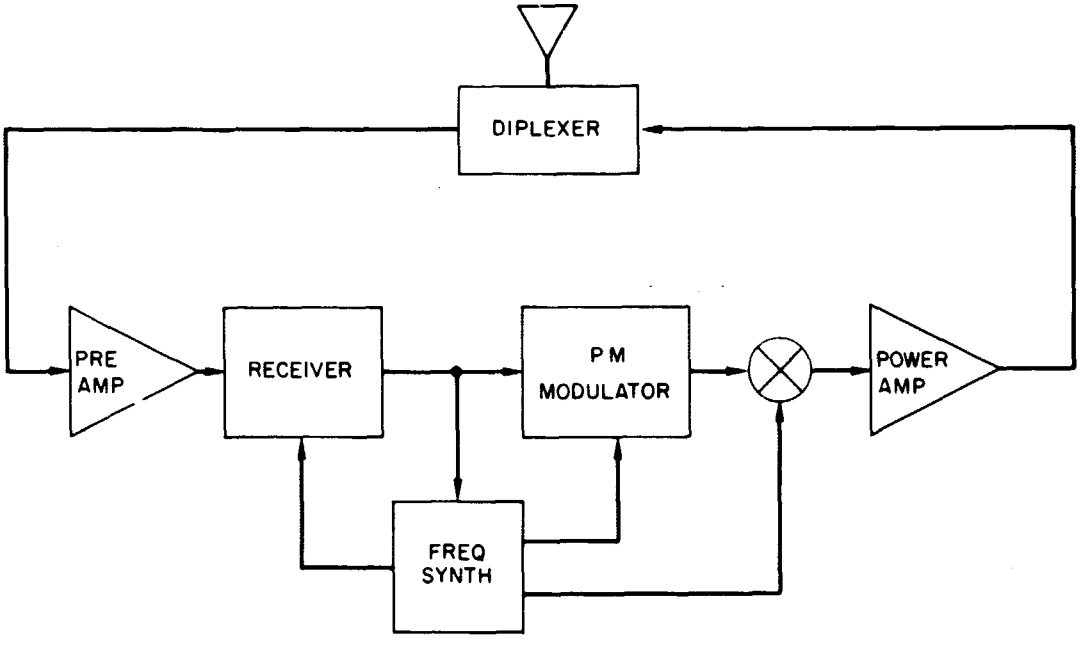

Figure 2-5–Simplified Block Diagram of Ground-to-Aircraft Transponder

stations and will modulate a carrier in the 1.5 GHz region. Phase coherence between the transmitted and received carrier frequencies is maintained by a phase-locked oscillator in conjunction with the synthesizer. The frequency synthesizer is locked to the received carrier from the Primary Ground Station and generates the transmitted carrier without the use of independent oscillators. The Primary Control Center will monitor the GA transmission to provide overall frequency and power control. In particular, the phase deviation of the GA transponder carrier will be maintained at the proper level by individual control exercised at each ground station. However, the Primary Control Center will provide additional control as may be required through the timing/control channel.

The satellite antenna will have an equivalent 3.5 ft. aperture with a receive gain of 32 db and an equivalent 3 db beamwidth of 4 degrees. The same antenna will be used for transmitting and receiving through the use of a diplexer. When transmitting, it will provide a half-power gain of 19 db with a 3 db beamwidth of 14 degrees. The transmitter output power will be 40 watts for an effective radiated power (ERP) of 37 dbw on boresight.

2.1.3 Aircraft Transceiver

The aircraft transceiver is shown in a functional block form in Figure 2-6. In a sense, it will operate as a coherent transponder in a similar fashion to the satellite GA transponder. That is, it will receive the 1.5 GHz signal from the satellite, phase-lock to the carrier component, and synchronize the frequency synthesizer. The frequency synthesizer will generate the aircraft transmitter carrier in the 1.5 GHz region. This carrier is phase coherent with the carrier received from the satellite; but is offset from the received carrier in frequency, under control of the channel selector. In terms of the carrier component then, the aircraft transceiver is a coherent transponder.

Operation of the portion of the aircraft transceiver described above is illustrated in Figure 2-7. With the receiver loop in equilibrium, the following two conditions are necessary.

$$\theta_4 = K_4 \, \theta_R$$

$$\theta_4 = \theta_1 - (K_1 + K_2 + K_3) \, \theta_R$$

With K written for the sum $(K_1 + K_2 + K_3 + K_4)$, the following relationship is obtained

$$\frac{\theta_R}{\theta_1} = \frac{1}{K}$$

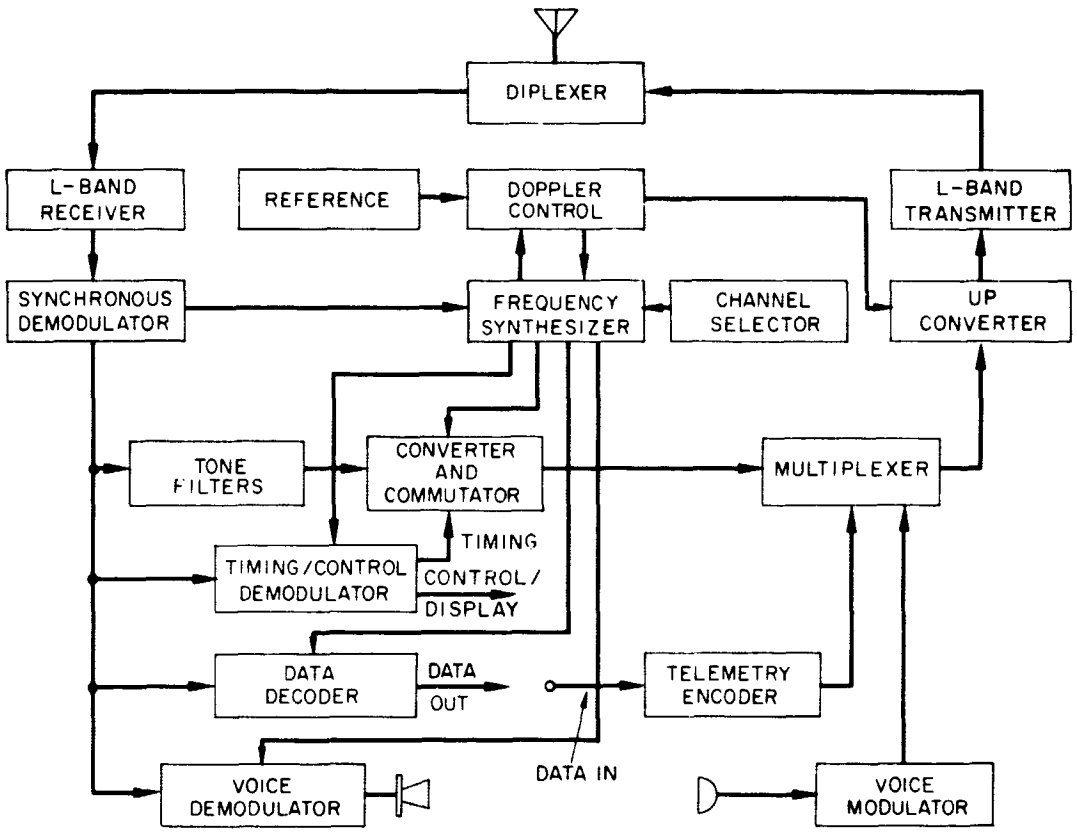

Figure 2-6–Functional Block Diagram of Aircraft Transceiver

If ψ in Figure 2-7 is assumed to be zero for the moment, a similar relationship for the transmitter is obtained. That is,

$$\frac{\theta_0}{\theta_R} = M$$

where $M = M_1 + M_2 + M_3 + M_4$. Therefore, the transmitter output is related to the receiver input by

$$\frac{\theta_0}{\theta_1} = M/K,$$

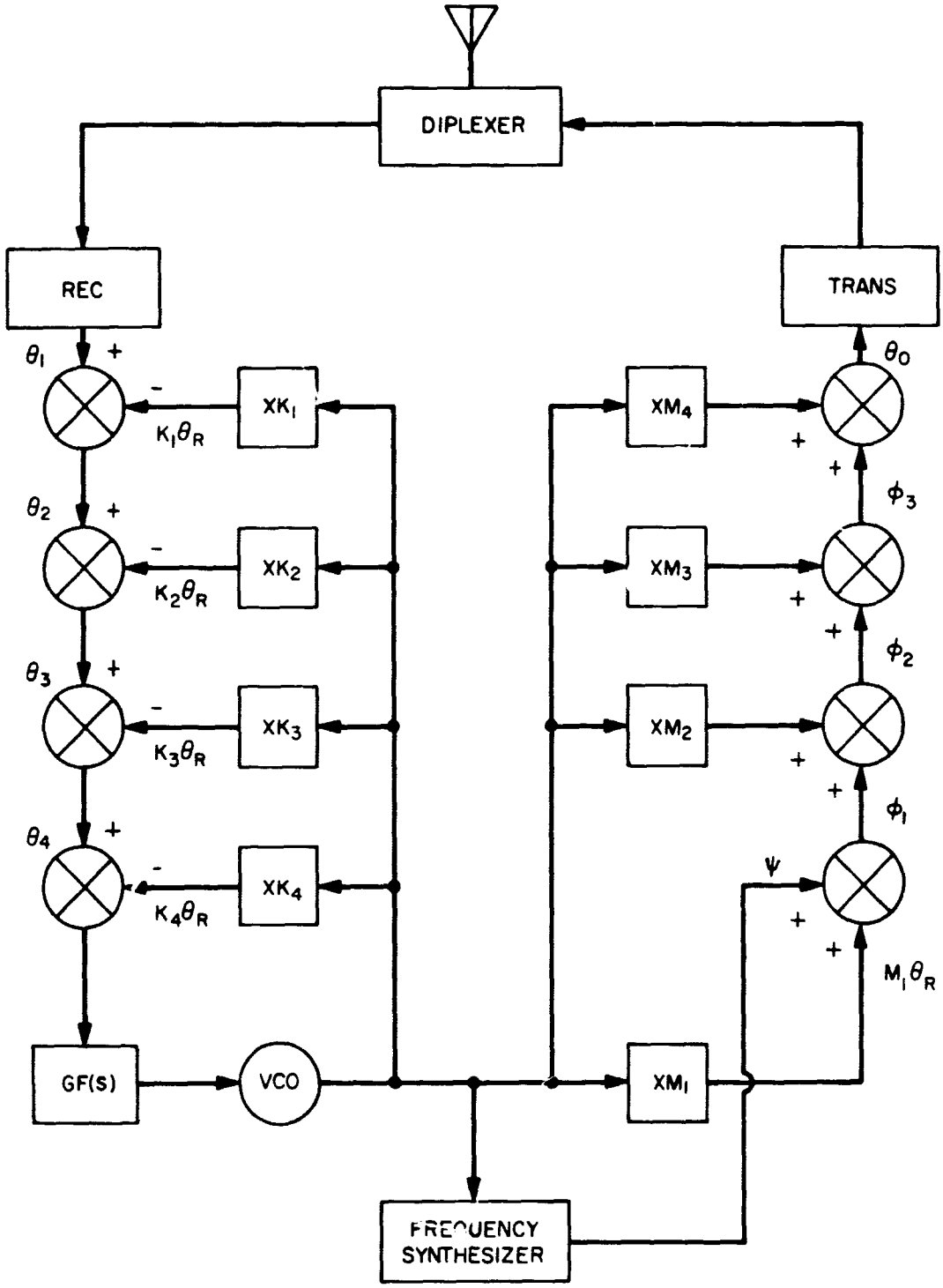

Figure 2-7–Simplified Block Diagram Illustrating Operation of the Aircraft Transceiver

where M/K is a rational fraction. The transmitter frequency is of course related to the received carrier frequency in the same way, so that any desired ratio between these two frequencies can be obtained. For example, if the two selected frequencies should be 1540 MHz and 1620 MHz, the corresponding ratio is 81:77. The following choices satisfy; $M_1 = 1$, $M_3 = 16$, $M_4 = 64$ and $K_1 = 1$, $K_2 = 4$, $K_3 = 8$, $K_4 = 64$. The multipliers and dividers can be cascaded to further simplify the circuitry.

Based on the results in Appendix A, it can be shown that the carrier component of the GA transmission is given by

$$P_{CAR} = \frac{A_0^2}{2} \exp(-\delta^2),$$

while the total signal (or continuum) power is

$$P_{CON} = \frac{A_0^2}{2} [1 - \exp(-\delta^2)].$$

In the above, $Ao^2/2$ is the unmodulated carrier power and δ^2 is the mean squared phase deviation. For $\delta = 1$ rad. rms, the carrier component is approximately 37 percent of the total power. In Section 3.1 it is shown that the minimum unmodulated carrier-to-noise power density ratio received by the aircraft will be 63.7 db. If the effective tracking bandwidth of the transceiver is 100 Hz, the signal-to-noise ratio in the tracking loop, S/N]TL, will be

$$\left.\frac{S}{N}\right]TL = 63.7 + 10 \log \frac{0.37}{100} \text{ db},$$

or approximately 38 db, so that excellent tracking performance is expected.

Based on the above, the continuum power is the remainder, or approximately 63 percent of the total power. Thus, the "power packing" efficiency of angle-modulation, in this case, exceeds that of linear modulation. However, only the first-order sideband portion of the continuum represents usable signal power. This portion can be found from

$$P_S = \frac{A_0^2}{2} \delta^2 \exp(-\delta^2),$$

which for $\delta = 1$ rad. rms results in approximately 37 percent of the total power.

The aircraft receiver IF bandwidth will be on the order of 2 MHz wide and the signal power and noise power will be at comparable levels at the input to the main demodulator. With this situation, it is clearly impossible to use an ordinary phase or frequency demodulator to any advantage. Instead, a linear (synchronous) demodulator is essential to prevent further deterioration of the signal-to-noise ratio. However, angle-modulation is a non-linear operation so that linear demodulation of such a signal necessarily produces distortion products. Appendix B deals with this situation in considerable detail. In particular, it is shown that the total interfering distortion products can be constrained to an acceptable level by holding the rms phase deviation to less than 1 radian and by spacing the subchannel carrier frequencies by an amount equal to three times the subchannel bandwidth as is indicated in Figure 2.4.

The transceiver phase-locked loop will demoduate the signal received from the satellite to produce the ranging pattern, the timing/control signal, and the subcarrier voice and data channels. By simple filtering, the signal will be separated into its three components. A simplified diagram of the receiver portion of the aircraft transceiver is shown in Figure 2-8 which also summarizes the important design parameters.

The timing/control signal is a binary data stream which is fed to the timing/control unit. This unit contains a timing clock generator which is synchronized by the timing/control signal and controls the range pattern processor. The range pattern processor is also fed the range-tone pattern from the phase-locked detector. All range tones are time commutated, under control of the timing signal, and then frequency translated, under control of the frequency synthesizer. The exact processing involved in this operation is a part of the position location scheme and does not pertain directly to the communications systems per-say. The voice and data subcarriers are fed to a demultiplexer where the data and voice channels are separated and demodulated.

The processed range patterns and the aircraft derived voice and data information are combined by frequency division multiplexing prior to transmission as shown in Figure 2-9a. This combined signal is modulated onto the transmitter carrier by a single sideband technique. The carrier component is used for both doppler tracking and signal recovery. Each aircraft is assigned a separate transmission channel which is offset in frequency from every other aircraft as determined by the frequency synthesizer settings. The input designated as ψ in

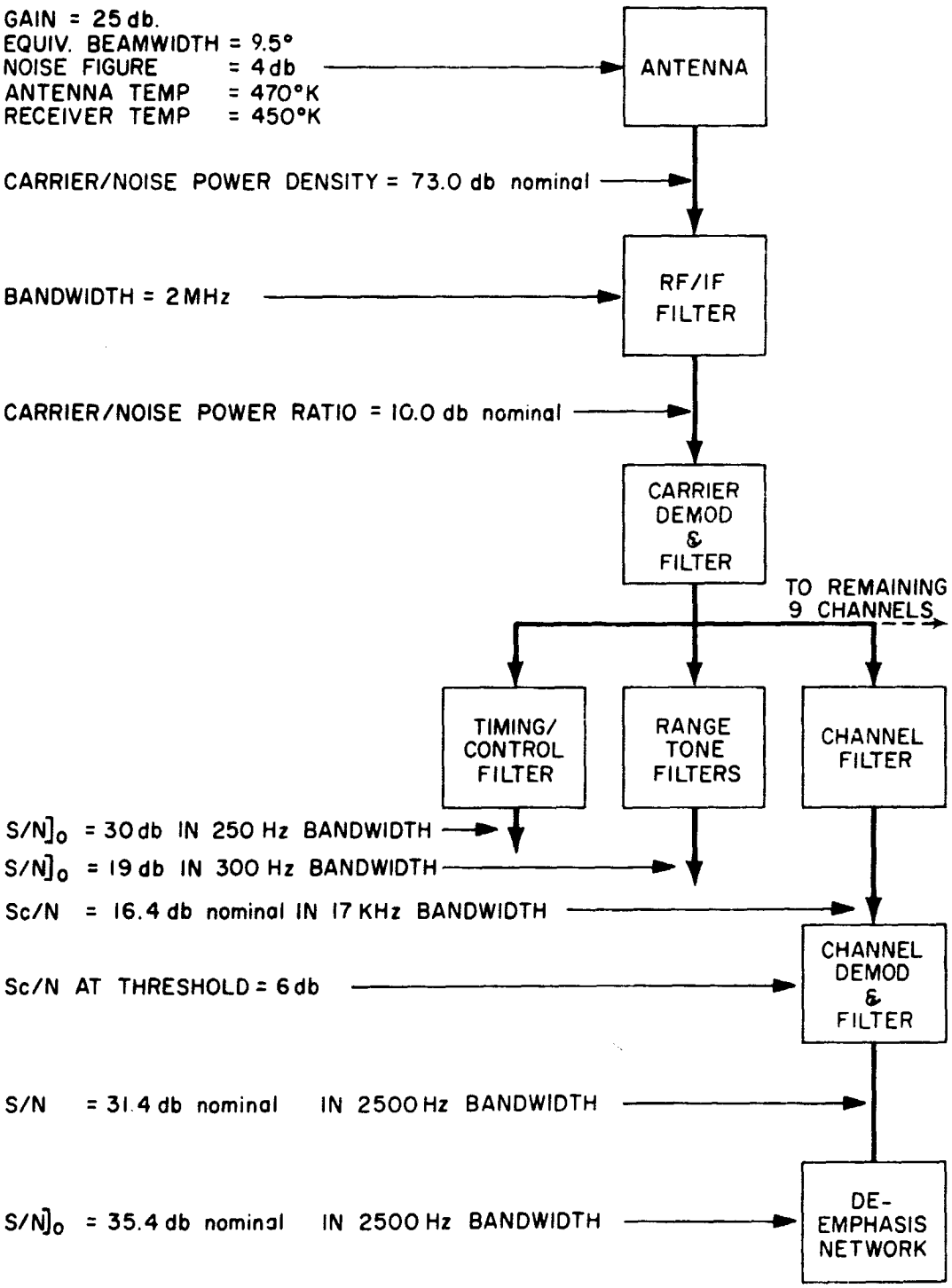

Figure 2-8–Summary of Aircraft Receiver Characteristics

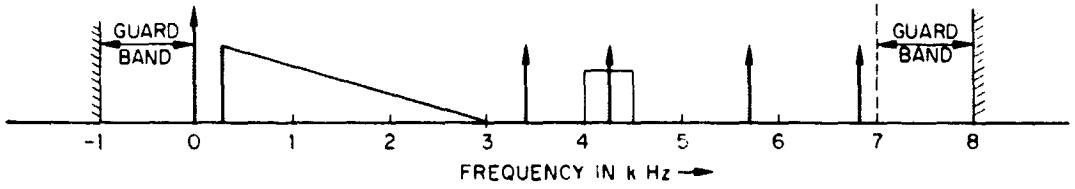

a. Baseband spectrum transmitted from each aircraft

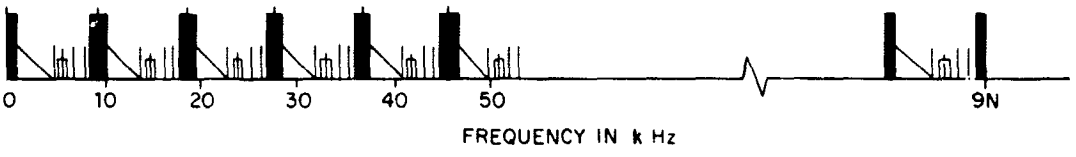

b. Composite spectrum received by the satellite

Figure 2-9–Aircraft-to-Satellite Spectral Diagram

Figure 2-7 can be chosen to provide the desired offset from the nominal transmit frequency. Thus a "stacking" of aircraft transmitter signals will be accomplished as shown in Figure 2-9b. The method by which doppler shift is compensated for is discussed in 3.4. The transceiver power output will be 50 watts. The aircraft antenna will have an effective gain of 25 db.

2.1.4 Satellite Transponder – Aircraft to Ground

Figure 2-10 shows a simplified block diagram of the satellite Aircraft-to-Ground (AG) transponder. The composite spectrum from all of the aircraft as received at the satellite is shown in Figure 2-9b. This signal is directly angle modulated, with an rms phase deviation of one radian, onto a carrier generated by the frequency synthesizer; and is then coherently translated to nominally 5 GHz for transmission back to the ground stations. The frequency synthesizer is common to both the GA and the AG transponders and is phase locked to the carrier of the Primary Ground Station. The AG transponder uses the same antenna for both reception and transmission as did the GA transponder. The AG transponder has a power output of 4 watts.

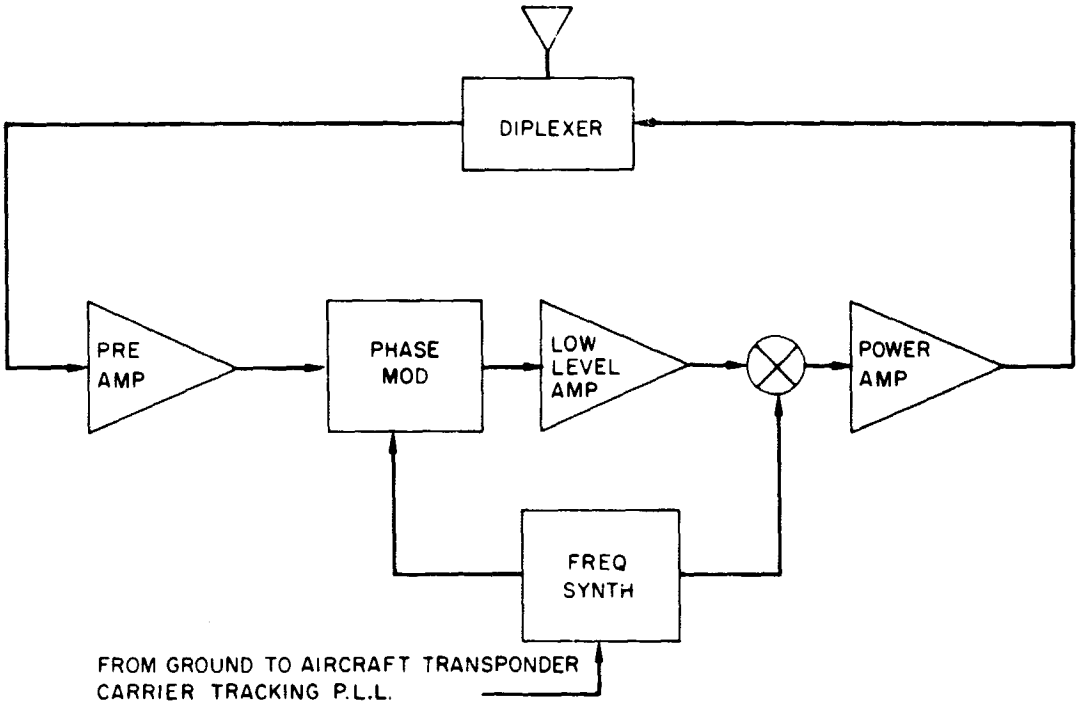

Figure 2-10–Simplified Block Diagram of Aircraft-to-Ground Transponder

2.1.5 Ground Station Receiver

The ground station receiver uses the same antenna as the ground station transmitter, and both the 1.5 GHz and the 5 GHz signals transmitted by the satellite are received. The 1.5 GHz signal is used for range measurements, power monitoring, and frequency control functions. Power monitoring is required to maintain the total phase deviation in the GA transponder to a constant value regardless of the number of channels being used. The 1.5 GHz signal is used for ground station-to-satellite doppler tracking. A carrier-tracking phase-locked loop is included to correct the transmission frequency of the ground station, so as to insure the correct frequency as received by the satellites. The aircraft signals are recovered by a phase-locked demodulator in the 5 GHz receiver. The composite signal from the aircraft is separated by channel selectors into ranging data and communication data for respective processing.

Figure 2-11 shows a simplified block diagram of the Primary Ground Station. The receiver uses the same antenna as the ground station transmitter; and both the 1.5 GHz and the 5 GHz signals, transmitted by the satellite, are received. The 1.5 GHz receiver and demodulators are similar to the aircraft

transponder's receiver section as described in Section 2.1.3. However, there are several distinct differences. The carrier-tracking phase-lock loop drives a doppler correction unit which introduces appropriate corrections in the ground station transmitter frequency. The function of the doppler correction unit is to effectively provide a frequency standard source at the satellite. The signal monitor is used for monitoring the transmissions from the other ground stations and the channel demodulator is used to monitor any or all of the ground-to-aircraft channels for operational purposes and overall control.

The 5 GHz receiver recovers the aircraft to ground signals through the use of a phase-locked demodulator. The composite signal from the aircraft is separated by channel selectors in a coherent manner. The individual channels are

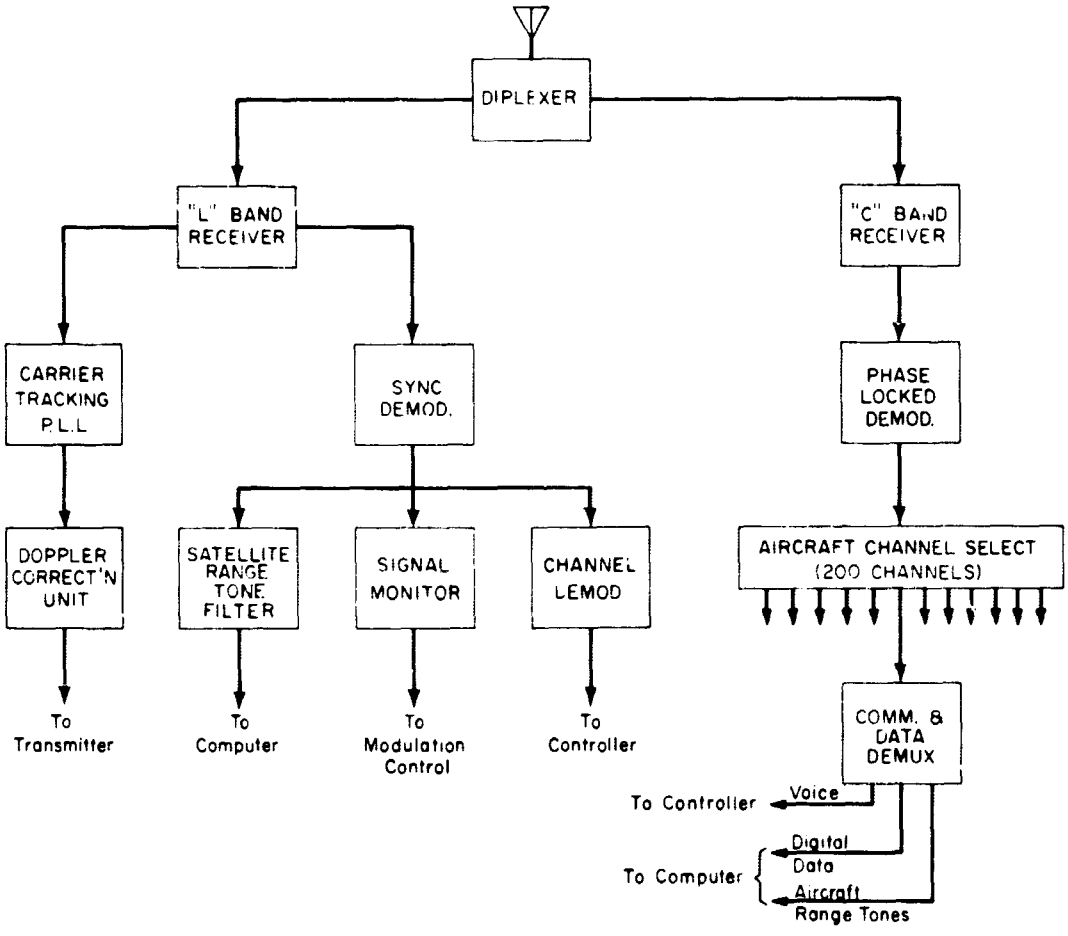

Figure 2-11–Simplified Block Diagram of Ground Receiver

further separated into their three component parts for respective processing. Namely, the voice signals are fed to the air traffic controller, and the ranging tones and digital telemetry data are fed to the position-location computer.

2.2 Position-Location System

The PLACE position-location technique will enable the Primary air traffic Control Center to continuously and simultaneously track 200 aircraft flying in the region of coverage of a single geosynchronous satellite. All functions required of the aircraft would be performed automatically and, after initial equipment adjustments, would be independent of the onboard navigation system. The Primary Control Center would perform all necessary signal processing and position-location computations for all aircraft. This facility would also perform the traffic surveillance functions and provide navigational information to all aircraft as required.

The position-location system employes a rho-rho technique whereby, the position of the aircraft is defined by the intersection of three spheres as is indicated in Figure 2-12. The first sphere is given by the known distance of the aircraft from the center of the earth, as determined by the aircraft altitude. The second sphere is determined by measuring the distance between the aircraft and the satellite. The intersection of these two spheres generates a circular line of position (LOP) which contains the aircraft. This LOP is centered on the

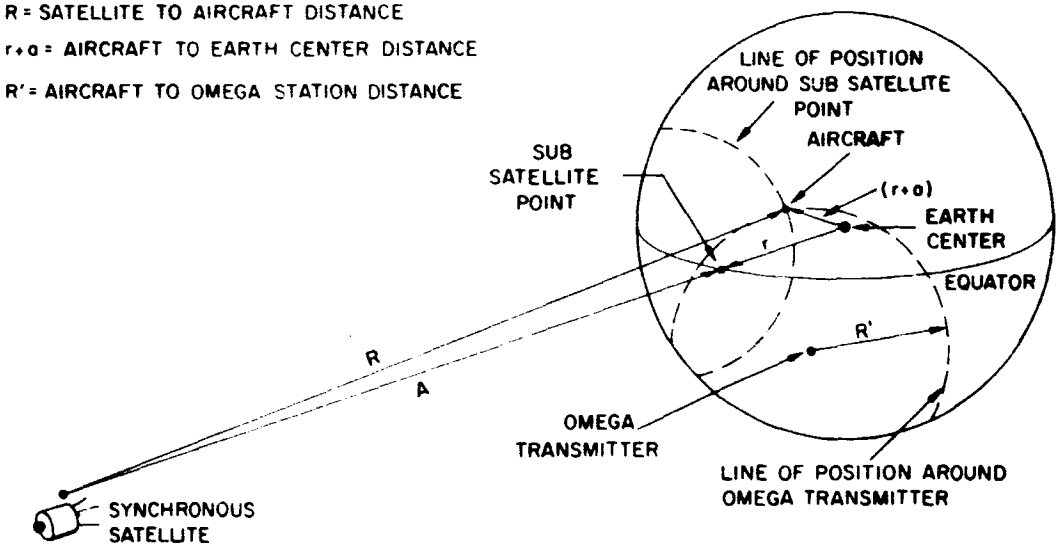

Figure 2-12–Position Determination Using Range Measurements

sub-satellite point. The required distance measurement is accomplished in a straight forward manner using side-tone ranging techniques similar to those used in the Goddard Range and Range Rate system. The third sphere is defined by the distance of the aircraft from an appropriately located VLF ground transmitter. This measurement is also performed by essentially the same side tone ranging technique.

2.2.1 Satellite Range Measurement

When the phase of a signal emitted by a distant transmitter is compared with the phase of a locally generated reference signal of precisely the same frequency and phase as that of the transmitter, the relative phase between the two will be a measure of the distance from the transmitting station. It is exactly this principle which is used in any side tone ranging system and is the technique which will be used to measure the distance from the satellite to the aircraft. In PLACE, the application of this technique differs somewhat from more conventional applications in that the range between the aircraft and the satellite is measured remotely at the ground station. In particular, the total two-way range is measured from the ground station-to-satellite-to-aircraft, along with the same return path. The ground station-to-satellite two-way range (which is the same for all aircraft) will also be continuously measured using the same ranging pattern. This known range can then be subtracted from the measured ground station-to-satellite-to-aircraft range to produce the satellite-to-aircraft range.

With this technique there is no need for a highly stable reference clock on either the aircraft or the satellite, since the phase comparison is made with respect to the transmitting clock at the ground station. The salient requirement on the aircraft and satellite equipments is to maintain phase coherence between the received and transmitted signals. The precision to which this range measurement can be made depends upon the dispersion introduced by the transmission medium and the signal-to-noise ratio maintained over the path.

2.2.2 Satellite Ranging Pattern

The ranging pattern transmitted over the above mentioned paths consists of a basic tone for fine range resolution and a set of sidetones which allow ambiguity resolution. The proposed pattern for PLACE is shown in Figure 2-3 where the lowest six tones are of primary interest at this point. The frequency of the highest tone is 6.8 KHz while the frequency of the second highest tone of interest is 3.4 KHz. The remaining four tones of interest (1.13 KHZ, 226.7 HZ, 45.3 HZ, and 11.3 HZ) are derived as differences between tones in the transmitted pattern. The fact that a tone delay is equivalent to the group delay over a transmission path allows construction of the lower frequency tones in the above stated manner.

Frequency	Period	λ/2 Km	λ/2 n. miles	λ/2 s. miles
6.8 KHz	147 μs	22.0	11.9	13.7
3.4 KHz	294 μs	44.1	23.8	27.4
1.13 KHz	882 μs	132.4	71.5	82
226.7 Hz	4.41 ms	662	357	411
45.3 Hz	22.1 ms	3,309	1786	2057
11.3 Hz	88.2 ms	13,236	7143	8229

Figure 2-13–Satellite Ranging Tones

Figure 2-13 lists the tones that will be used to perform the range measurements.

In such a multitone system, the relative phase measurement of any one tone alone would define the range. In particular, the lowest tone of 11.33 Hz would define the range unambiguously to more than 8000 statute miles. This degree of range separation is adequate for PLACE since the greatest range difference for aircraft anywhere in the region of coverage is less than this figure and the measurement obtained would be unique. However, the lowest tone could not provide the required precision of measurement at the signal-to-noise ratios that can be reasonably expected. In particular, the next highest tone frequency is 45.3 Hz; and with equal signal-to-noise ratios (and propagation dispersion), the higher tone (45.3 Hz) will define the range to a precision four times better than that of the lower tone (11.33 Hz). However, the measured range will be ambiguous in that a set of four admissable ranges would be obtained. The two tones together permit measurements with ambiguity determined by the lower tone and precision determined by the higher tone.

The set of six tones will be used in this manner to provide the precision of measurement afforded by the 6.8 KHz tone which is plotted as a function of signal-to-noise ratio in Figure 2-14. It should be noted that the ambiguity steps are not constant, but vary between 2:1 and 5:1. The reasons for this choice will become apparent later, but the significance of this fact is that the required signal-to-noise ratio for each of the tones is not the same for equal probabilities

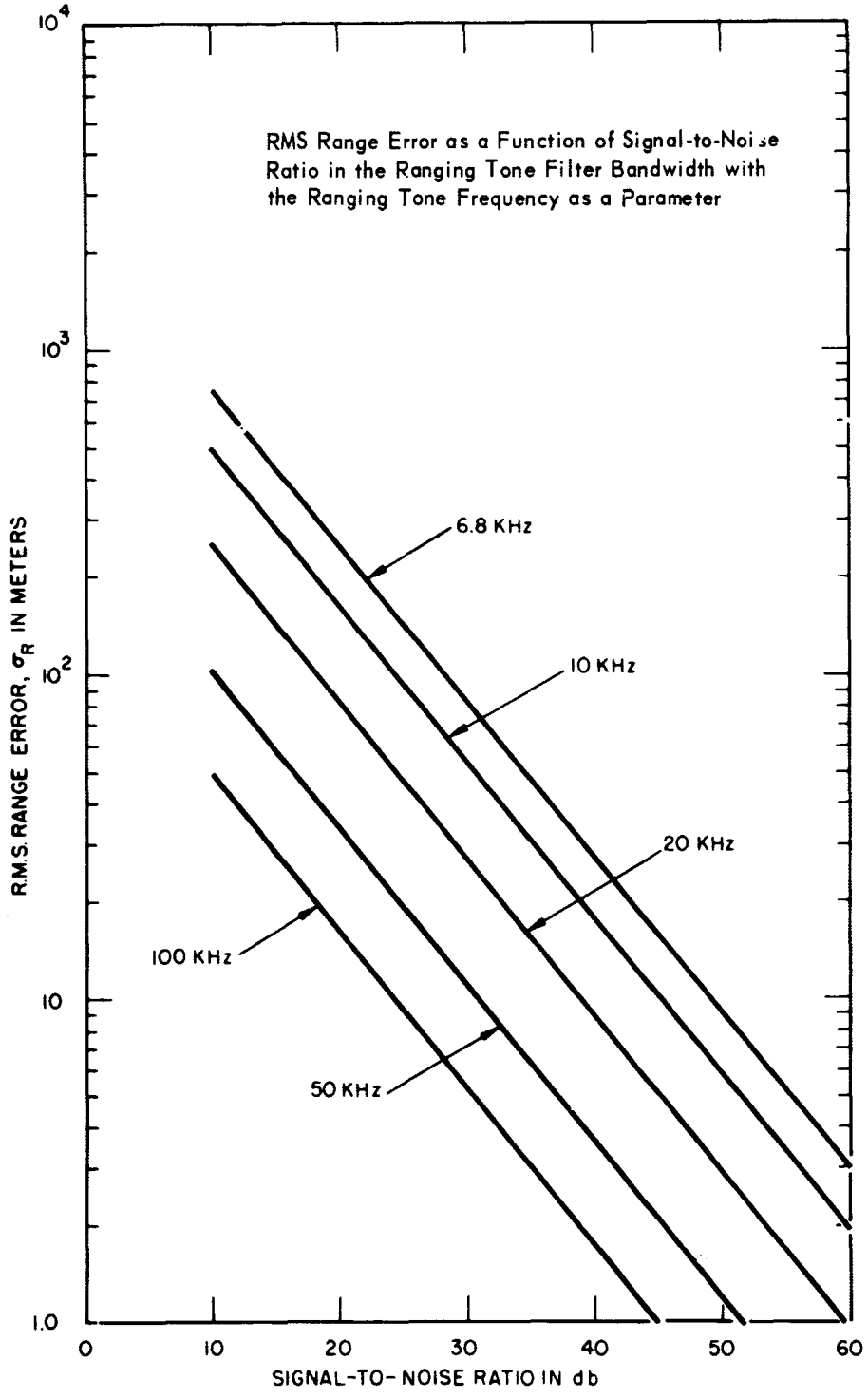

Figure 2-14—Range Error vs Signal-to-Noise Ratio

of correct ambiguity resolution as is indicated in Figure 2-15. For this reason, the relative amplitude of the tones will be adjusted accordingly.

2.2.3 Satellite Range Errors

An instructive relationship between positional and range measurement errors can be obtained by considering the geometry shown in Figure 2-16. Using the quantities identified in this figure, the following triangular relationship is easily obtained.

$$R^2 = S^2 + P^2 - 2SP \cos \gamma$$

By taking partial derivatives, and with the assumption that errors in measuring S and P are negligible, we obtain the following equation.

$$\Delta R = (SP \, \Delta\gamma \sin \gamma)/R$$

By simple substitution, the above equation can be written as

$$\Delta R = \frac{S \sin D/P}{[S^2 + P^2 - 2SP \cos D/P]^{1/2}} \Delta D$$

where $D = P\gamma$ is the great circle distance between the subsatellite point, SS, and the aircraft position, P, and $\Delta D = P\Delta\gamma$ is the measured error in D. The last equation provides the functional relationship which is plotted in Figure 2-17 with ΔD as a parameter.

From this figure it can be determined that if it is desired to hold the error in D to less than one mile for aircraft positions greater than 700 miles from the subsatellite point, the range error must be less than 0.2 miles or approximately 300 meters. Returning to Figure 2-14, the minimum required signal-to-noise ratio for the 6.8 KHZ tone is approximately 18 db.

2.2.4 VLF Range Measurement

The aircraft position on the circular LOP defined by the satellite range measurement described in 2.2.1 could be determined by a second independent

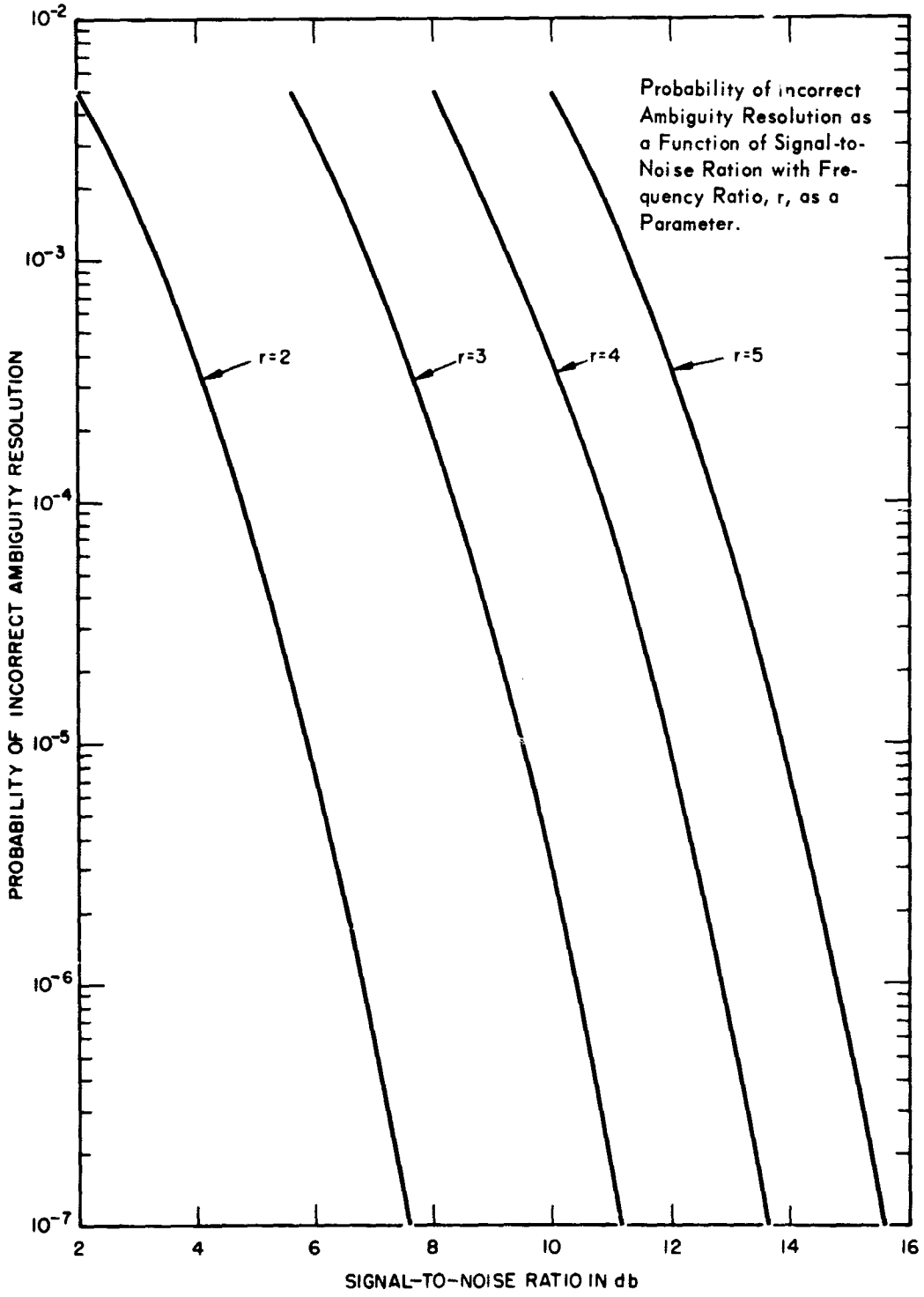

Figure 2-15–Ambiguity Resolution vs Signal-to-Noise Ratio

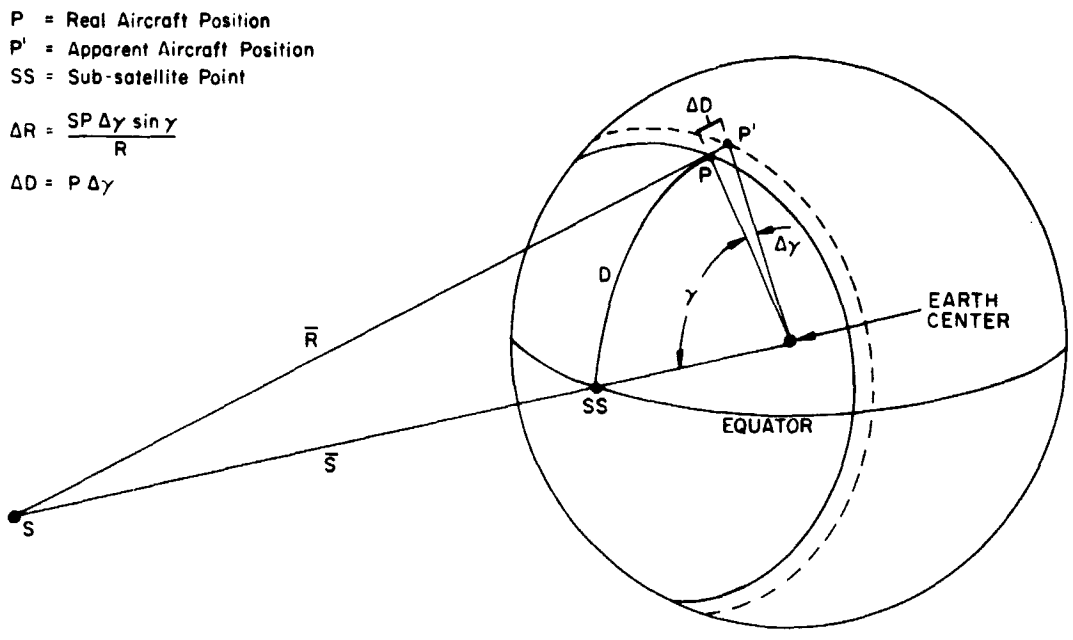

Figure 2-16–Diagram Pertaining to Relationship Between Positional and Range Errors

range measurement from another location – such as a second synchronous satellite. It is the method by which this range determination is made that sets PLACE apart from previously proposed air traffic control systems. In PLACE, the range from an appropriately located VLF transmitter provides the remaining essential measurement.

In the case of a VLF signal received at some distance from a transmitter, it is of course not practical to coherently transmit the VLF signal back to the source for phase comparison (two-way range measurement). Nor is it desirable to carry a reference clock of the required precision along with the attendant measuring equipment on board the aircraft. The problem is circumvented in PLACE by transmitting reference clock tones from the primary control center to the aircraft through the satellite. Relative phase measurements are derived analytically at the primary control center by the control center computer in conjunction with a VLF monitor receiver. In addition to the elimination of the requirement for a frequency standard on the aircraft, the aircraft equipment is simplified by eliminating the need for any on-board measurements. This is accomplished by a simple process of time commutating the received VLF signals with the reference clock signals and relaying them back through the same satellite to the primary central control facility where common equipment can perform the measurements for all aircraft.

Just as in the case of satellite ranging previously discussed, the precision of measurement of the VLF station to aircraft range is limited by the signal-to-noise ratio over the transmission path, but more important it is limited by the ionospheric propagation properties at VLF. Extensive investigations of VLF propagation characteristics have been made throughout the last decade. One result of these investigations had been to show that the 10 to 15 KHz region of the VLF spectrum exhibits a remarkable phase stability along with a very low rate of attenuation as a function of distance from the transmitter. These characteristics permit world-wide propagation of VLF radio waves and allows short-term phase measurements with rms variations of less than five microseconds.

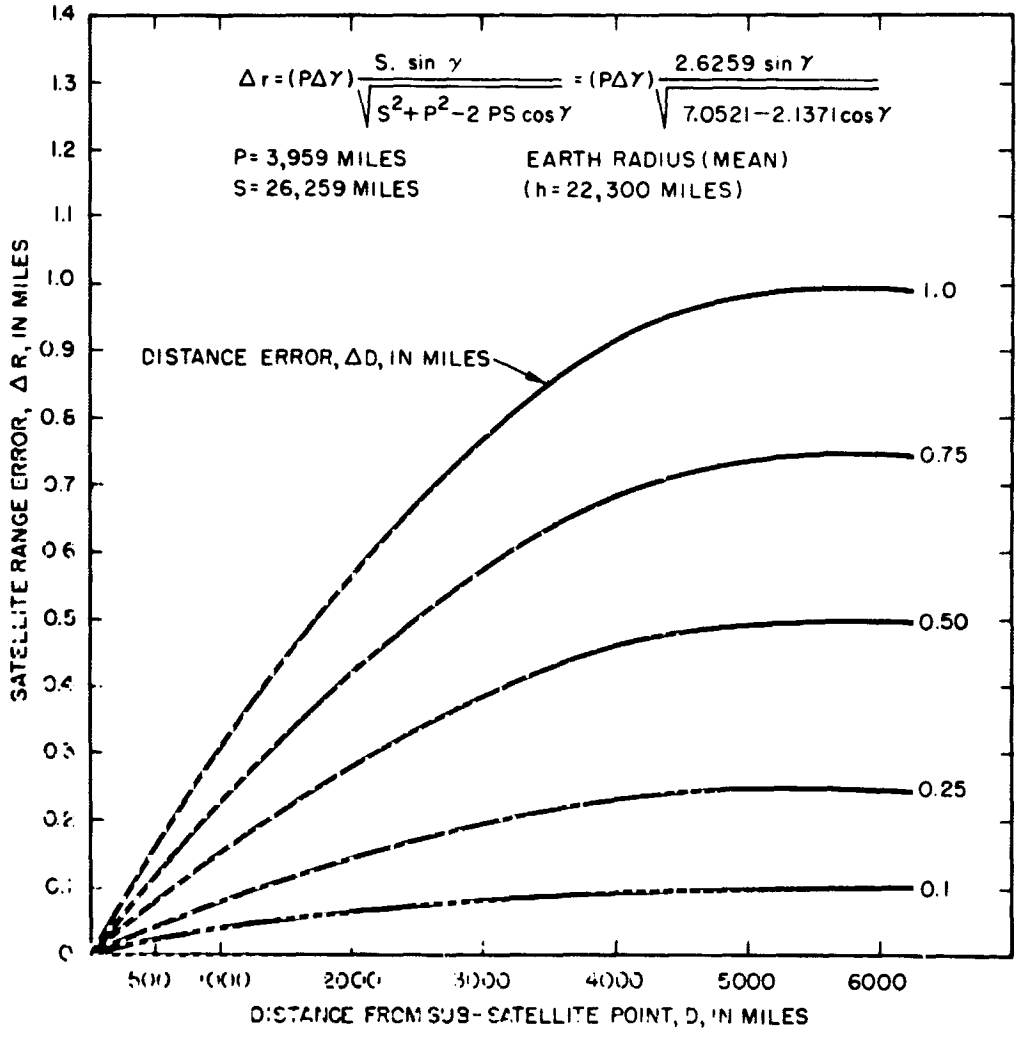

Figure 2-17.-Curve Pertaining to Relationship Between Positional and Range Errors

Within this frequency range, the radiated energy is propagated principally as a guided wave in the space between the earth and the reflecting ionosphere and it is this dominant single-mode of transmission, characteristic of VLF, that results in both the highly stable phase condition along with an attenuation rate near that which would be expected from inverse spreading loss. There are regular diurnal and annual changes in the velocity of propagation due to changes in the earth-sun geometry and there are certain geographic and magnetic irregularities that may result in variations in measured position of several miles. However, it is quite feasible to generate compensation or correction charts as is regularly done for LORAN systems. The difficulty of applying corrections to achieve an accuracy on the order of a mile is exactly the problem of charting the area of interest to this precision for various times of the day and year. For a fixed receiving position and a given time of day, the extreme variations throughout the year correspond to three or four miles in position. It is therefore apparent that approximately one chart per month, or six or seven charts for the entire year (since spring and fall charts will be essentially the same) will suffice to present the temporal variations in adequate detail.

2.2.5 Ambiguity Resolution by Continuous Tracking

As with the satellite ranging system, it is possible to resolve the inherent ambiguity of a single VLF tone in the 10 to 14 KHz range by means of a set of harmonic sidetones. In fact, the Navy's Omega navigation system, which is presently envisioned as the source of the VLF transmissions for PLACE, operates in exactly this fashion. The method by which Omega is commonly used eliminates the need for a highly stable clock at the receiver by generating hyperbolic LOP's resulting from phase difference measurements between VLF station pairs. PLACE has been designed to be completely compatible with the Omega system; that is, if the Omega network is operating, the received Omega signals will be relayed to the control center and the aircraft position can be located only on the basis of the Omega signals. If this mode of operation were to be adopted, the satellite range measurement would be redundant and could be used to increase the reliability and improve the accuracy of the overall system.

In PLACE, the mode of operation described above has not been adopted as the primary mode. Instead two separate provisions for ambiguity resolution have been included to make the system independent of the Omega network so that any suitably located VLF source of adequate frequency stability can be used.

The primary mode for resolving the ambiguity of the VLF range measurement depends on the continuous tracking feature of PLACE. Consider a system wherein only the fine resolution tone is used for position fixing. As long as a

continuous plot of the movement of each aircraft is made as the aircraft proceeds away from its known initial departure point, no ambiguity will exist. This continuous plot can be accomplished by a technique commonly called lane counting. Ambiguous concentric equiphase circles of position separated by the wavelength of the ground transmitter will exist, since the measured phase delay will repeat for every range increase equal to a wave length at the transmitted frequency. Any given phase difference can be used to define lanes, with the region between two adjacent equal phase difference lines being called a lane. Lane counting can be accomplished by assigning a number to each such lane. As an aircraft crosses a given phase difference line the count in a counter, located at the ground station, can be automatically increased or decreased depending on the direction of motion. In the event that the measured phase should erroneously advance or retard by one or more full periods (because of loss of signal due to aircraft maneuvers, equipment errors, or noisy environments) errors in the position fix will occur. Since an aircraft may be moving as rapidly as 0.5 mile per second, and the smallest lane widths are approximately 16 n miles, momentary outages on the order of a few seconds might be tolerated. An estimate of the likelihood that the measured phase might erroneously advance or retard by one or more full periods due to fluctuation noise or aircraft maneuvers is derived in 3.3 where it is shown that very acceptable performance should be possible.

2.2.6 Ambiguity Resolution By SIND

For the purpose of increasing the overall reliability of aircraft surveillance, a second method of ambiguity resolution will be implemented in PLACE. This subsystem, designated SIND for Satellite Inertial Navigation Determination, requires only four parameters to completely derive the aircraft position: aircraft altitude; aircraft velocity vector; range and range rate between the aircraft and the satellite. The aircraft-to-satellite range rate is derived from a doppler measurement on the carrier component of the signal received from each aircraft. The velocity vector is obtained from aircraft installed accelerometers whose outputs are telemetered to the Primary Control Center where velocity is computed. These sensors can be independent of any on-board inertial navigation equipments since neither a torqued platform nor on-board integration is required. Basically the SIND performs a position fix from the concept that there are only two possible aircraft locations on the circle of position (defined by the satellite-to-aircraft range) where the component of the aircraft velocity vector in the direction of the satellite will equal the measured aircraft-to-satellite velocity.

Consider the system geometry shown in Figure 2-18 which includes: a spherical coordinate system with origin at the center of the earth; a geo-stationary

SPECIFICATION OF LINE OF POSITION FROM ALTITUDE AND RANGE TO SATELLITE - LOP PROJECTS AS A CIRCLE ON SPHERE.

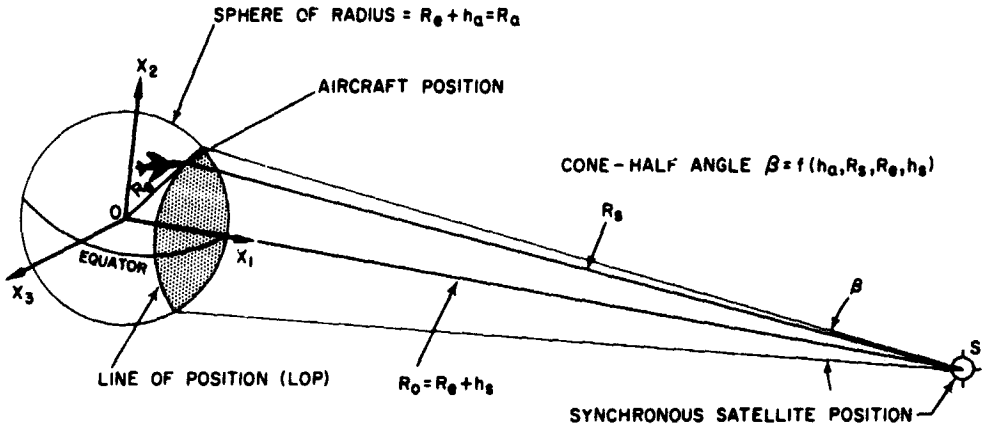

Figure 2-18-Geometry of SIND System

satellite, S; and an aircraft positioned on a spherical surface concentric with the earth. For simplicity, the earth may be assumed spherical. The distance from the center of the earth to the satellite is given by $R_o = R_e + h_s$, where R_e is the radius of the earth and h_s is the altitude of the satellite.

The distance from the center of the earth to the aircraft is denoted by $R_a = R_e + h_a$ where R_e is the radius of the earth and h_a is the aircraft altitude. Thus, R_a is the radius of a "sphere of position" on which the aircraft is located.

The distance between the aircraft and the satellite is represented by R_s. The locus of points on the surface of the "sphere of position" separated from the satellite by a distance R_s describes a circle which is the base of a cone with apex at the geo-stationary satellite position S, and apex angle β. The described circle, which is the intersection of the conical surface with the surface of the "sphere of position," is a circular line of position on which the aircraft is located.

If the satellite is assumed as specifying a Greenwich meridian, the sub-satellite point would be located on the equator at the Greenwich meridian. Thus, the satellite azimuth angle and the elevation angle are both zero. The aircraft azimuth angle and elevation angle are ϕ and θ, respectively.

Employing the rectangular coordinate system shown with the unit vectors $\bar{i}$, $\bar{j}$, and $\bar{k}$, the range vector $\bar{r}_s$, from the satellite to the aircraft is given by.

$$\bar{r}_s = \bar{r}_a - \bar{r}_o$$

or

$$\bar{r}_s = [r_a \cos\theta \cos\phi - r_o]\,\bar{i} + [r_a \cos\theta \sin\phi]\,\bar{j} + [r_a \sin\theta]\,\bar{k}. \qquad (1)$$

Let $r_s = |\bar{r}_s|$, the absolute value of the range vector. Let the aircraft velocity over the surface of the earth be represented by:

$$\bar{V} = V_x\,\bar{i} + V_y\,\bar{j} + V_z\,\bar{k}.$$

Since the satellite is assumed stationary with respect to the surface of the earth, range rate $\dot{r}_s$, between the satellite and the aircraft is obtained by taking the dot product of aircraft true airspeed $\bar{V}$, and the normalized satellite to aircraft range vector $\bar{r}_s$.

Thus, range rate $\dot{r}$, is given by

$$\dot{r}_s = \frac{\bar{r} \cdot \bar{V}}{r_s},$$

or

$$\dot{r}_s = \frac{1}{r_s}\left[[r_a \cos\theta \cos\phi - r_o]\,V_x + [r_a \cos\theta \sin\phi]\,V_y + [r_a \sin\theta]\,V_z\right]. \qquad (2)$$

Symbol	Quantity	Value Determined from
r	Range Satellite to Aircraft	Measured
$\dot{r}$	Range Rate Satellite to Aircraft	Measured
V_x	Component Aircraft Velocity	Aircraft Accelerometer
V_y	Component Aircraft Velocity	Aircraft Accelerometer
V_z	Component Aircraft Velocity	Aircraft Accelerometer
r_a	Distance from Center of Earth to Aircraft	Aircraft Altimeter and Earth Radius
r_o	Distance from Center of Earth to Satellite	Satellite Altitude and Earth Radius
$\emptyset$	Aircraft Azimuth Angle with Respect to Fixed Meridian Described by Synchronous Satellite	Simultaneous Solution of Equations (1) and (2)
θ	Aircraft Elevation Angle with Respect to Equator	Simultaneous Solution of Equations (1) and (2)

Figure 2-19–Tabulation of Known and Unknown SIND Quantities

Equations (1) and (2) constitute the system mathematical model consisting of two expressions in two unknowns for range and range rate between the satellite and the aircraft. The unknown quantities are the aircraft azimuth angle ϕ, and elevation angle θ. All other quantities are known or can be determined in any real situation. Figure 2-19 lists these known and unknown quantities and the sources from which actual values can be determined. Range and range-rate errors resulting from atmospheric effects are considered in Appendix A, while an error analysis of the SIND system is given in Appendix C.

2.2.7 Aircraft Transceiver

A functional block diagram of the aircraft transceiver is shown in Figure 2-20. The frequency control section of the transceiver has already been discussed; so that, the portion of primary concern, at this point, are those having to do with the tone processing. There are three district tone paths corresponding to the three possible modes of operation. First, the tones received from the satellite, by the L-Band receiver, are separated out by the 3-7 KHz bandpass filter and coherently transponded through the transmitter to the Central

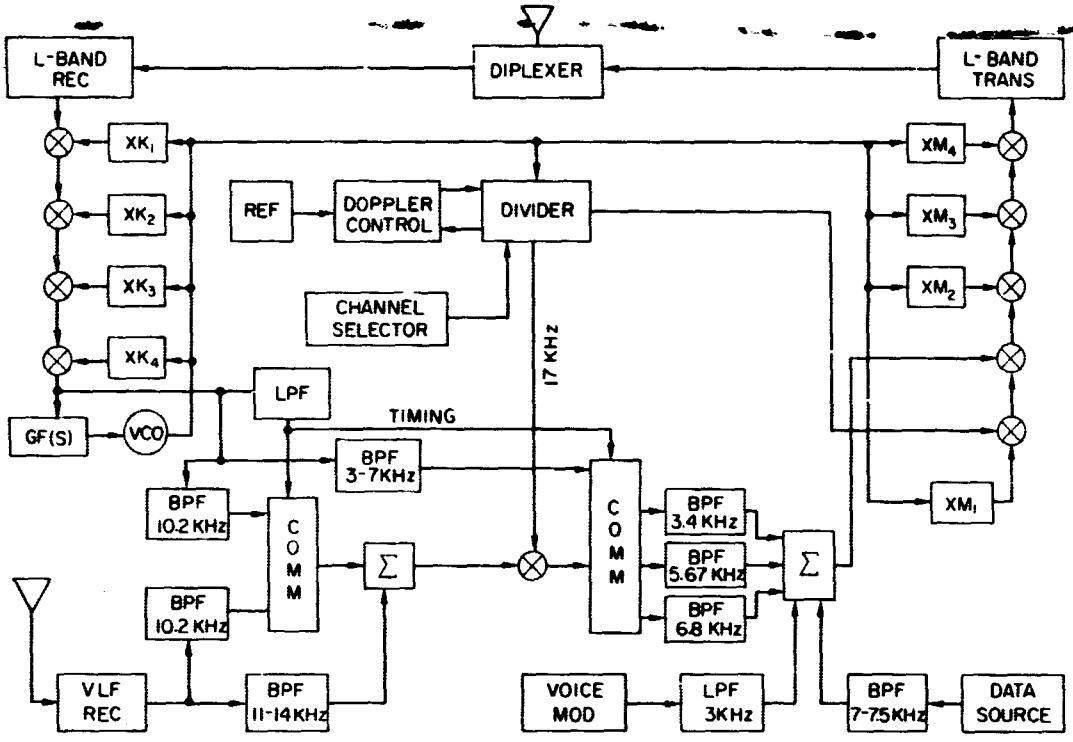

Figure 2-20–Functional Diagram of Aircraft Transceiver

Control. This operation permits the measurement of the ground-to-satellite-to-aircraft two-way range.

A second path exists, with the VLF receiver serving as the source of tones. Figure 2-20 has been drawn so that the transceiver will be compatible with Omega in this mode of operation. If the output of the 10.2 KHz filter is connected through the commutator to the summer in Figure 2-20, then the output of the VLF receiver will be relayed to the Control Center. In this mode, the position of the aircraft can be determined using only the inverse hyperbolic geometry of Omega.

If the VLF transmissions are to be used in the range mode, a third signal path has been provided. The output of the 10.2 k Hz filter from the L-Band receiver is time commutated with the output of the VLF receiver. If Omega stations are being used, this tone will be inserted during time intervals when the four least useful Omega transmitters are radiating. The purpose of this tone is to provide an absolute reference for the VLF tones so that range as well as range-differences can be measured. The relative phase and time delay relationships of importance to the system are listed in Figure 2-21.

Aircraft Receiver	Frequency as Received		Delay	Relative Phase Delay at Aircraft	Frequency as Transmitted		Return Delay (app.)	Total Delay	Relative Phase Delay as Received Primary Control Center
	Nomenclature	KHz			Nomenclature	Hz			
L BAND	ω_{2L}	3.4	τ_1	θ_{R_2}	ω_{2L}	3.4	τ_1	$2\tau_1$	$2\theta_{R_2}$
	$\omega_{3L}-\omega_{1L}$	5.6	τ_1	$\theta_{R_3}-\theta_{R_1}$	$\omega_{3L}-\omega_{1L}$	5.6	τ_1	$2\tau_1$	$2(\theta_{R_3}-\theta_{R_1})$
	ω_{3L}	6.8	τ_1	θ_{R_3}	ω_{3L}	6.8	τ_1	$2\tau_1$	$2\theta_{R_3}$
	$\omega_{3L}+\omega_{2L}$	10.2	τ_1	$\theta_a-(\theta_{R_3}+\theta_{R_2})$	$\omega_0-(\omega_{3L}+\omega_{2L})$	6.8	$\tau_1+\tau_a$	$2\tau_1+\tau_a$	$\theta_a-\theta_{R_2}$
VLF	$\omega_{3v}+\omega_{2v}$	10.2	τ_2	$\theta_a-(\theta_{\Omega_3}+\theta_{\Omega_2})$	$\omega_0-(\omega_{3v}+\omega_{2v})$	6.8	$\tau_1+\tau_a$	$\tau_1+\tau_2+\tau_a$	$\theta_a+\theta_{R_3}-(\theta_{\Omega_3}+\theta_{\Omega_2})$
	$\omega_{2v}+\omega_{2v}+\omega_{1v}$	11.3	τ_2	$\theta_c-(\theta_{\Omega_3}+\theta_{\Omega_2}+\theta_{\Omega_1})$	$\omega_0-(\omega_{3v}+\omega_{2v}+\omega_{1v})$	5.6	$\tau_1+\tau_a$	$\tau_1+\tau_2+\tau_a$	$\theta_a+(\theta_{R_3}-\theta_{R_1})-(\theta_{\Omega_3}+\theta_{\Omega_2}+\theta_{\Omega_1})$
	$2\omega_{3v}$	13.6	τ_2	$\theta_a-(2\theta_{\Omega_3})$	$\omega_0-(2\omega_{3v})$	3.4	$\tau_1+\tau_a$	$\tau_1+\tau_2+\tau_a$	$\theta_a+\theta_{R_1}-(2\theta_{\Omega_3})$

Figure 2-21 - Relative Phase of Ranging Tones

Referring to Figure 2-21, the use of the reference tone becomes apparent. In particular, the total delays for the 6.8 k Hz and the 10.2 k Hz (ω_{3L} and $\omega_{3L} + \omega_{2L}$ respectively) should be noted. These tones together provide a means for determining the arbitrary delay, τ_a, introduced by the frequency conversion process in the transceiver.

3. PERFORMANCE ANALYSES

3.1 Communication Link Power Budgets

Consideration of the PLACE communication links will begin with the satellite-to-aircraft link since this is the critical link of the system which determines many of the other design choices. To begin, the power budget for this link is given in Figure 3-1. As previously stated, the output power of the satellite L-Band transmitter is established by the constraints of presently programmed ATS spacecraft. For example, the primary power available with the ATS-C type of spacecraft is 185 watts which must be de-rated to approximately 165 watts of useful power. The telemetry and spacecraft control systems require 30 watts of power and it should be assumed that other on-board experiments (including other PLACE equipments) will require at least an additional 55 watts. Thus, about 80 watts of input power is a reasonable assumption for the transmitter which, with an efficiency of 50 percent results in 40 watts for the transmitter output power. In the present stage of planning for the ATS F and G spacecraft, it is reasonable to state that the transmitter output power that can be provided will not be very much different from the assumed 40 watts.

The satellite antenna gain at L-band is determined by the requirement for nearly earth disc coverage; although for experimental purposes it is possible to form a somewhat more directive beam without serious penalty. The synchronous satellite-earth geometry establishes the beamwidth, and hence gain, of this antenna independent of the choice of operating frequency. In the case of the ATS-C class of spacecraft, the assumed gain of this antenna is realizable; whereas in the case of the ATS F and G class of spacecraft, considerably greater gain could be provided. However, the requirement for nearly earth disc coverage obviates the use of the full potential of the ATS F and G antenna.

The path loss given in Figure 3-1 is of course determined by the choice of the operating frequency (1500 MHz) as well as the satellite-to-earth geometry. For communication purposes alone, the 136 MHz (VHF) frequency region is a more desirable choice. However, as shown in Appendix A, the range and range-rate errors introduced by propagation through the ionosphere preclude adequate position-location accuracies in this frequency range. Tropospheric errors are

Satellite To Aircraft – Down Link (freq. = 1500 MHz)			
	Nominal Value	Worst-Case Value	Units
Transmitter			
Output Power	40	40	watts
	16.0	16.0	dbw
Coupling Loss	-1.0	-1.5	db
Antenna Gain	22.0	19.0	db
Effective Radiated Power	37.0	33.5	dbw
Path Loss	-187.0	-188.3	db
Dispersion Margin	—	-3.0	db
Receiver			
Antenna Gain	25	24.0	db
Coupling Loss	-1.0	-1.5	db
Thermal Noise Power Density	-204.0	-204.0	dbw/Hz
Effective Noise Temperature	5.0	5.0	db
Receiver Noise Power Density	-199.0	-199.0	dbw/Hz
Received Carrier Power	-126.0	-135.3	dbw
Carrier/Noise Power Density	73.0 max.	63.7 min.	db/Hz
Carrier/Noise Power Into Channel Demod.	16.4 max.	7.1 min.	db
Demod. Threshold	6.0	6.0	db
System Margin	10.4 max.	1.1 min.	db

Figure 3-1–Satellite-to-Aircraft Power Budget

essentially independent of frequency while ionospheric errors decrease with frequency. In the region of 500 MHz, the separate errors introduced by both effects can be expected to be of the same order of magnitude. For position-location purposes then, a choice of operating frequency above 500 MHz is essential. In PLACE, the L-Band was chosen specifically because of the aeronautical services frequency assignment in this band.

The aircraft antenna gain of 25 db listed in Figure 3-1 was chosen to compensate for the path loss difference between 136 MHz and 1500 MHz if it is assumed that the aircraft were to employ a nominal 3 db gain antenna at 136 MHz. In this way, no penalty is imposed in the communication link by the choice of L-band operation. However, the development of the required aircraft antenna is a considerable problem.

Figure 3-1 shows the nominal carrier-to-noise power density received at the aircraft to be 73 db/Hz. Additional calculations pertaining to this link are given in Figure 3-2 where the essential portions of the aircraft receiver are shown. In this figure, (1) makes use of (3) derived in 3.2. Equation (2) is a standard relationship which can be easily derived from frequency demodulation analysis and Figure 3-3 has been included to assist in its interpretation. The main demodulator relationship used in (5) is based on results given in Appendix B. Figure 3-4 pertains to the threshold characteristics of the Channel Demodulators and this figure was derived from the results given in References (6) and (7). The remaining link power budgets are shown in Figures 3-5 through 3-7.

3.2 Signal Pre-emphasis

The power spectrum of a voice signal is primarily concentrated in the frequency range below 1000 Hz, but the spectral content up to at least 2500 Hz is essential for intelligibility. Typical airborne specifications for a voice channel require a passband from 350 to 2500 Hz with an overall frequency response flat within 6 db of that at 1000 Hz. The power spectrum produced by a male speaker is anything but uniform over this range however. Instead, the power spectrum will more normally drop off at something close to 6 db per octave for frequencies above 1000 Hz. Advantage can be taken of this fact, through pre-emphasis prior to modulation and de-emphasis following demodulation, to improve the operating signal-to-noise ratio while still maintaining a nearly flat overall response. Additional gains are possible through certain non-linear signal processing techniques such as amplitude clipping, but such operations quickly get into subjective questions having to do with operational tradeoffs. Due to difficulties in establishing fidelity criteria and in estimating resulting improvements, such techniques have not been considered in the PLACE design. Instead, any such potential improvements which can be incorporated will add directly to the overall system performance.

The high-frequency components of each voice signal will be emphasized at the ground station by means of a simple linear network. The aircraft receiver will perform a complementary operation to restore the original power spectral shape by de-emphasizing the high-frequency components by means of another simple linear network. The received noise enters the system after the

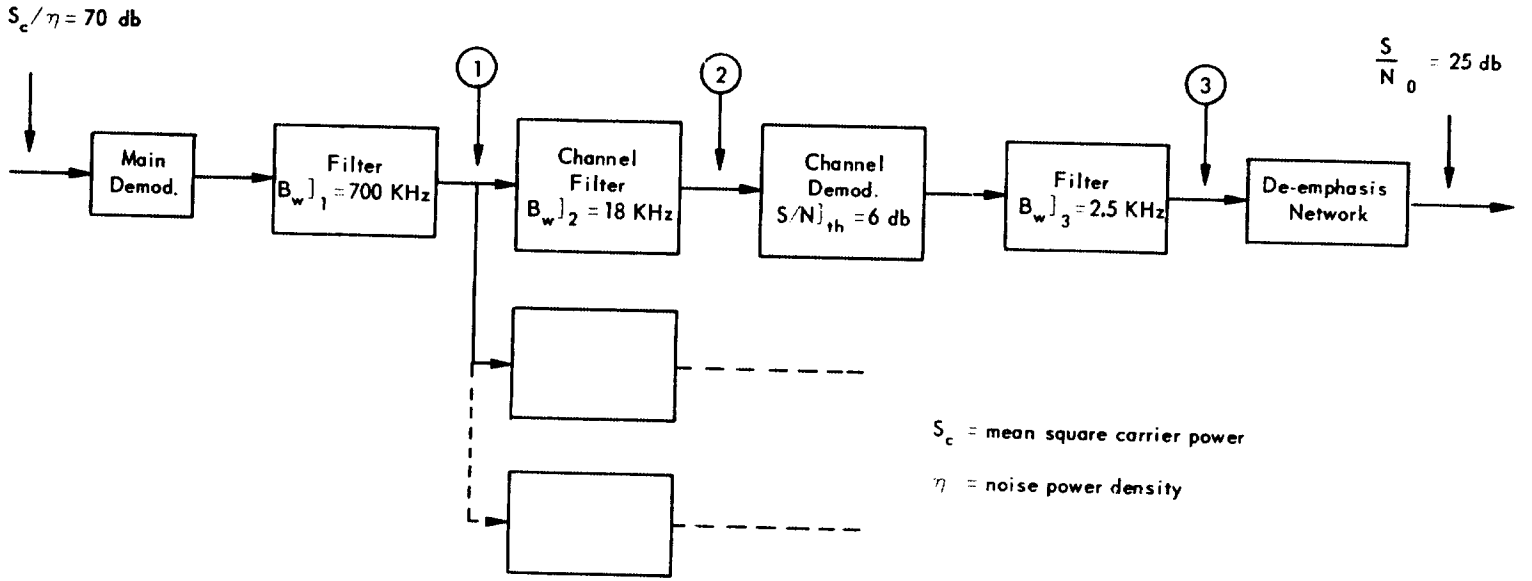

Figure 3-2(a)–Aircraft Receiver P rformance

De-emphasis Network

$$\left[\frac{S}{N}\right]_0 = \frac{1}{3}\left(\frac{f_u}{f_1}\right)^2 \left[\frac{S}{N}\right]_3 \qquad (1)$$

where;

f_1 = break frequency of de-emphasis network = 1 KHz

f_u = upper frequency limit of voice channel = 2.75 KHz

$$\left[\frac{S}{N}\right]_3 = \left[\frac{S}{N}\right]_0 - 10 \log \frac{1}{3}\left(\frac{f_u}{f_1}\right)^2 \text{ db}$$

$$= 25.0 - 4.0 = 21 \text{ db}$$

Channel Demodulation

$$\left[\frac{S}{N}\right]_3 = \frac{3}{2} \frac{(\Delta f_u)^2 B_2}{(f_u^3 - f_L^3)} \left[\frac{S_c}{N}\right]_2 \qquad (2)$$

where;

Δf_e = effective peak frequency device

f_2 = lower frequency limit of voice channel = 250 Hz

$S_c = A_s^2/2$ = rms carrier power

$$\frac{3}{2} \frac{(\Delta f_e)^2 B_2}{(f_u^3 - f_L^3)} = 31.6 \longleftarrow (21 - 6) = 15 \text{ db} \qquad (3)$$

Using the relation $B_2 = 2 f_u (\alpha + 1) = 2 (\Delta f_e + f_u)$, (3) becomes (4)

$$\frac{3 (\Delta f_e)^2 (\Delta f_e + f_u)}{f_u^3 - f_L^3}$$

where; $f_u^3 = (2750)^3$, $f_L^3 = (250)^3$ $\Rightarrow$ $f_u^3 - f_L^3 = 20.9 \times 10^9$

Dividing (3) by f_u^2 and substituting $\alpha^2 = (\Delta f_e / f_u)^2$, the result is $\alpha^2 (\alpha + 1) = 10.5$

Solution for α provides $\alpha = 2$

$\therefore B_2 = 2(2750)(2 + 1) = 16.5$ KHz

Take $B_2 = 17.0$ KHz

Main Demodulation

$$\left[\frac{S_c}{N}\right]_1 = \frac{2 \delta^2 S_c}{2 \eta B_1 \exp \delta^2} \qquad (5)$$

where; δ^2 = mean square phase deviation = 1 rad^2

B_1 = 700 KHz

$$= \frac{1}{B_1 e} \cdot \frac{S_c}{\eta} \longrightarrow \begin{cases} 73.0 - 10 \log e B_1 = 10.2 \text{ db – nom.} \\ 63.7 - 10 \log e B_1 = 0.9 \text{ db – min.} \end{cases}$$

Channel Filter

$$\left[\frac{S_c}{N}\right]_2 = \frac{B_1}{10 B_2} \left[\frac{S_c}{N}\right]_1 \longrightarrow \begin{cases} 10.2 + 10 \log \frac{700}{10.17} = 16.4 \text{ db – nom.} \\ 0.9 + 10 \log \frac{700}{10.17} = 7.1 \text{ db – min.} \end{cases}$$

Margin

$$\left[\frac{S_c}{N}\right]_{2\,(max)} - \left[\frac{S_c}{N}\right]_{2\,(Thresh)} = (16.4 - 6.0) \text{ db} = 10.4 \text{ db – nom.}$$

$$\left[\frac{S_c}{N}\right]_{2\,(min)} - \left[\frac{S_c}{N}\right]_{2\,(Thresh)} = (7.1 - 6.0) \text{ db} = 1.1 \text{ db – min.}$$

Figure 3-2(b)–Aircraft Receiver Performance

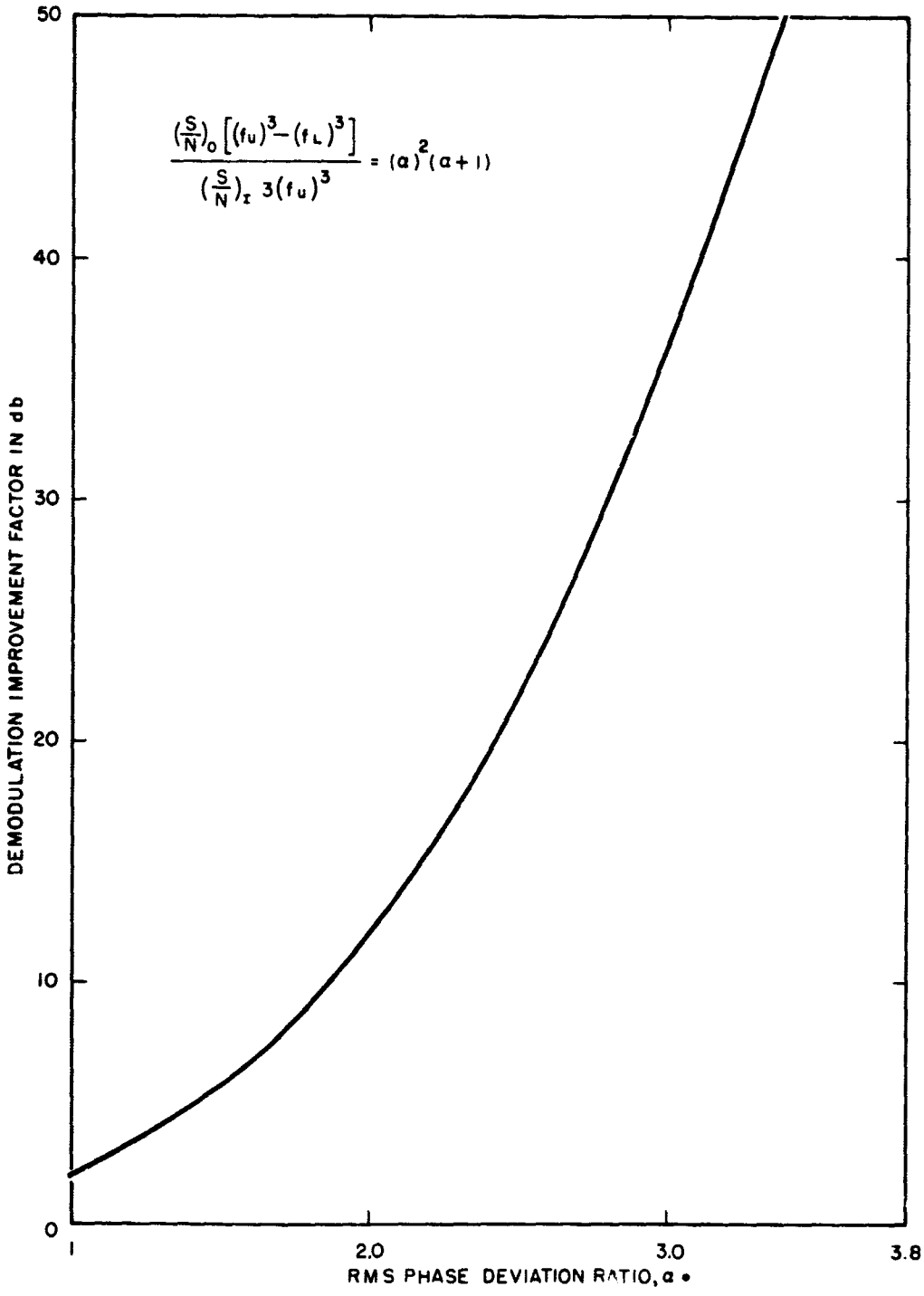

Figure 3-3–Pertaining to Aircraft Demodulator

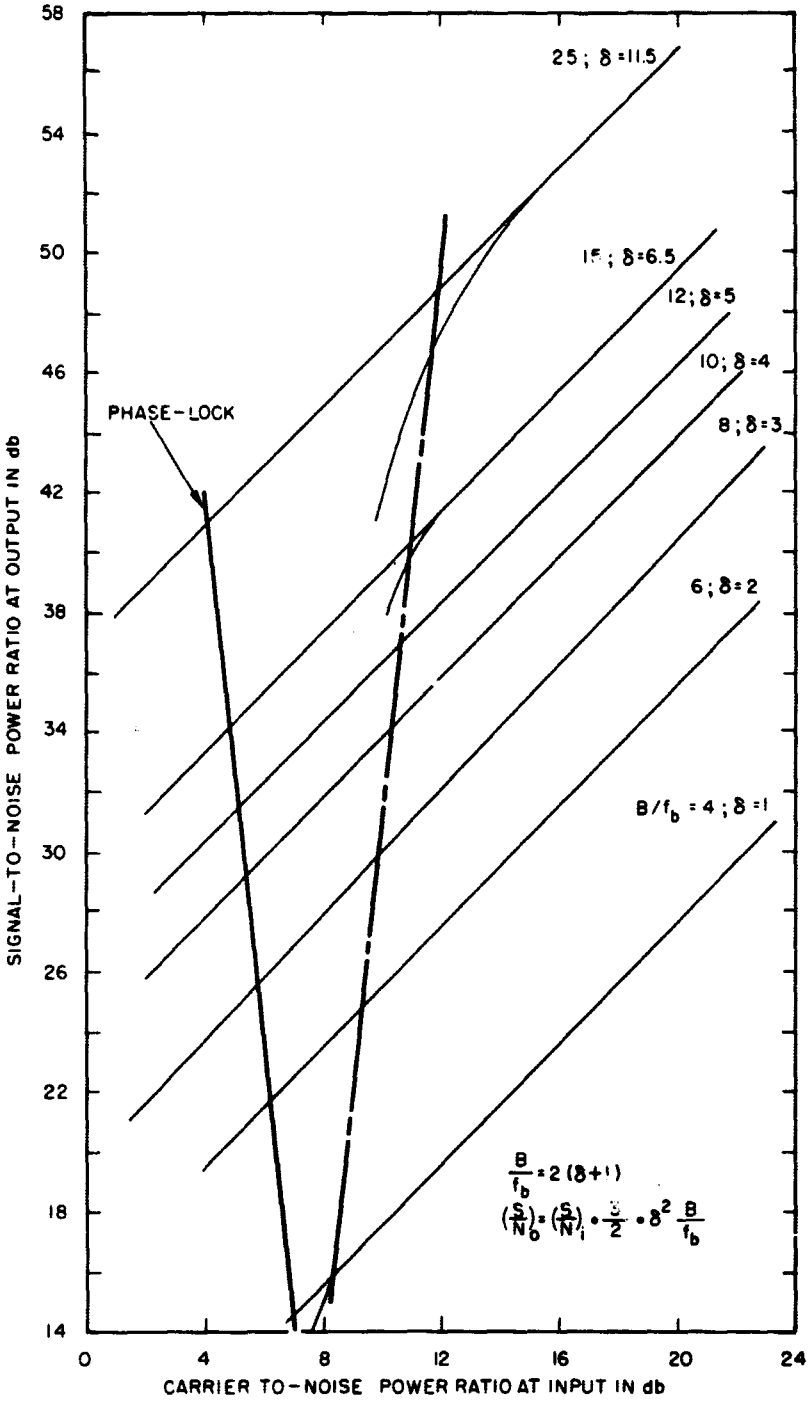

Figure 3-4–Demodulator Threshold Characteristics

Aircraft To Satellite – Up Link (freq. = 1500 MHz)		
	Value	Units
Transmitter		
Output Power	50	watts
	17.0	dbw
Antenna Gain	25.0	db
Coupling Loss	-3.0	db
Pointing Loss	-1.0	db
Effective Radiated Power	38.0	dbw
Path Loss	-189.0	db
Dispersion Margin	-3.0	db
Receiver		
Antenna Gain	22.0	db
Coupling Loss	-2.0	db
Pointing Loss	-3.0	db
Received Signal Power	-131.0	dbw
Thermal Noise Power Density	-204.0	dbw/Hz
Effective Noise Temperature	5.5	db
Channel Bandwidth	40.0	db
Received Noise Power	-158.5	dbw
Signal To Noise Ratio per Channel	27.5	db

Figure 3-5–Aircraft-to-Satellite Power Budget

Satellite To Ground – Down Link (freq. = 5 GHz)		
	Value	Units
Transmitter		
Output Power	4	watts
	6.0	dbw
Antenna Gain	32.0	db
Coupling Loss	-2.0	db
Pointing Loss	-1.0	db
Effective Radiated Power	35.0	dbw
Path Loss	-198.0	db
Receiver		
Antenna Gain	60.0	db
Coupl ıg Loss	-1.5	db
Received Carrier Power	-104.5	dbw
Thermal Noise Power Density	-204.0	dbw/Hz
Effective Noise Temperature	4.0	db
Receiver Bandwidth	68.5	db
Received Noise Power	- 131.5	dbw
Carrier-to-Noise Ratio	27.0	db
Signal-to-Noise Ratio Out	30.0	db

Figure 3-6–Satellite-to-Ground Power Budget

Ground To Satellite – Up Link (freq. = 5 GHz)		
	Value	Units
Transmitter		
Output Power	100	watts
	20	dbw
Antenna Gain	60	db
Coupling Loss	-5	db
Effective Radiated Power	75	dbw
Path Loss	-198	db
Receiver		
Antenna Gain	32.0	db
Coupling Loss	-3.0	db
Received Signal Power	-94.0	dbw
Thermal Noise Power Density	-204.0	dbw/Hz
Effective Noise Temperature	8.0	db
Channel Bandwidth	43.0	db
Received Noise Power	-153.0	dbw
Signal-To-Noise Ratio per Channel	59.0	db

Figure 3-7–Ground-to-Satellite Power Budget

pre-emphasis but before the de-emphasis network and therefore the high-frequency components of the noise will be reduced as will the total noise power. The procedure is a matter of capitalizing on differences in the characteristics of the signal and noise spectral distributions to provide an actual improvement in the received signal-to-noise ratio.

The pre-emphasis network that will be used can be described by a simple frequency transfer function given by

$$H_1(s) = \frac{s + \omega_1}{s + \omega_2}, \tag{1}$$

where $\omega_1 = 1/R_1C$ and $\omega_2 = R_1 + R_2/R_1R_2C$. The corresponding circuit and asymptotic logarithmic amplitude plot is shown in Figure 3-8. The choice for ω_1 is based on the assumption that a typical voice power spectrum will decrease at the rate of approximately 6 db per octave for frequencies above 1 KHz. Whereas ω_2 is simply chosen to be well beyond the maximum modulating signal frequency – say 6 KHz. Thus, the circuit performs as a single pole, high-pass network with a break frequency at 1 KHz.

The receiver de-emphasis network, following the discriminator must have the inverse characteristic

$$H_2(s) = \frac{\omega_1}{s + \omega_1}, \tag{2}$$

which serves to restore the signal spectrum to its original relative values when ω_1 has the same value in (2) as it does in (1) above. The required circuit is shown in Figure 3-8 along with the asymptotic logarithmic amplitude plot.

From standard angle-modulation noise analysis, the two-sided spectral density for the noise at the output of a frequency demodulator is given by

$$w(f) = \frac{b^2 \eta f^2}{2S_c}, \tag{3}$$

where b is the demodulator transfer constant, η is the input noise spectral density, and $S_c = A_c^2/2$ is the mean carrier power. If the noise is now passed through the de-emphasis network of (2), the modified spectral density is

$$w'(f) = w(f) \cdot |H_2(j\omega')|^2. \tag{4}$$

From (2)

$$|H_2(j\omega')|^2 = \frac{1}{1 + (f/f_1)^2},$$

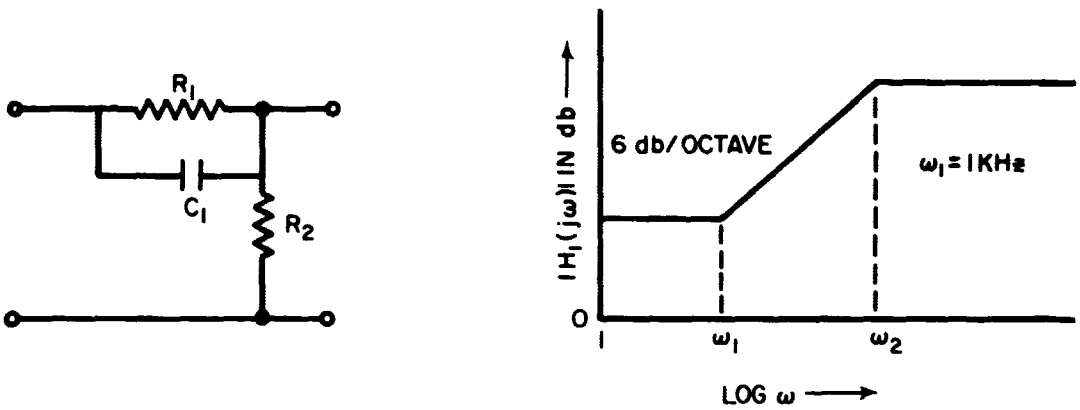

a. PRE-EMPHASIS NETWORK AND CORRESPONDING ASYMPTOTIC AMPLITUDE PLOT

b. DE-EMPHASIS NETWORK AND CORRESPONDING ASYMPTOTIC AMPLITUDE PLOT

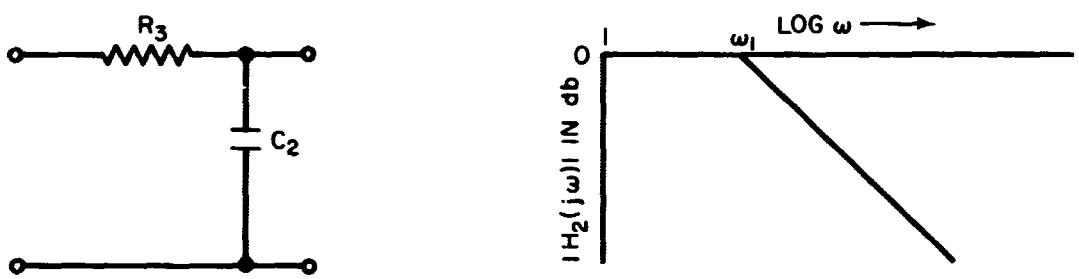

Figure 3-8–Circuit Diagrams and Transfer Plots Pertaining to Signal Pre-emphasis

so that (4) becomes

$$w'(f) = \frac{b^2 \eta f^2}{2S_c} \cdot \frac{1}{1 + (f/f_1)^2} . \qquad (5)$$

The total noise power at the output of the de-emphasis network is

$$w_0 = 2 \int_0^{fm} w'(f)\, df$$

$$\approx \frac{b^2\eta}{S_c} \left[\int_0^{f_1} f^2 df + \int_{f_1}^{f_m} f_1^2 df \right]. \tag{6}$$

For $f_m = 3$ KHz and $f_1 = 1$ KHz, (6) has the approximate value of

$$w_0 \approx f_1^2 f_m b^2\eta / S_c .$$

Without de-emphasis, the output noise power, w_0', is

$$w_0' = \frac{b^2\eta}{S_c} \int_0^{fm} f^2 df = \frac{b^2\eta}{3S_c} f_m^3 ,$$

so that the output noise is reduced by the factor

$$F = \frac{w_0'}{w_0} = \frac{1}{3} \left(\frac{f_m}{f_1} \right)^2 . \tag{7}$$

3.3 Phase Tracking Analysis

The purpose of the analysis which follows is to provide quantitative estimates of the performance characteristics that can be provided by the VLF ranging method presented in previous sections. The approach used here is based on a phase-locked tracking filter. It is not expected that such a tracking filter will be used in any final design primarily because of the equipment complexity that would be involved with a large number of tracking filters. Instead, it is expected that a single high-speed computer will be utilized to simultaneously track all of the aircraft. In addition, the computer processing can be optimized to generate maximum likelihood estimates and to take advantage of several other factors

which are ignored in the following analysis. Nonetheless, confidence can be gained in the reliability that can ultimately be achieved through the relatively simple analysis which follows.

The basic tracking filter system to be considered is shown in Figure 3-9. The output of the system is taken from the voltage-controlled oscillator (VCO) which is fed by the closed feed-back loop so as to follow the variations in frequency and phase of the input signal $e_1(t)$. The input signal is taken to be represented by

$$e_1(t) = \sqrt{2}\, V_s \sin [\omega_0 t + \theta_1(t)]. \tag{1}$$

The phase of the input signal can be resolved into two components: (1) a uniformly increasing function of time and (2) a phase function which depends on the motion of the aircraft relative to the VLF transmitter.

The VCO output has a sinusoidal form described by

$$e_0(t) = \sqrt{2}\, V_1 \sin [\omega_0 t + \theta_2(t)]. \tag{2}$$

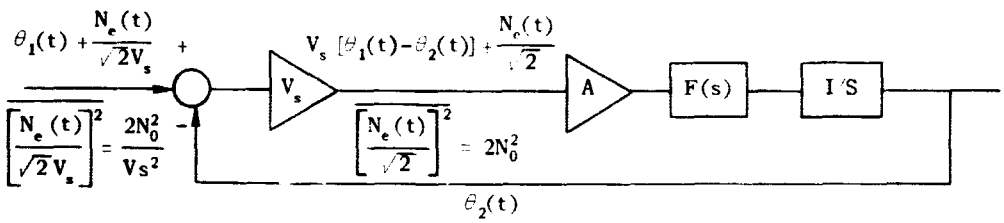

a. Linearized equivalent diagram of a phase-lock loop.

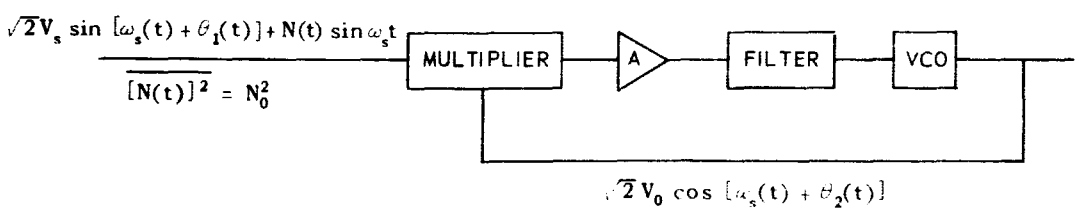

b. Typical phase-lock loop with which (a) is associated.

Figure 3-9–Equivalent Phase-Lock Loop Diagram

In the locked condition, the output phase $\theta_2(t)$, must differ from the input phase $\theta_1(t)$, by $\pi/2$ plus some, integral multiple of 2π, within a small error angle $\epsilon(t)$ which depends on the forward gain of the loop. That is,

$$\theta_1(t) - \theta_2(t) = \theta_E(t) = \frac{\eta}{2}(4\eta + 1) \pm \epsilon(t).$$

For the loop to remain in lock, it is necessary that the instantaneous error be constrained to remain within some range of values say $\pm\epsilon_m$. Ignoring the steady-state frequency and phase offset, this condition becomes

$$|\theta_E(t)| = |\theta_1(t) - \theta_2(t)| \leq \epsilon_m. \tag{3}$$

For the idealized linearized case, a value for $\pm\epsilon_m$ of $\pm\pi/2$ is the limit of lock since an error in excess of this results in a change in sign of the open loop gain and the VCO is driven in the opposite direction from lock.

The input signal also includes additive narrow band noise of bandwidth Δf which can be represented as $N(t) \sin \omega_{st}$, as is indicated in Figure 3-9b. It is assumed that the noise has a uniformly distributed spectral density of $No^2/\Delta f$. Also, the effective closed loop bandwidth is taken to be small compared with Δf so that the VCO output which is multiplied with the input can be considered to be noise free and the multiplier to act as a synchronous detector. The output of the multiplier (neglecting higher order terms) is

$$\frac{V_E}{V_s} = [\theta_1(t) - \theta_2(t)] + \frac{N_E(t)}{\sqrt{2}V_s},$$

where $N_E(t)/\sqrt{2} = \sqrt{2}N(t)$ has been substituted to account for the doubling of the noise power at the output of the multiplier. Since the actual input noise power is $(No)^2$, the noise power at the point between the amplifiers is $2(No)^2$ so that the effective input noise power is $2(No)^2/(V_s)^2$ with a double sided spectral density of $w = (No^2/V_s^2)\Delta f$.

The mean-squared phase jitter, or noise power σ_n^2 at the output due to noise power at the input is determined by the usual contour integral,

$$\sigma_n^2 = \frac{1}{2\pi j}\int_{-j\infty}^{j\infty} |Y_L(s)|^2 w_n ds = 2w_n B_L \text{ rad}^2, \tag{4}$$

where B_L is the loop bandwidth. The variance of $\theta_2(t)$ is the variance of $\theta_1(t) - \theta_2(t)$ due to noise while the mean of $\theta_1(t) - \theta_2(t)$ is the error in $\theta_2(t)$ from the desired value $\theta_1(t)$. Should the output deviate from the input by more than $\pm \epsilon_m$, loss of lock will occur. The probability of $\theta_2(t)$ exceeding $\pm\epsilon_m$ can be calculated from

$$P = \Phi\left[-\frac{\epsilon_m}{\sigma_n}\left(1 - \frac{2\theta_E}{\pi}\right)\right] + \Phi\left[-\frac{\epsilon_m}{\sigma_n}\left(1 + \frac{2\theta_E}{\pi}\right)\right], \tag{5}$$

where $\Phi(-v)$ is the commulative distribution function

$$\Phi(-v) = \sqrt{\frac{2}{\pi}} \int_{-\infty}^{-v} \exp\left(\frac{-x^2}{2}\right) dx.$$

When the transient error, θ_E, is zero, the probability of losing lock reduces to

$$P_0 = 2\Phi(-\epsilon_m/\sigma_n) = \sqrt{\frac{2}{\pi}} \int_{-\infty}^{-\epsilon_m/\sigma_n} \exp\left(-\frac{X^2}{2}\right) dx. \tag{6}$$

In (5) and (6),

$$\sigma_n^2 = 2(N_0^2 B_L/V_s)\,\Delta f$$

is the normalized noise power at the output of the tracking loop. A plot of (6) is shown in Figure 3-10 with the probability of losing lock as a function of the signal to noise ratio for $\epsilon_m = \pi/2$ and 1 radian with zero transient error.

From this figure, the anticipated time before loss of lock can be inferred. For example, for $\epsilon_m = \pi/2$, a tracking bandwidth of 0.1 Hz, and a loop signal to noise ratio of 11 db, the expected times between loss of lock should be about 280 hours. The loop transient errors that can result even in the absence of noise will now be considered.

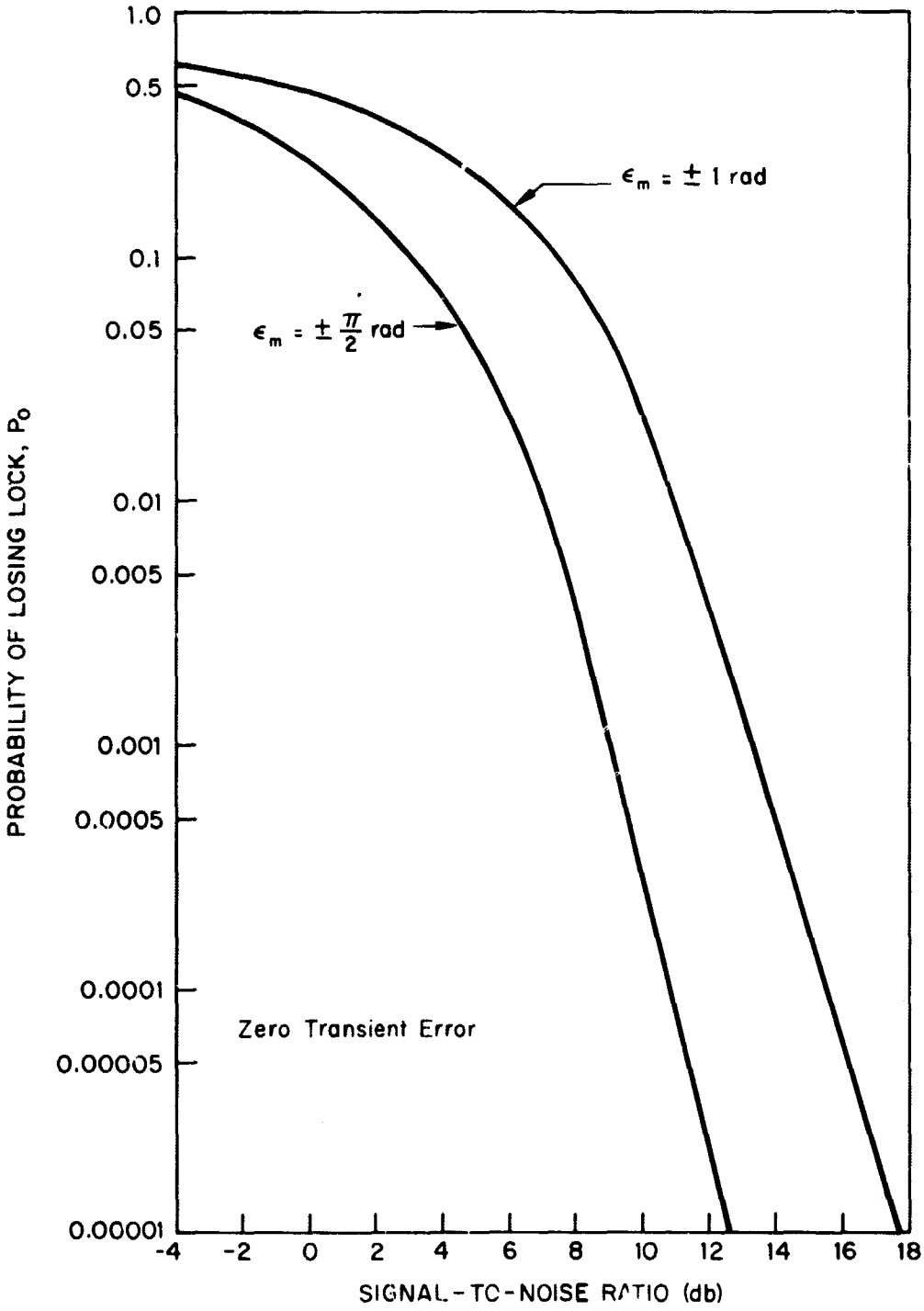

Figure 3-10–Probability of Losing Lock vs Signal-to-Noise Ratio

For this purpose, it is necessary to again refer to the linearized equivalent phase lock loop shown in Figure 3-9 for which the following error function applies,

$$Y_E(s) = \frac{\theta_E(s)}{\theta_2(s)} = \frac{s}{s + GF(s)}. \tag{7}$$

To proceed further, the form of F (s) must be specified. If the filter is chosen so that

$$F(s) = \frac{(s + \omega_0/3)^2}{s^2} \tag{8}$$

a third order loop results and substitution of (8) into (7) provides

$$\frac{\theta_E(s)}{\theta_i(s)} = \frac{s^3}{(s + \omega_0/4)(s^2 + 2\omega_0 s + \omega_0^2)}, \tag{9}$$

where $G = 9\omega_0/4$ is the gain constant.

The steady state-error can be evaluated by means of a Maclaurin series of the form

$$\frac{\theta_E(s)}{\theta_1(s)} = \sum_{n=0}^{\infty} C_n s^n/n! \tag{10}$$

where $C_n = f^n(o)$. This is equivalent to the form

$$\theta_E(t) \underset{t \to \infty}{=} C_0\theta_1(t) + C_1 \frac{d\theta_1(t)}{dt} + \frac{C_2}{2!} \frac{d^2\theta_1(t)}{dt^2} + \cdots \tag{11}$$

where

C_0 = position error coefficient

C_1 = velocity error coefficient

C_2 = acceleration error coefficient

It follows that to keep the dynamic tracking error to a minimum, C_0, C_1, and C_2 must be zero to prevent steady-state errors arising from the derivatives known to exist in the input. The basic filter chosen herein meets the requirement for position, velocity and acceleration which can be verified by the final value theorem. For $\theta_1(t) = \ddot{\theta}_1(t)$ ($\ddot{\theta}_1$ is a constant), we have $\theta_1(s) = \ddot{\theta}_1 / S^3$ and

$$\lim_{t \to \infty} \theta_2(t) = \lim_{s \to 0} s\theta_E(s)$$

$$= \lim_{s \to 0} \frac{s}{(s + \omega_0/4)(s^2 + 2\omega_0 s + \omega_0^2)} = 0$$

so that the steady-state error due to acceleration (and all lower ordered) inputs is zero.

To evaluate the transient error for an acceleration input, it is necessary to have the complete solution of (9) which is given below and plotted in Figure 3-11

$$\theta_E(t) = \frac{16\ddot{\theta}_1}{9\omega_0^2} \left[\exp(-\omega_0 t/4) - (1 + 3\omega_0 t/4) \exp(-\omega_0 t)\right]. \quad (12)$$

The peak value of (12) is

$$\theta_{E_{(max)}} = \frac{0.552}{\omega_0^2} \ddot{\theta}_1 . \quad (13)$$

To make use of (13), a further relationship involving ω_0 is needed. This can be obtained by using (9) in the standard relation as follows,

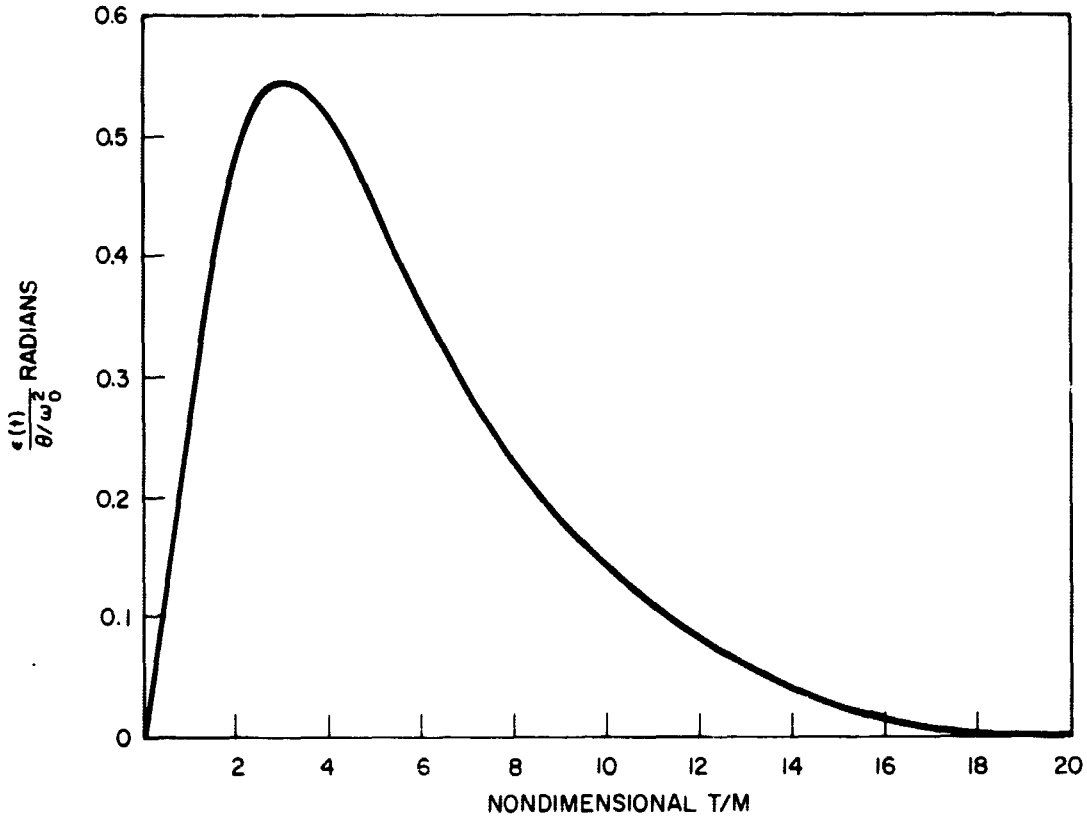

Figure 3-11–Transient Phase Error

$$B_L = \frac{1}{2\pi} \int_0^\infty |Y_L(j\omega)|^2 \, d\omega$$

and performing the indicated integration to obtain the effective loop bandwidth, B_L, in Hz. The result is $B_L = 0.743\,\omega_0$ and (13) can be written in the following useful form

$$\theta_{E\,(max)} = \frac{0.304\,\ddot{\theta}_1}{B_L^2}. \qquad (14)$$

The only remaining problem is to relate the input $\ddot{\theta}_1$ to the aircraft flight path. First, assume that the aircraft velocity vector is constant. In this case,

the relative velocity vector, with respect to the transmitting station, changes continuously and results in an acceleration input to the loop. Figure 3-12a shows the situation under consideration from which it is easily deduced that the greatest acceleration will occur when the velocity vector is normal to the distance vector and the acceleration, α, is

$$\alpha = \frac{d|\overline{V}|}{dt} = \frac{V^2}{D} \frac{1}{\left[1 + \left(\frac{Vt}{D}\right)^2\right]^{3/2}} \tag{15}$$

The maximum acceleration occurs when $t = 0$ and (15) reduces to

$$\alpha_{(max)} = 7.7 \times 10^{-8} \frac{V^2}{D} \text{ nm/sec}^2$$

which, using the relation $\ddot{\theta} = 2\pi/\lambda \, \alpha$, results in

$$\ddot{\theta}_{(max)} = \frac{2\pi}{\lambda} \frac{V^2}{D} \times 7.7 \times 10^{-8} \text{ rad/sec}^2, \tag{16}$$

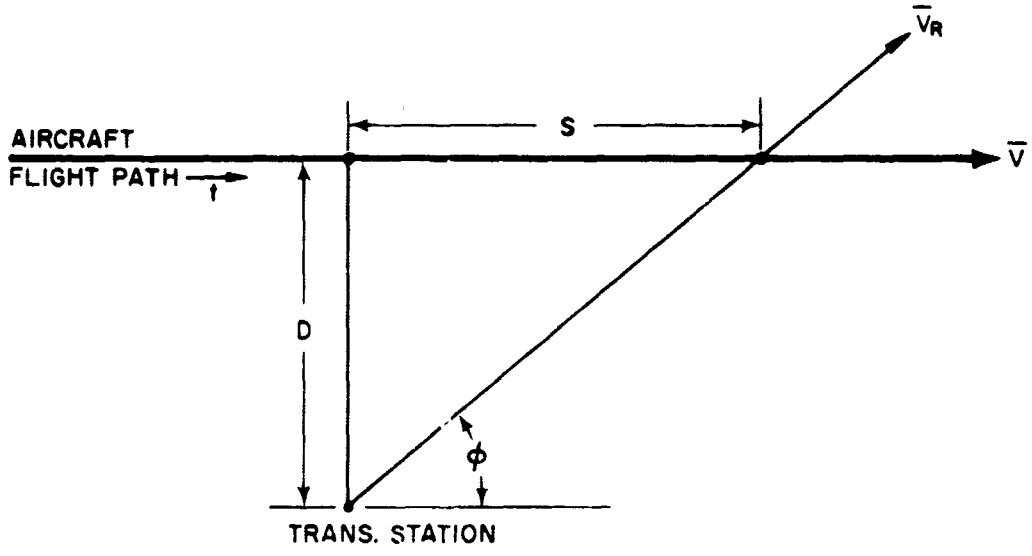

Figure 3-12–Diagram Illustrating Relative Aircraft Acceleration

for V and D in consistent units. For an aircraft velocity of 1800 knots, a minimum distance of 1000 nautical miles, and a transmitting frequency of 10 KHz, (16) provides

$$\ddot{\theta}_{(max)} = 9.8 \times 10^{-5} \text{ rad/sec}^2.$$

Substituting the above into (14) results in

$$\theta_{E\ max} = 0.17 \text{ degrees}.$$

It can be concluded that this error is negligible.

A second situation will now be considered which results from aircraft maneuvers. Consider the aircraft velocity vector under the condition of a 2 "g" acceleration. The resulting value for $\ddot{\theta}_{max}$ is 2.07×10^{-4} rad/sec. Substituting this value into (14) shows θ_E max. to be equal to 0.126 rad. or 7.2 degrees. Since this error is nearly an order of magnitude less than the limit of lock for the tracking loop, it can be concluded that satisfactory performance can be obtained.

3.4 Doppler Compensation

The relative motion of a transmitter with respect to a receiver causes a frequency translation of the entire transmitted spectrum as seen by the receiver. The magnitude of this frequency translation is directly proportional to the relative motion between the transmitter and the receiver, and the transmitter frequency as is shown in the following equation,

$$f_R = f_T + f_D = f_T \left(1 + \frac{\dot{R}}{C}\right),$$

where the above parameters are defined as follows:

f_R = frequency seen by receiver

f_T = frequency of transmitter

f_D = doppler frequency (frequency translation)

$\dot{R}$ = range rate (relative velocity between transmitter and receiver)

C = speed of light

This situation exists in PLACE where the aircraft motion can have a component of velocity in the direction of the synchronous transponding satellite. The doppler frequency shift of the aircraft transmissions is a necessary consideration in the assignment of the aircraft transmitter channels. The composite spectrum received by the satellite (Figure 2-3) consists of the transmissions from all cooperating aircraft. These aircraft transmissions are separated by frequency division multiplexing, wherein each aircraft is assigned a different carrier frequency (i.e., a different channel). In addition to the normal guardbands assigned to each aircraft channel, it is necessary to allocate additional guardbands for each channel to avoid an overlap of two adjacent (in frequency) aircraft transmissions caused by doppler-created frequency translations. It would be very simple to allocate additional guardbands equal to the maximum possible doppler shift; however, this unnecessarily increases the total system bandwidth.

An ideal doppler compensation technique would exactly compensate the transmitter frequency for frequency shifts that occur; so that, the receiver always received exactly the same frequency from the transmitter. This is not practical, so in PLACE an approximate or "gross" doppler compensation technique will be used. The consideration of doppler compensation in PLACE is complicated by the use of a coherent transceiver on the aircraft. The aircraft transceiver derives its output frequency from the carrier frequency transmitted by the satellite. Therefore the total doppler shift seen by the satellite is affected not only by the relative velocity on the aircraft to satellite uplink, but is also a function of the relative velocity on the satellite to aircraft downlink. Since it is required that the aircraft transceiver remain coherent, the compensation cannot be derived from an independent oscillator on board the aircraft but must take place in the output multiplier chain.

The gross compensation technique makes a rough measurement of the doppler shift seen by the aircraft and inserts an offset (derived from the frequency synthesizer which is locked to the received carrier) in the output frequency, thereby maintaining the output frequency within the required channel at the satellite. This offset is not a continuous function but occurs in steps. As the aircraft detects the output frequency nearing one band edge, it shifts the output back to near the other band edge, actually changing the value of a multiplier in the output frequency translation chain. This technique inserts no unknown frequencies into the output, deriving the output frequency only from the phase locked

frequency synthesizer, thereby maintaining the coherence of the aircraft transmissions. Figure 3-13 shows a simple conceptual diagram of how this technique could be implemented. The expression for the frequency received by the satellite from an aircraft as a function of the satellite transmitter frequency is derived as follows.

The satellite transmitter frequency is f_{TS}. The frequency received at the aircraft (f_{RA}) varies with range rate ($\dot{R}$) as follows:

$$f_{RA} = f_{TS}\left(1 + \frac{\dot{R}}{C}\right),$$

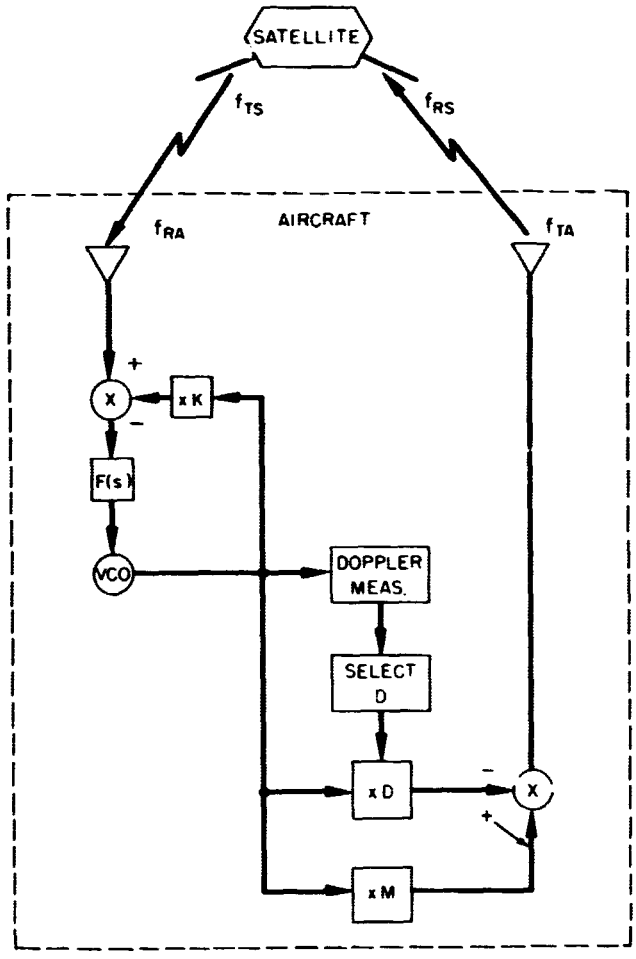

Figure 3-13–Doppler Compensation Functional Diagram

where C is the speed of light. The frequency transmitted by the aircraft (f_{TA}) after doppler compensation is

$$f_{TA} = f_{RA}\left(\frac{M-D}{K}\right) = f_{TS}\left(\frac{M-D}{K}\right)\left(1+\frac{\dot{R}}{C}\right)$$

The frequency received at the satellie (f_{RS}) is

$$f_{RS} = f_{TA}\left(1+\frac{\dot{R}}{C}\right) = f_{TS}\left(\frac{M-D}{K}\right)\left(1+\frac{\dot{R}}{C}\right)^2.$$

This may be approximated as follows;

$$f_{RS} \cong f_{TS}\left(\frac{M-D}{K}\right)\left(1+\frac{2\dot{R}}{C}\right).$$

Without the doppler compensation at the aircraft the frequency received by the satellite would be,

$$f_{RS} \cong f_{TS}\frac{M}{K}\left(1+\frac{2\dot{R}}{C}\right).$$

Ideally, the following frequency is desired at the satellite.

$$f_{RS} = \frac{M}{K} f_{TS}$$

To receive the above frequency, the following equation must be satisfied.

$$-f_{TS}\frac{D}{K}\left(1+2\frac{\dot{R}}{C}\right) + 2\frac{M}{K}\frac{\dot{R}}{C} f_{TS} = 0$$

We can now solve for the "D" required on the aircraft as a function of range rate.

$$D\left(1 + \frac{2\dot{R}}{C}\right) = 2M\frac{\dot{R}}{C}$$

$$D = \frac{2M\dot{R}}{C + 2\dot{R}} \cong 2M\frac{\dot{R}}{C}$$

From the preceeding set of equations we can extract the following functions. The uncompensated doppler frequency (f_d) at the satellite is

$$f_d = 2\frac{M}{K}\frac{\dot{R}}{C} f_{TS}.$$

The magnitude of doppler compensation by the aircraft (f_g) is

$$f_g = \frac{D}{K}\left(1 + 2\frac{\dot{R}}{C}\right) f_{TS} \cong \frac{D}{K} f_{TS}.$$

The value of doppler frequency seen at the satellite after doppler compensation is f_a.

$$f_a = f_d - f_g \cong \left(\frac{2M\dot{R}}{C} - D\right)\frac{f_{TS}}{K}$$

Figure 3-14 is a plot of the preceeding three equations, as a function of the doppler frequency measured at the aircraft (f_d'), with the following assumptions.

f_{TS} = 1500 MHz

$\dot{R}$ = 0 to ±2000 mi/hr

D = N × 1/625 (where N = ±1, 2, 3 etc.)

K = M = 1500

C = 6.7×10^8 mi/hr

Due to the desire to avoid the requirement for an extremely precise frequency standard on board the aircraft, the doppler compensation is not a continuous function. Instead as the aircraft detects that the received frequency at the satellite has shifted to within a certain distance from the band edge, an offset in the output frequency will be inserted at the aircraft; that is, the value of D is stepped to a new value, driving the signal received at the satellite away from the bandedge it was approaching. Hysteresis is added in the doppler compensation technique to prevent the aircraft transmitter frequency (which has a doppler frequency coincident with a step value) from alternating between two different carrier frequencies. Since the doppler frequency seen at the satellite is directly proportional to the doppler shift measured at the aircraft, and this proportionality factor is known, it is not necessary to perform any measurements at the satellite. The control for the doppler compensation can be derived entirely on the aircraft, provided the doppler frequency at the aircraft can be measured with the following limit on the measurement error.

$$E = \text{doppler measurement error}$$

$$E \leq \frac{f_x}{2\, f_{TS}}$$

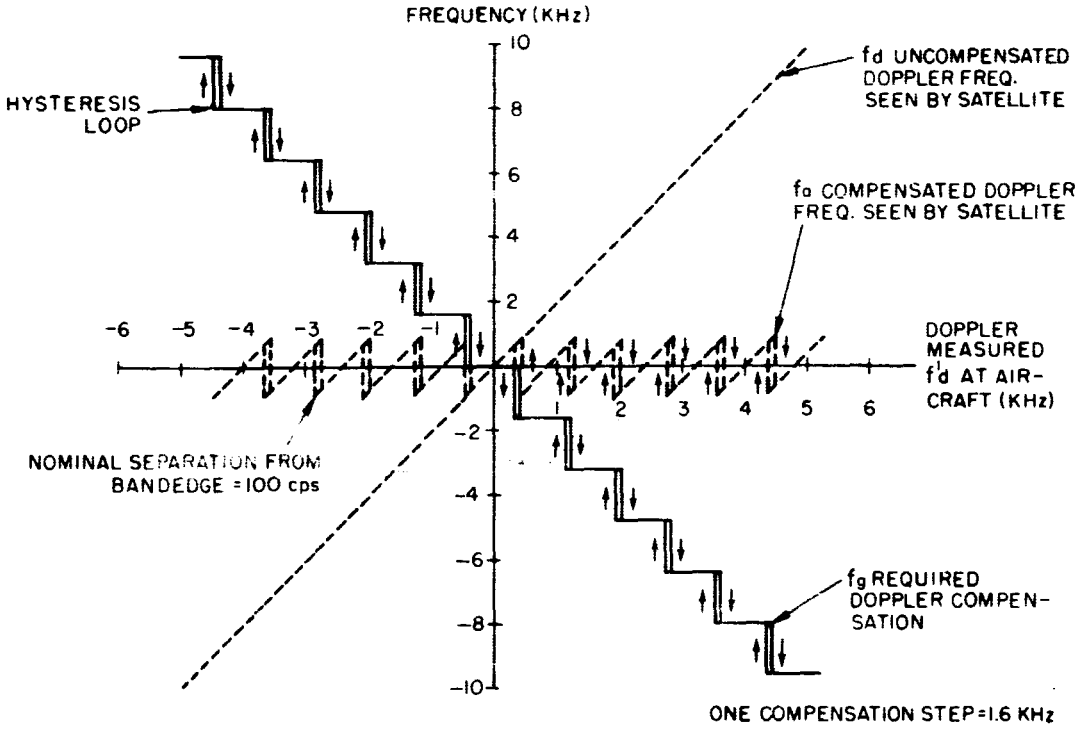

Figure 3-14–Doppler Compensation Curves

where f_x = difference between allocated bandedge and the nominal controlled bandedge, and f_{TS} = the satellite carrier frequency. For the values assumed in Figure 3-14; f_x = 100 Hz and f_{TS} = 1500 MHz, E must be equal to or less than 3.3×10^{-8} Hz/Kz. We can reduce the measurement accuracy requirements by increasing the value of f_x. The value of f_x chosen for use in Figure 3-14 was only for discussion purposes and could be increased to reduce the accuracy requirements to a more reasonable value.

Figure 3-15 is a tabulation of how the bandwidth of the composite spectrum received by the satellite from all aircraft can be reduced by compensating for doppler shifts in the manner just described. The numbers for this table are derived from the assumption that the guards bands allocated for doppler shift protection are for the worst case. The worst case for PLACE is that wherein the maximum range rate between the aircraft and the satellite is 2000 miles/hour which conceivably could occur under certain geometries for a supersonic transport.

BANDWIDTHS REQUIRED BETWEEN AIRCRAFT AND SATELLITE WITH AND WITHOUT DOPPLER COMPENSATION

	With Compensation	Without Compensation
Single Aircraft Channel	7 KHz	7 KHz
200 Aircraft Channels	1.4 MHz	1.4 MHz
Guard Band per Aircraft	± 1 KHz	± 10.5 KHz
200 Guard Bands	0.4 MHz	4.2 MHz
TOTAL	1.8 MHz	5.6 MHz

Figure 3-15–Bandwidth Requirements

3.5 SIND Performance Characteristics

The Satellite Inertial Navigation Determination (SIND) study indicates that all significant results are embodied in one expression. This single relationship, which is derived in Appendix C, describes the total aircraft positional error.

$$\text{Total Error} = \sigma_D = \frac{R_s}{V \cos \alpha} \sqrt{\sigma_v^2 + \sigma_{\dot{R}}^2}$$

The intrack and crosstrack components of the total error are close approximations based on the simplified model, and are given by:

$$\text{Intrack Error} = \sigma_{IT} \approx \frac{R_s}{V} \sqrt{\sigma_v^2 + \sigma_{\dot{R}}^2}$$

$$\text{Crosstrack Error} = \sigma_{ct} \approx \frac{R_s}{V} \sqrt{\sigma_v^2 + \sigma_{\dot{R}}^2} \tan \alpha,$$

where the intrack error is defined tangent to the flight path and the cross track error is defined perpendicular to the flight path.

The positional error is a function of the range between the aircraft and the satellite; the aircraft velocity component tangent to the circle of position; the angle, α, at which the aircraft flight path intersects the line of position; and the one sigma measurement errors inherent in determining the aircraft velocity vector, V, and the range rate or Doppler, $\dot{R}$, between the aircraft and the satellite. The utilization of the error relationships is relatively simple and straightforward, providing easy visualization of the Satellite Inertial Navigation Determination system errors.

In general the length to diameter ratio of the SIND error ellipsoid is very large resulting in a cigar shaped characteristic with the major axis, or long dimension, of the ellipsoid tangent to the aircraft circle of position.

The required inputs for the operational SIND system, which are shown in Figure 3-16, include measured parameters and the accuracy or error associated with these measurements. Range and range rate between the aircraft and satellite are derived from the aircraft transmitter-receiver system operating in conjunction with the satellite transponder. Aircraft altitude is determined from the aircraft altimeter. The velocity vector of the aircraft can be developed from the aircraft inertial navigation system (or gyros) or possibly by Doppler radar. The SIND system must be programmed with the input errors, or accuracies, associated with each of the measured parameters. The output accuracies are then obtained from an error analysis. A description of the output parameters and errors determined are shown in Figure 3-17.

The geometry of the SIND system is indicated in Figure 2-18. Utilizing the earth centered coordinate system, X_1, X_2, X_3, a circle or line of position for the

FOR SYSTEM OPERATION AND ERROR ANALYSIS
INPUTS ARE MEASURED PARAMETERS AND MEASUREMENT ERRORS

PARAMETERS, MEASURED ON-BOARD A/C		DERIVED FROM
R, σ_R	RANGE TO SATELLITE RANGE ERROR	A/C TRANSMITTER-RECEIVER SYSTEM AND SATELLITE TRANSPONDER
$\dot{R}$, $\sigma_{\dot{R}}$	RANGE-RATE BETWEEN A/C AND SATELLITE RANGE-RATE ERROR	
h, σ_h	ALTITUDE OF A/C ALTITUDE ERROR	A/C ALTIMETER
$\vec{v}$, $\sigma_{\vec{v}}$	VELOCITY VECTOR OF A/C VELOCITY ERROR	A/C INERTIAL SYSTEM (OR GYROS); POSSIBLY BY DOPPLER RADAR

$\vec{v} = f(\dot{x}, \dot{y}, \dot{z})$ A/C

$\sigma_{\vec{v}} = f(\sigma_{\dot{x}}, \sigma_{\dot{y}}, \sigma_{\dot{z}})$

Figure 3-16–SIND Inputs

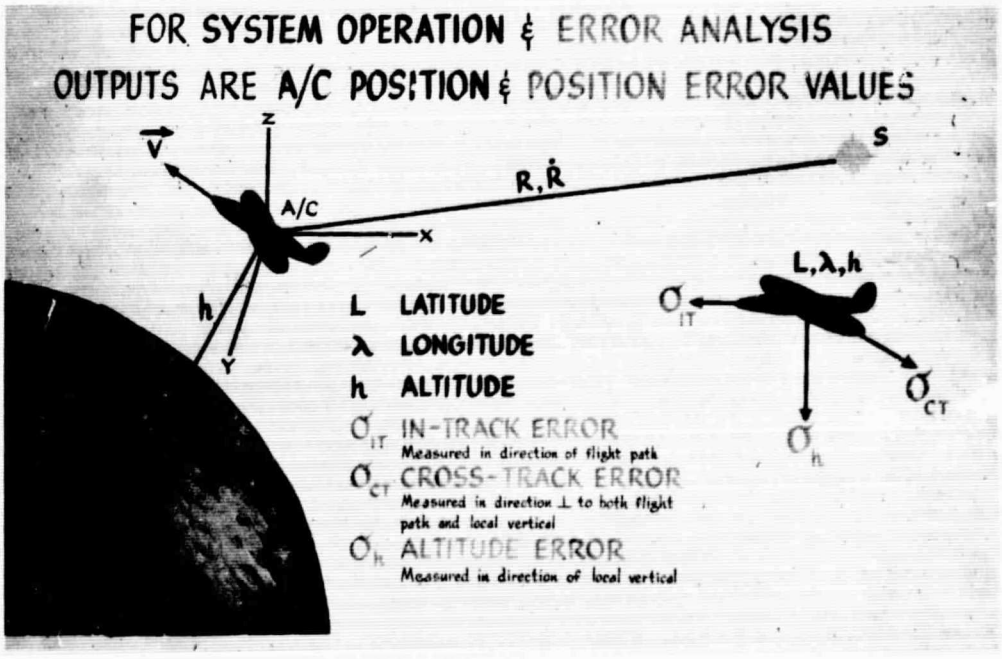

Figure 3-17–SIND Outputs

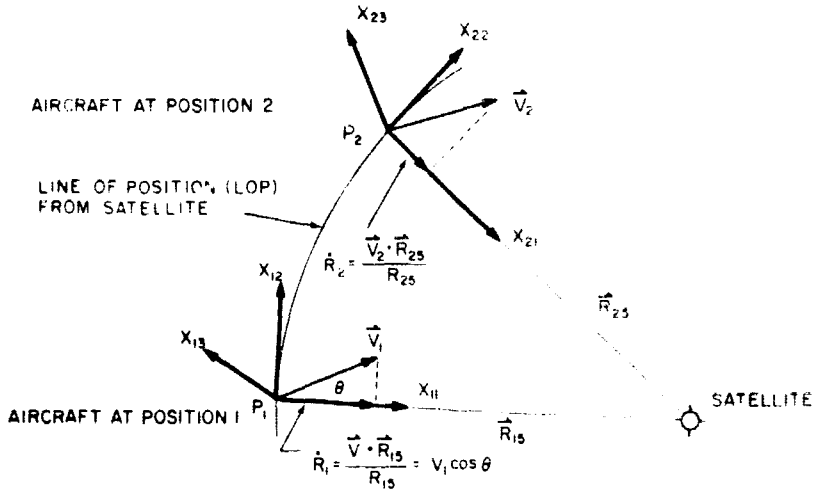

FROM ANY POINT ON THE LINE OF POSITION, SAY P_1 OR P_2, THE INERTIAL VELOCITY VECTOR CAN BE PROJECTED ONTO THE DIRECTION TO THE SATELLITE, $\vec{R}_{15}$ OR $\vec{R}_{25}$ THIS PROJECTION WILL AGREE WITH THE OBSERVED VALUE OF $\dot{R}$ AT ONLY TWO POINTS: AMBIGUITY IS EASILY RESOLVED FOR FLIGHT PATHS NOT NORMAL TO LOP. FIGURE SHOWS TYPICAL CHANGE IN $\dot{R}$ PROJECTION OF $\vec{V}_{A/C}$ ONTO $\vec{R}_5$ AS LOP CHANGES FOR SPECIFIED FLIGHT PATH.

Figure 3-18–Determination of Position on Line of Position

aircraft is determined on the surface of the sphere of radius, $R_a = R_e + h$, by the range, R_s, between the aircraft and the satellite. The determination of the location of the aircraft on the line of position is indicated for two aircraft in Figure 3-18. Consider an aircraft situated at position 1. The aircraft inertial velocity vector, V_1, can be projected onto the direction of the satellite, R_{1s}. This projected magnitude, $V_1 \cos \theta$ is equal to the magnitude of the range rate at only two points on the circle of position. The ambiguity between these two points is easily resolved for flights not normal to the line of position.

The results of the error analysis are summarized in simplified form in Figure 3-19 which shows the error ellipsoid along the line of position at an angle α with respect to the aircraft flight path. An approximation of the total intrack and crosstrack positional error is given in terms of the distance from the aircraft to the satellite, the aircraft inertial velocity, the angle of intersection of the aircraft inertial velocity vector with the line of position, and the standard deviations of aircraft velocity and range rate error. The approximations are valid within 5 percent within the limits on α from $\pm 2°$ to $\pm 85°$.

Figure 3-21 shows typical lines of position which might be obtained over the North Atlantic principal area employing a stationary equatorial satellite positioned at 30°W longitude. The navigational accuracy of a great circle flight over

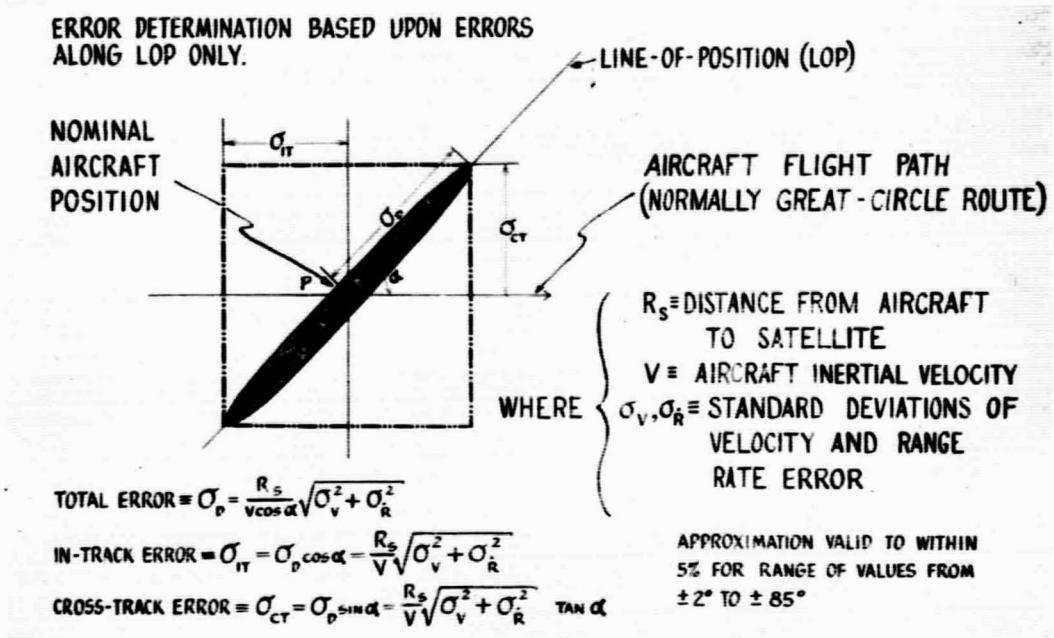

Figure 3-19–Simplified Error Relation

this area between Washington, D.C. and Paris, France, is presented in Figure 3-22 for two cases.

In case I, the standard deviation is 10 meters for range error and 0.01 meters per second for range rate error. For Case II, the standard deviation is 100 meters for range error and 0.1 meters per second for range rate error. In both cases, the navigation satellite is equatorial and stationed at 30°W longitude. Aircraft velocity is considered to be 2000 knots. The standard deviation of the intrack error is 6400 meters for Case II and 640 meters for Case I. The standard deviation for crosstrack error may be read directly from the curve, either in nautical miles or meters, as a function of distance traveled.

Modern aircraft are capable of traveling at extremely high speeds and thus covering substantial distances in relatively short periods of time. An appreciation of this can be seen by reference to Figure 3-23 which shows distance traveled versus time for selected velocities.

The SIND intrack error and aircraft separation distance are shown in Figure 3-24 as a function of aircraft velocity in knots. Two cases of SIND intrack error are considered corresponding to two scaling relations for the standard deviation of the intrack error. Note that for both Case I and Case II,

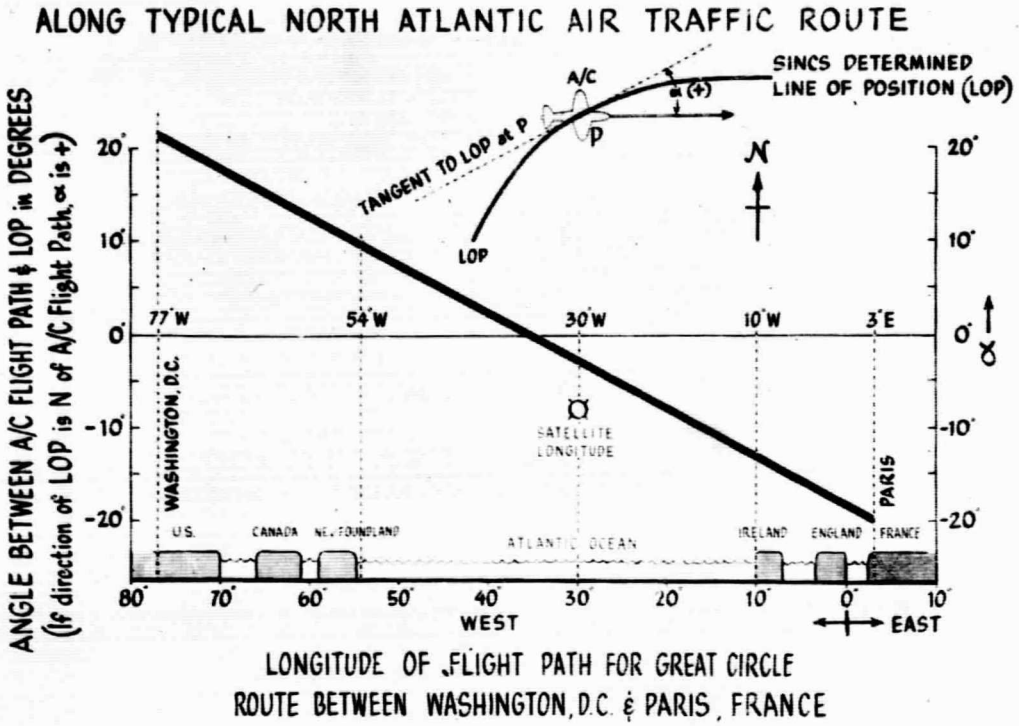

Figure 3-20–Variation of α Along Typical North Atlantic Air Traffic Route

the error decreases as the aircraft velocity increases, which suggests that the SIND system may be more effectively employed with high speed aircraft.

Figure 3-24 also shows aircraft longitudinal separation distances in nautical miles as a function of aircraft speed for the current rules governing flights over the North Atlantic. These rules generally prescribe an intrack separation time of 30 minutes but under special conditions permit a reduction to 20 minutes. In this report, the allowable error in separation distance has been arbitrarily selected as one-tenth of the general 30 minute separation and is shown in Figure 3-27 as three-minute distance – allowable error. Based on this allowable error, the SIND system is useful only below the three-minute distance allowable error line shown in Figure 3-24.

Figure 3-25 illustrates aircraft crosstrack error and lateral separation distances for two cases. For each case, the nominal error is plotted within an indicated maximum and minimum variation. As before, the error decreases as the aircraft velocity increases. Although the minimum lateral separation allowed on North Atlantic flights is 90 miles, the majority of current flights are

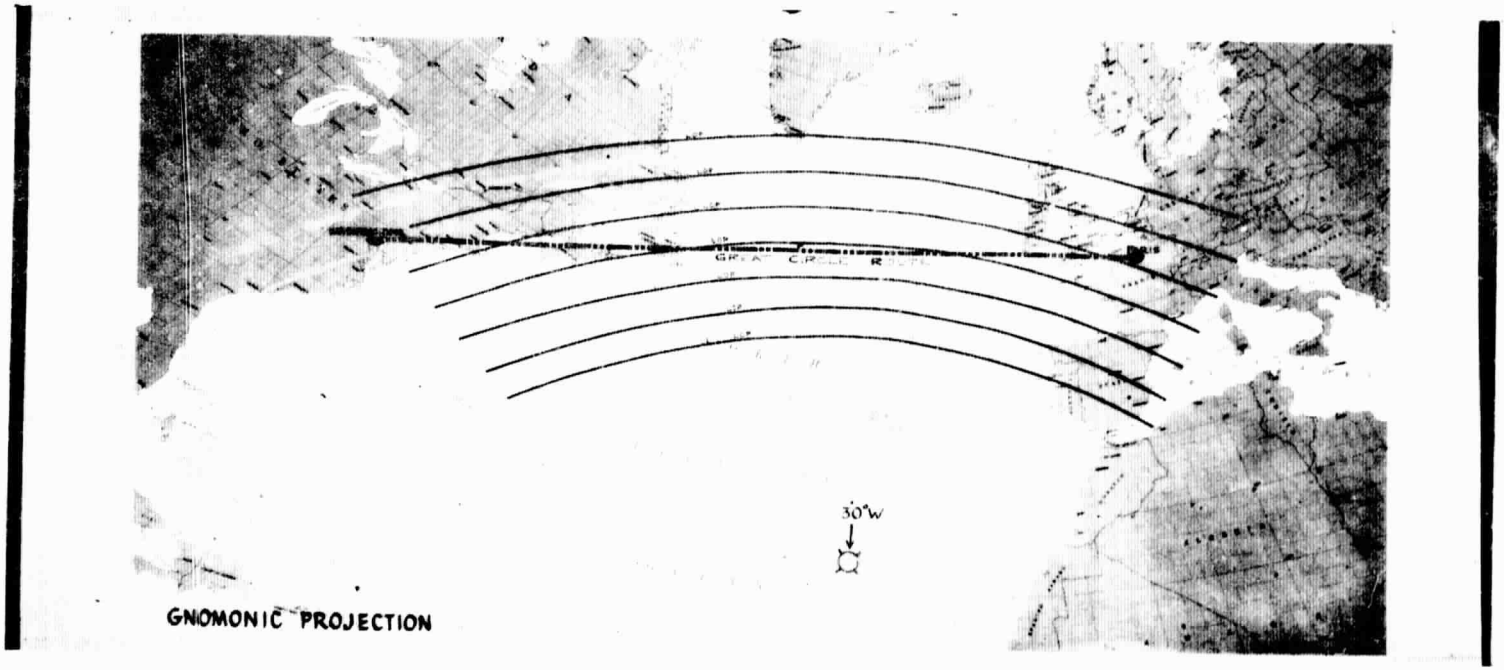

Figure 3-21–Typical Lines of Position for Satellite at 30° W Longitude

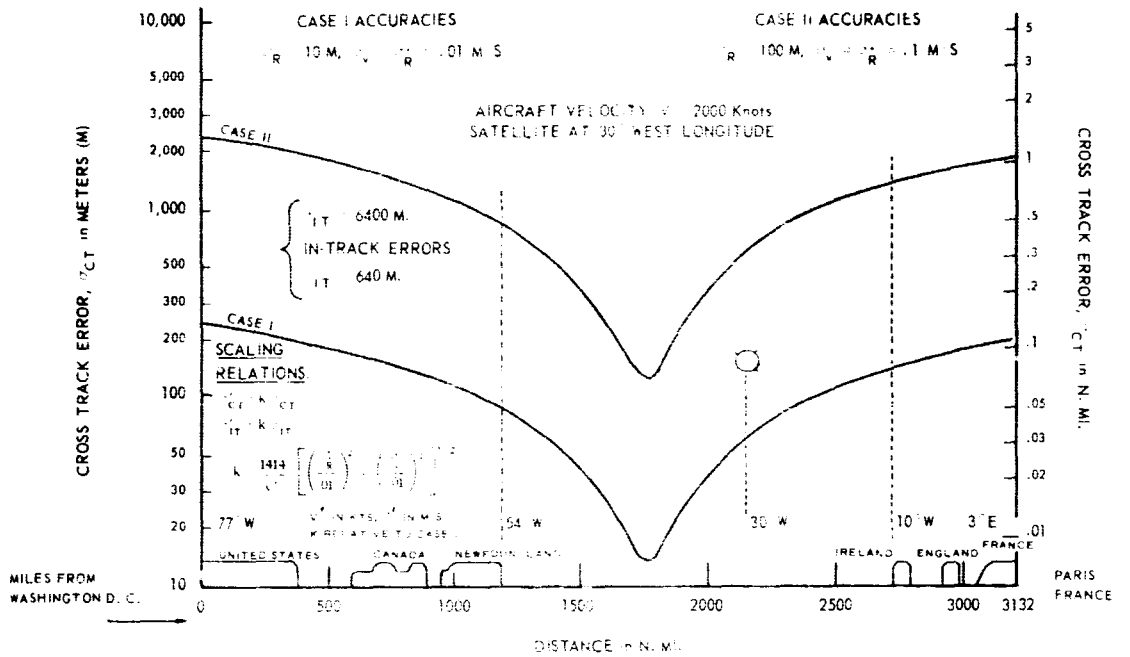

Figure 3-22–Intrack and Crosstrack Errors for a Typical Flight From Washington, D.C. to Paris, France

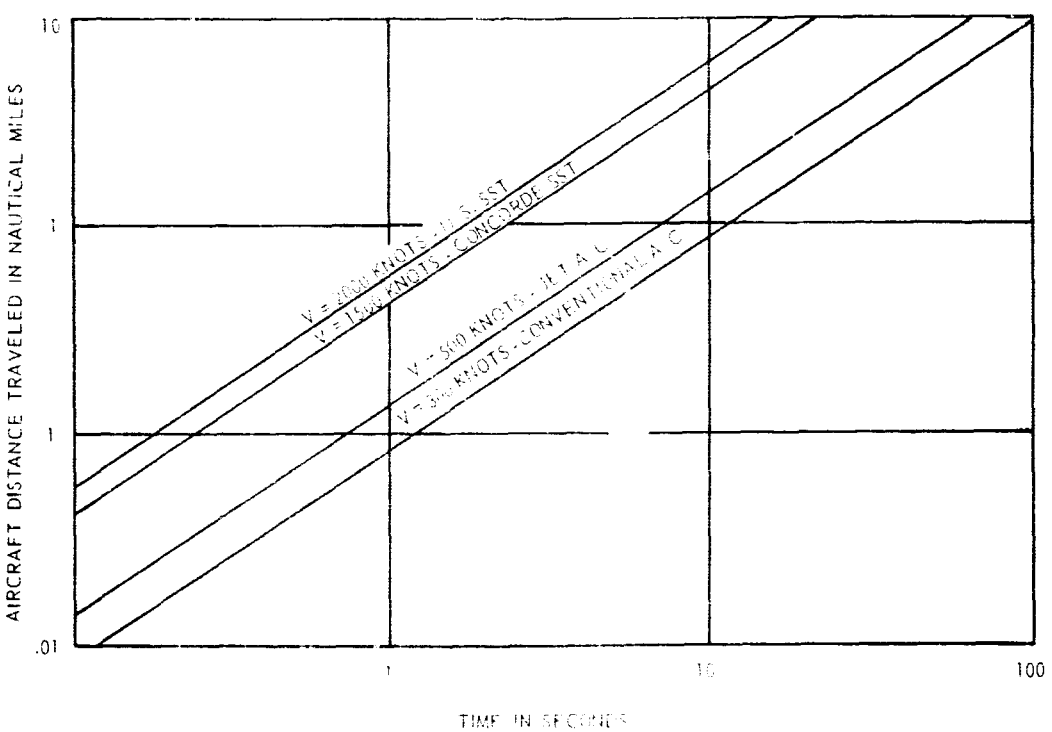

Figure 3-23–Aircraft Distance Traveled vs. Time for Selected Aircraft Velocities

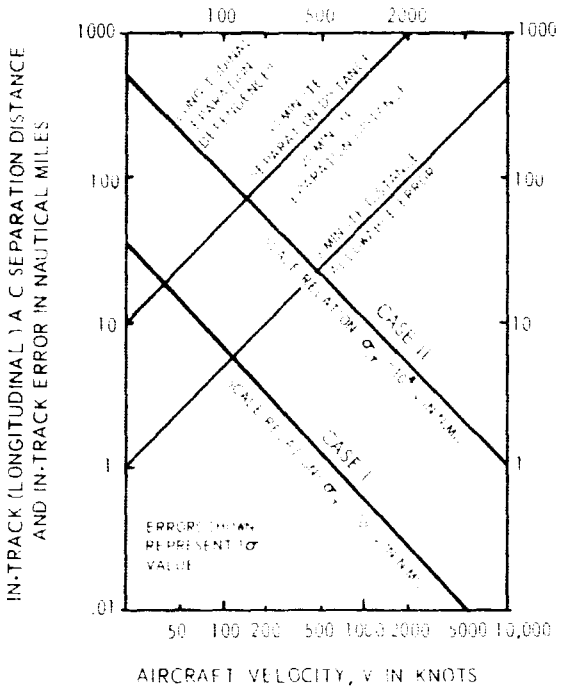

a. NORTH ATLANTIC LONGITUDINAL SEPARATIONS ESTABLISHED BY ICAO REGIONAL SUPPLEMENTARY PROCEDURES, DOCUMENT 7030," SECTION 2.1 AS AMENDED JUNE 1966. U. S. OCEANIC CONTROL PROCEDURES CONSISTENT WITH ICAO BUT GOVERNED BY FAA "AIR TRAFFIC PROCEDURES MANUAL, ATP-7110.18, SECTION 600 NOV. 12, 1964.

Figure 3-24–Intrack Error and Aircraft Separation vs. Aircraft Velocity

assigned 120-mile separations. Plots of lateral separation distance for both 90 and 120 miles are shown in Figure 3-25. If the allowable error is arbitrarily taken as approximately one-tenth of the actual separation, then the allowable error in lateral separation is approximately 10 miles as shown in Figure 3-25. With this allowable crosstrack error, the SIND system is useful only below the lateral separation allowable error line.

Two areas appear to require further study. One area involves the precise determination of accelerometer and gyro errors for torqued platforms and the effect of such errors on system performance. Also, a study should be initiated relative to the use of time histories for improving system performance. Of particular importance in this area is the use of time histories in determining accelerometer and gyro errors.

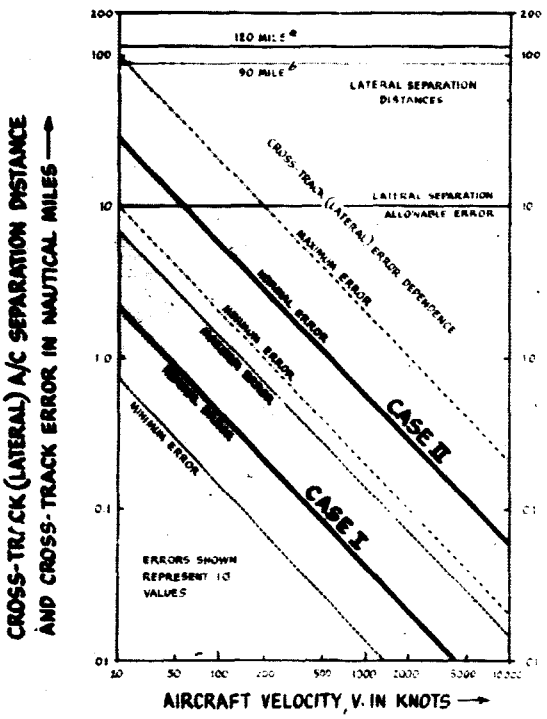

a. NORTH ATLANTIC LATERAL SEPARATION OF 120 MILES PRESCRIBED BY AGREEMENT BETWEEN CANADA, UNITED STATES, AND UNITED KINGDOM. FAA ISSUED COVERING FLIGHT INFORMATION BULLETIN, JUNE 1966.

b. 90 MILE FIGURE IS THE MINIMUM LATERAL SEPARATION FOR NORTH ATLANTIC ROUTES AS ESTABLISHED BY ICAO "REGIONAL SUPPLEMENTARY PROCEDURES, DOCUMENT 7030", SECTION 2 2 AS AMENDED, JUNE 1966.

Figure 3-25–Crosstrack Error and Aircraft Separation vs. Aircraft Velocity

ACKNOWLEDGMENTS

The error analysis of the SIND concept was performed for Goddard Space Flight Center by Messers. K. McDonald, R. Leach, and R. Nickell of the Systems Science Corporation under NASA Contract NAS 5-9758, Task Order No. 9758-67.

REFERENCES

1. J. A. Deveiet, Jr., "Fundamental Accuracy Limitations in a Two-Way Coherent Doppler Measurement System," I.R.E. Transactions, Vol. SET-7, No. 3, pp. 80-85, September 1961.

2. J. K. Holmes, "A Consideration of VCO and Thermal Phase Noise in a Coherent Two-Way Doppler Communication System," IEEE Transactions on Space Electronics and Telemetry, pp. 1-6, March 1965.

3. J. H. Hutcheson, J. D. Mallet, and H. S. Schwimmer, "Navigation by Satellite Using Two-Way Range and Doppler Data," Memorandum RM-4815-NASA, Rand Corporation prepared for NASA under Contract NO. NAS-21, December 1965.

4. G. C. Kronmiller, Jr. and E. J. Baghdady, "Goddard Range and Range Rate Tracking System: Concept, Design and Performance," NASA Document X531-65-403, Goddard Space Flight Center, Greenbelt, Maryland, Oct. 1965.

5. J. A. Pierce, W. Palmer, A. D. Watt, and R. H. Woodward, "OMEGA, A World-Wide Navigational System," System Specification and Implementations Prepared by the Implementation Committee for the U. S. Navy Department Bureau of Ships, published by Pickard and Burns Electronics, P&B Pub. No. 886, P&B Project No. 347, June 1964.

6. L. H. Enloe, "Decreasing the Threshold in FM by Frequency Feedback," Proceedings of the IRE, Vol. 50, No. 1, pp. 18-30, January 1962.

7. J. J. Spilker, Jr., "Threshold Comparison of Phase-Lock, Frequency-Lock and Maximum-Likelihood Types of FM Discriminators," presented at WESCON, San Francisco, August 1961.

8. B. D. Martin, "The Pioneer IV Lunar Probe: A Minimum-Power FM/PM System Design," Technical Report No. 32-215, Jet Propulsion Laboratory, March 1962.

9. P. I. Richards, "Computing Reliable Power Spectrum," IEEE Spectrum, pp. 83-90, January 1967.

10. J. L. Stewart, "The Power Spectrum of a Carrier Frequency Modulated by Gaussian Noise," Proceedings of the I.R.E. pp. 1539-1542, Vol. 42, Oct. 1954.

11. N. Abramson, "Bandwidth and Spectra of Phase-and-Frequency-Modulated Waves," IEEE Transactions on Communications Systems, pp. 407-414, December 1965.

12. W. D. Peterson, "Signal-Power Comparison of Coded and Tone Ranging Systems for Spacecraft Vehicles," IEEE Transactions on Aerospace and Navigational Electronics, pp. 140-148, June 1965.

13. M. L. Livingston, "The Effect of Antenna Characteristics on Antenna Noise Temperature and System SNR," I.R.E. Transactions on Space Electronics and Telemetry, pp. 71-79, September 1961.

14. D. L. Miller, "Presentation to Joint US/UK/Canada Aeronautical Satellite Communications Working Group," September 1966.

15. D. L. Miller, "Letter to Raymond Spence, Federal Aviation Agency," Aug. 1966.

16. E. J. Martin, "Status of the Comsat Aeronautical Satellite Program" presented at RTCA Fall Assembly, September 1966.

17. R. J. Adams, "Polarization Protection from Multipath in Satellite Communications for Aeronautical Mobile Service," Hughes Aircraft Company, SSD 60231R, June 1966.

APPENDIX A

TROPOSPHERIC AND IONOSPHERIC EFFECTS ON RANGE AND RANGE-RATE MEASUREMENTS

I. INTRODUCTION

The primary purpose of this appendix is to provide a realistic estimate of the tropospheric and ionospheric influences upon the range and range-rate measurements. The PLACE study made it necessary to provide a basis for selecting a suitable operating frequency where the range and range-rate errors introduced by the atmosphere will allow precise determination of the location of high speed aircraft by means of a synchronous altitude satellite. The regions of the atmosphere which affect the propagation of electromagnetic waves are; the troposphere (0-30.5 km), where the index of refraction is greater than unity, and the ionosphere (85-1000 km), where the index of refraction is less than unity. Free space prevails between the tropospheric and ionospheric region (30.5-85 km) where the index of refraction is essentially unity.

Signal deterioration results from the fact that there exists in the atmosphere spatial inhomogeneties which are continuously varying as a function with time. A radio wave traveling from some object in space and incident upon the earth's surface has of necessity traversed the earth's atmosphere; a region in which the refractive index may deviate significantly from unity. Particularly at frequencies below 1000 MHz the atmosphere may affect any or even all of the five parameters that can be used to define the radio wave (i.e., its amplitude, direction of propagation, phase, frequency, and polarization). The time and space variations of these five parameters may be affected by atmospheric irregularities of various sizes and, for a moving source, even by a smooth, nonvarying ionosphere.

A study of the effects of the atmosphere on radio wave propagation necessitates a knowledge of the height-variations of the dielectric constant, or refractive index, in the tropospheric and ionospheric regions. Since the magnitude of the dielectric constant is a function of such parameters as the geographic location on the earth, weather, time of day and season of the year, it becomes an overwhelming task to completely analyze atmospheric propagational effects under all parametric conditions.

To simplify the analytical problem, atmospheric models[1,2,3] which are representative of average conditions are employed to estimate the influence of the earth's atmosphere (tropospheric and ionospheric regions) upon measurements of range and range-rate at various frequencies. The effects of the troposphere and ionosphere upon radio wave propagation can best be predicted if an accurate refractive profile of the atmosphere is available. To a certain extent, the systematic or biasing effects of the atmosphere are predictable and can be corrected for if sufficient data regarding the atmospheric state are available.

II. TROPOSPHERIC RANGE ERROR

Figure A-1 indicates the physical relationship between the troposphere and ionosphere above the earth's surface. In the troposphere, the index of refraction, n, can be found from the following equation[4].

$$N = (n - 1) \times 10^6 = \frac{77.6}{T} \left[P + \frac{4810\, e}{T} \right], \tag{1}$$

where N is the refractivity, T is temperature in degrees Kelvin, P is total atmospheric pressure, and e is the partial pressure of water vapor (both P and e in millibars). The above expression for the refractivity of air is independent of frequency in the 100 MHz to 10,000 MHz range.

Bean and Thayer[3,5] describe the tropospheric refractivity profile by the following equation:

$$N = N_s \exp\left[- k(h - h_s) \right], \tag{2}$$

where

N_s = refractivity at earth's surface

k = decay constant (per km)

h = height above surface corresponding to N (km)

h_s = height of reference point above mean sea level (km)

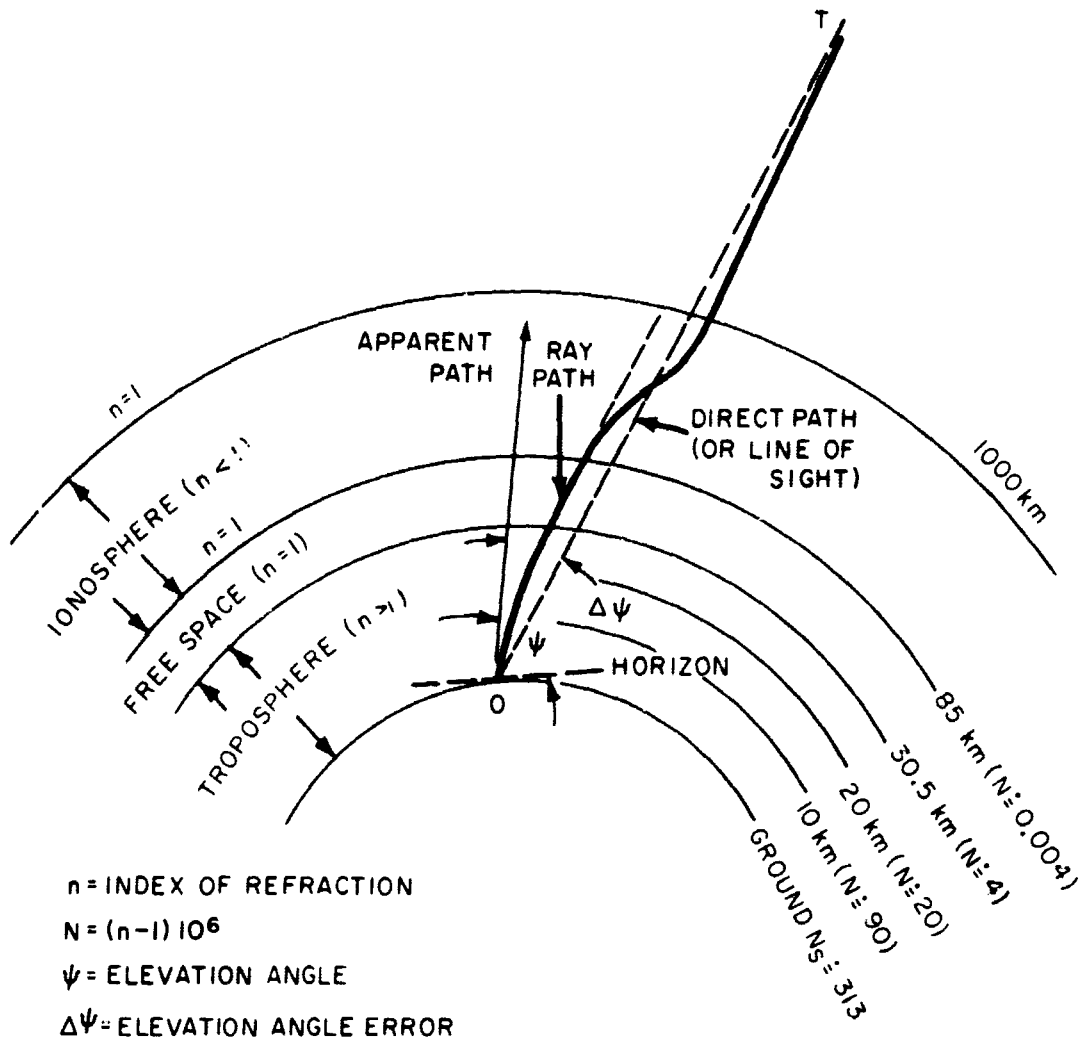

Figure A-1–Typical Ray Path Trajectory Through the Atmosphere

The decay constant is generally calculated from a refractivity measurement at a height of 1 km. That is,

$$k = \ell n \frac{N_s}{N_s + \Delta N} \cdot \tag{3}$$

$N_s + \Delta N$ is the refractivity at a height of 1 km above the earth surface[3]. The calculated exponential profile by NBS is in agreement with the measured tropospheric index of refraction profile[6].

The tropospheric range measurement error is primarily due to the electrical path length difference between a line-of-sight path measured in terms of the velocity of light in vacuum and the line-of-sight electrical path length due to the actual velocity of propagation associated with the troposphere.

When electromagnetic waves are propagated through a medium whose dielectric constant or index of refraction is a varying function of the path, the wave undergoes a change in direction, or refractive bending, and a retardation in the velocity of propagation.

The path length between ground station and target is given by

$$R_0 = \int_1^2 ds = \text{line-of-sight range (or true range)}. \tag{4}$$

The "apparent range" due to a velocity of propagation less than that of light in vacuum is given by

$$R = \int_1^2 nds = \text{apparent range}. \tag{5}$$

The range error ΔR is the difference between apparent range R and the true range R_0.

$$\Delta R = \int_1^2 (n - 1)\, ds \tag{6}$$

Using (1) and

$$ds = \frac{dh}{\sin \psi}$$

where

ψ = elevation angle,

h_1 = height of surface above sea level,

h_2 = target height,

equation (6) can (for elevation angles $\psi > 10$ angles) be approximated by the following equation:

$$\Delta R \doteq \frac{10^{-6}}{\sin \psi} \int_{h_1}^{h_2} N dh. \tag{7}$$

Equation (7) indicates that the range error is a function of the refractivity profile and elevation angle. Figure A-2 shows tropospheric range errors represented by the exponential model[3] and by the standard atmospheric models[7] (see Tables A-1 and A-2).

Tropospheric range errors decrease rapidly with increasing elevation angle and are independent of frequency. The tropospheric error is appropriate for lunar distances as well as earth orbits.

III. IONOSPHERIC RANGE ERROR

In the troposphere the index of refraction is independent of frequency. For the ionosphere, however, the refractive index of the medium is a function of the transmitted frequency.

The effects of the ionosphere can be described to a sufficient approximation for $f \geq 100$ MHz by ascribing to the ionosphere an equivalent index of refraction given by[9];

$$n = \left[1 - \frac{N_e e^2}{\epsilon_0 m \omega^2}\right]^{1/2}, \tag{8}$$

where

N_e = electron density = electrons/meter^3,

e = electron charge = 1.602×10^{-19} Coulombs,

m = electron mass = 9.11×10^{-31} kilograms

ϵ_0 = free space dielectric constant = 8.855×10^{-12} farad/meter.

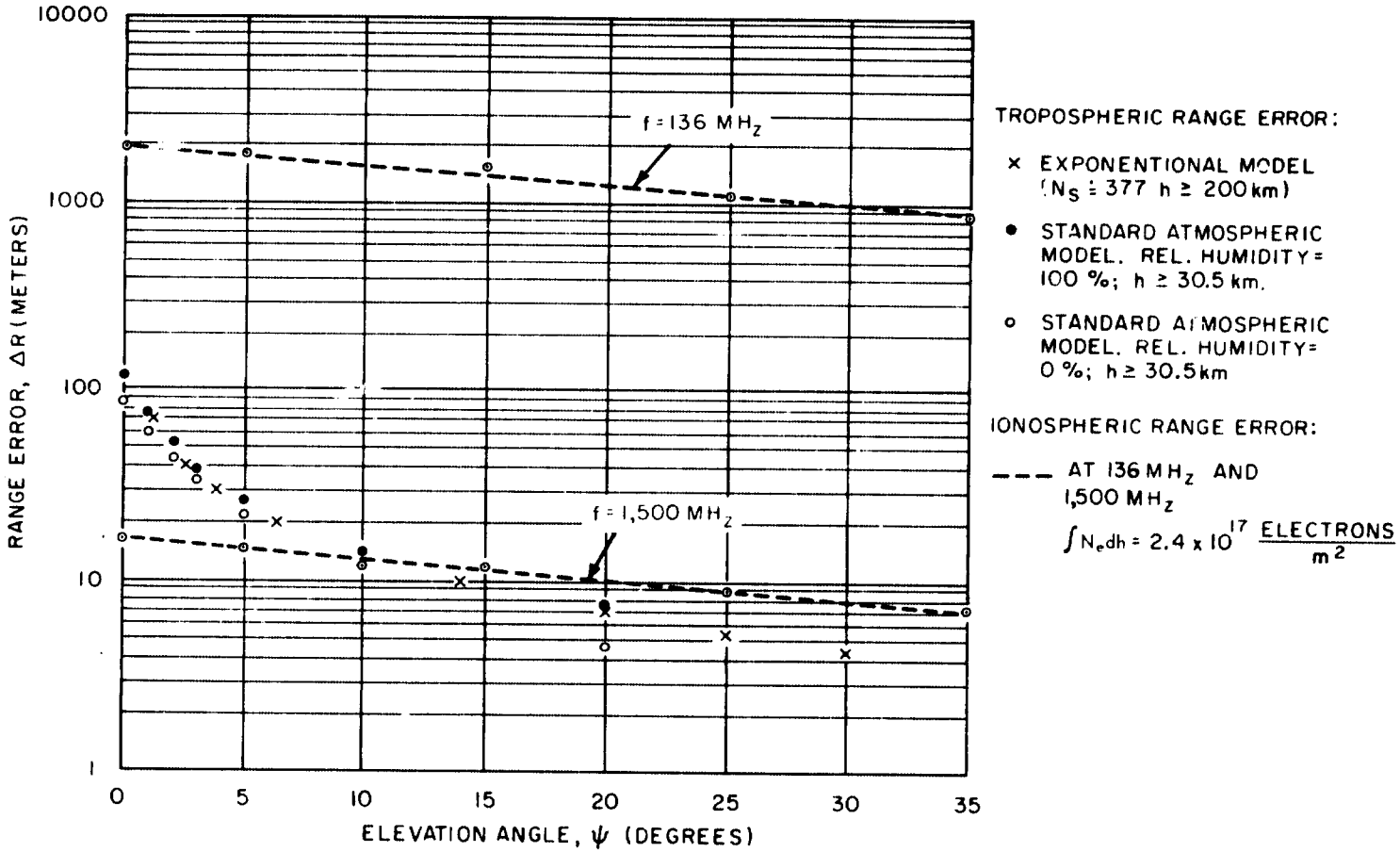

Figure A-2–Tropospheric and Ionospheric Range Errors Vs. Elevation Angle.

Table A-1

Tropospheric range errors for a standard atmosphere with 100% relative humidity, one way transmission path at the altitude $\geq$ 30.5 km.

ψ (degrees)	0	1	2	3	5	10	20
ΔR (meters)	116	73	51.3	38.2	26	12.8	7.6

Table A-2

Tropospheric range error for a standard atmosphere with 0% relative humidity, one way transmission path at the altitude $\geq$ 30.5 km.

ψ (degrees)	0	1	2	3	5	10	20
ΔR (meters)	88.5	60	44	33.8	22	11.6	4.6

The ionospheric range error due to time delay can be calculated when

$$R_0 = \int_1^2 ds = \text{line of sight range (or true range)}. \tag{9}$$

The "apparent range," due to a phase velocity greater than that of light in vacuum, is given by;

$$R = \int_1^2 \frac{ds}{n} = \text{measured range}, \tag{10}$$

where n = ionosphere index of refraction ($n < 1$).

Equation (10) describes the apparent increase in range due to a group velocity less than the speed of light. The ionospheric range error ΔR is given by

$$\Delta R = R - R_0 = \int_1^2 \left(\frac{1}{n} - 1\right) \, ds. \tag{11}$$

By using (1) and (8), equation (11) can be written as,

$$\Delta R = \frac{1.6 \times 10^3}{(2\pi f)^2} \int_1^2 N_e \, ds. \tag{12}$$

Reference (10) shows that if ψ is the angle between the horizontal and the direction of propagation, then

$$\int_1^2 N_e \, ds = (1 - 0.928 \cos^2 \psi)^{-1/2} \int N_e \, dh. \tag{13}$$

By using (13), and for elevation angle $\psi = 0$, equation (12) can be written as;

$$\Delta R = \frac{152}{f^2} \int N_e \, dh, \tag{14}$$

where f is in Hertz, ΔR is in meters, and $\int N_e dh$ is in electrons per square meter.

Figure A-3 and Table A-3 show the ionospheric range error for zero elevation angle and various integrated electron densities versus frequency.

Range biasing effects due to the atmosphere as shown in Figure A-2 decrease with increasing elevation angle ψ. The tropospheric range error is frequency independent while ionospheric range error is inversely proportional to the square of the operating frequency. The electron density, N_e, is a function of time of day, the magnitude of recent sun spot activity, the effect of local ionospheric storms, and the local latitude; therefore, the integrated electron density will vary in a non-deterministic manner as a function of time. Several investigators[10] have observed a strong diurnal variation in the total electron content of the

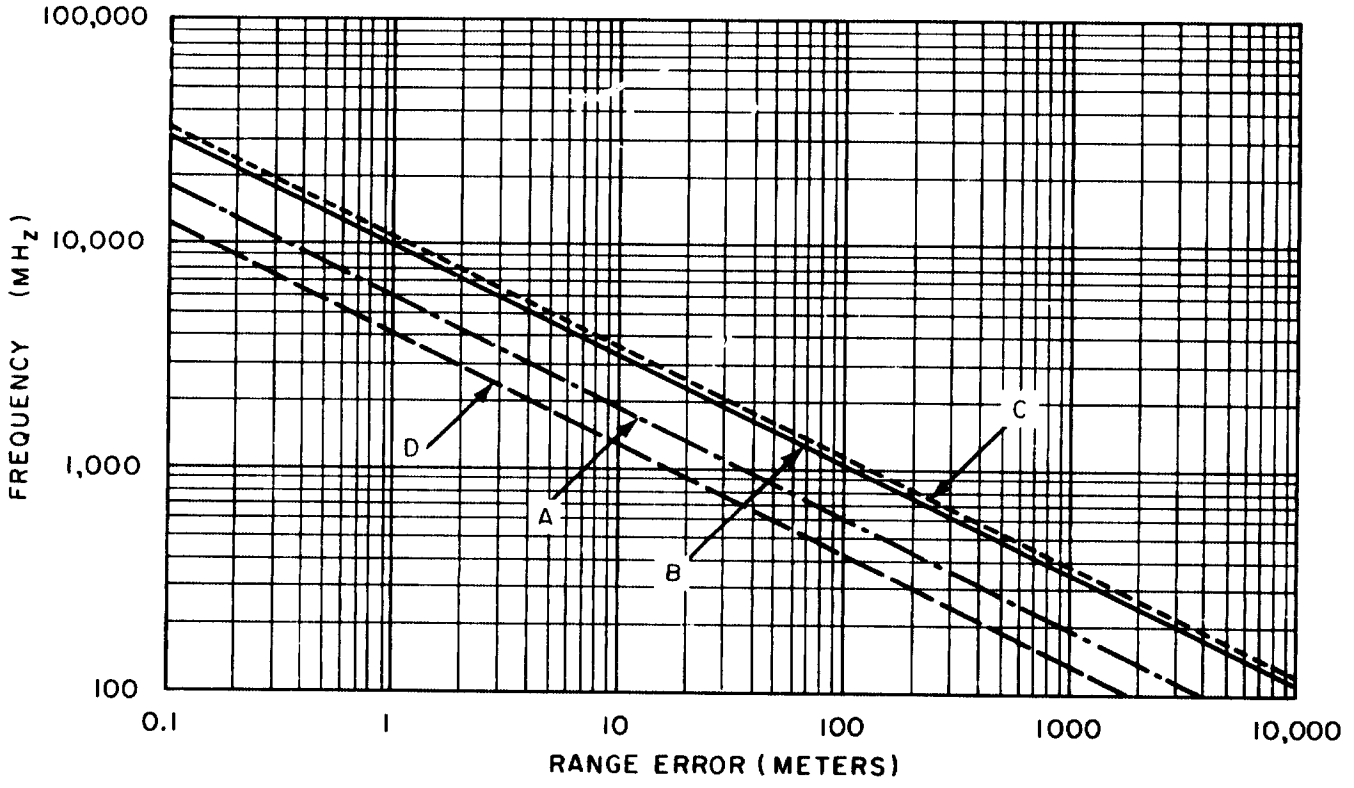

Figure A-3—Ionospheric Range Error for 0° Elevation and Various Integrated Electron Densities.

Table A-3
Ionospheric Range Error at 0° Elevation Angle, Various Integrated Electron Densities, and Frequencies

Frequency f (MHz)	DAYTIME			MIDNIGHT
	A Average Value $\int N_e dh = 2.4 \times 10^{17}$ el/m²	B Mean Value $\int N_e dh = 6.9 \times 10^{17}$ el/m²	C Maximum Value $\int N_e dh = 8.5 \times 10^{17}$ el/m²	D Mean Value $\int N_e dh = 1.1 \times 10^{17}$ el/m²
	ΔR (meters)	ΔR (meters)	ΔR (meters)	ΔR (meters)
100	3,640	10,200	12,700	1,670
136	1,960	5,650	6,860	902
200	910	2,620	3,182	418
400	228	657	798	105
500	154	447	539	71
800	56.8	164	199	26
1,000	36.4	102	127	16.7
1,500	16.2	46.7	56.7	7.5
2,000	9.1	26.2	31.8	4.2

Ionospheric range error for different elevation angles ψ can be computed from the above data using the following relation,

$$\Delta R_{\psi} = k \, \Delta R_{(\psi=0)}$$

where

$$k = \frac{0.268}{\sqrt{1 - 0.928 \cos^2 \psi}}$$

ψ°	15	25	35
k	0.74	0.55	0.44

ionosphere. There is agreement that the daytime peak (early afternoon) is six to eight times greater than the nighttime minimum.

As might be expected, the highest values for the integrated electron density occur in the early afternoon with a range of 5.5×10^{17} to 8.5×10^{17} electrons per square meter (satellite height between 1227 and 1350 km). A typical mean value of the integrated electron density at midnight is 1.1×10^{17} electrons per square meter[11, 12]. Reference (13) gives the integrated electron density as a function of time of day measured on Sputnik III. An average value of the integrated electron density is shown to be about 2.4×10^{17} electrons per square meter, with a maximum value of approximately 8×10^{17} electrons per square meter, depending on the time of day.

It is evident that the ionospheric range error is a maximum during the daytime. The major portion of the time delay occurs below an altitude of 500 km. At 200 MHz, for a one-way transmission path, the maximum error (Figure A-3, Curve A) ΔR is on the order of 910 meters. This value is approximately eight times larger than the maximum error introduced by the troposphere. At a frequency of about 580 MHz the tropospheric and ionospheric contributions to the propagational time delays are of the same order of magnitude. Above 580 MHz the tropospheric error is predominant.

IV. TROPOSPHERIC RANGE-RATE ERROR

The one way range error, ΔR, due to the troposphere was

$$\Delta R = \int_1^2 (n - 1)\, ds. \tag{6}$$

The tropospheric refraction contribution to the Doppler shift of the signal received from a passing satellite for a transmitter frequency f is;

$$\Delta f_{tro} = -\frac{f}{c}\left[\frac{\partial(\Delta R)}{\partial t}\right] = -\frac{f}{c}\dot{\Delta R}, \tag{15}$$

where Δf_{tro} = tropospheric Doppler frequency error,

$$\frac{\partial(\Delta R)}{\partial t} = \Delta\left(\frac{\partial R}{\partial t}\right) = \Delta\dot{R} = \text{range-rate error},$$

$$\frac{\partial R}{\partial t} = \dot{R} = \text{range-rate},$$

$$c = \text{speed of light}.$$

The computed refraction contributions to the Doppler shift produced by the troposphere, as shown in Table A-4, has been derived from the observed data by Hopfield[14]. Table A-4 indicates that the tropospheric Doppler frequency error decreases very rapidly with increasing elevation angle.

V. IONOSPHERIC RANGE-RATE ERROR

The ionospheric range error ΔR was

$$\Delta R = \frac{1.6 \times 10^3}{(2\pi f)^2} \int_1^2 N_e \, ds. \tag{12}$$

Similar to Δf_{tro}, by using (12) and (13), we can write for the ionospheric Doppler error Δf_{ion},

$$\Delta f_{ion} = -\frac{f}{c}\Delta\dot{R} = -\frac{1.6 \times 10^3 \left[\frac{\partial}{\partial t}\int N_e \, dh\right]}{(2\pi)^2 \, f \, c(1 - 0.928 \cos^2 \psi)^{1/2}} \tag{16}$$

In (16), Δf_{ion}, the ionospheric Doppler frequency error, is at maximum during the daytime and at low elevation angles. The ionospheric Doppler frequency error is inversely proportional to frequency.

Table A-4

Maximum Ionospheric and Tropospheric Doppler Errors (Δf) and Range-Rate Errors ($\Delta \dot{R}$):

IONOSPHERE

Frequency 136 MHz	ELEVATION ANGLE (degrees)					
	0	5	15	25	35	70
Doppler Error Δf_{ion} (c/s)	28	26.3	20.7	15.4	12.30	7.98
Range-Rate Error $\Delta \dot{R}$ (meters/sec)	62	58	45.7	34	27.10	17.60
Frequency 1,500 MHz	ELEVATION ANGLE (degrees)					
	0	5	15	25	35	70
Doppler Error Δf_{ion} (c/s)	2.34	2.2	1.74	1.3	1.03	0.67
Range-Rate Error $\Delta \dot{R}$ (meters/sec)	0.47	0.43	0.35	0.26	0.21	0.13

TROPOSPHERE

Frequency 136 MHz	ELEVATION ANGLE (degrees)					
	0	2	5	8	15	
Doppler Error Δf_{tro} (c/s)	0.88	0.38	0.13	0.06	0.025	
Range-Rate Error $\Delta \dot{R}$ (meters/sec)	1.96	0.83	0.28	0.14	0.05	
Frequency 1,500 MHz	ELEVATION ANGLE (degrees)					
	0	2	5	8	15	
Doppler Error Δf_{tro} (c/s)	9.8	4	1.4	0.7	0.27	
Range-Rate Error $\Delta \dot{R}$ (meters/sec)	1.96	0.8	0.28	0.14	0.05	

A study and an experimental investigation of the behavior of ionospheric contributions to the Doppler shift was done at the University of Texas[15]. The purpose of this study was to present experimental data which illustrate the separation of frequency dependent refraction errors. The experimental data gave evidence of the presence of ionospheric refraction errors of unusually high magnitude.

The data in Table A-5 are derived from this study by assuming the maximum observed values of total refraction error, first order refraction error, and third order refraction error, 27, 18.5, and 10 Hz respectively (referenced to 54 MHz).

The values of Table A-5 exceed previous estimates by a substantial amount[16,17]. During periods where the ionosphere is not seriously disturbed, the magnitude of the various ionospheric contributions to the Doppler shift are most likely a factor of 3 to 10 lower.

Table A-5

Maximum Ionospheric Doppler Errors (Range-Rate Errors)

Elevation Angle $\psi = 0°$	FREQUENCY (MHz)								
	54	100	136	150	324	400	1,000	1,500	2,000
Doppler Error Δf_{ion} (c/s)	100	40.5	28	24.8	11	8.8	3.5	2.34	1.75
Range-Rate Error $\Delta\dot{R}$ (meters/sec)	552	121.5	62	49.7	10.18	6.67	1.15	0.47	0.26

Elevation Angle $\psi = 70°$	FREQUENCY (MHz)								
	54	100	136	150	324	400	1,000	1,500	2,000
Doppler Error Δf_{ion} (c/s)	28.5	11.57	7.98	7.1	3.13	2.52	1.01	0.67	0.5
Range-Rate Error $\Delta\dot{R}$ (meters/sec)	158	34.70	17.60	14.20	2.90	1.90	0.30	0.13	0.07

The maximum range-rate error due to the ionosphere for 0°, 25° and 70° elevation angles versus frequency can be seen in Figure A-4.

Figure A-5 shows a comparison of tropospheric and ionospheric range-rate errors versus elevation angle at 136 MHz and 1,500 MHz. It can be seen that at a frequency of 1,500 MHz or higher the tropospheric range-rate error will predominate by a factor of approximately four or more for an elevation angle of zero; but with increasing elevation angle the tropospheric range-rate error falls off quite rapidly. As seen in Figure A-5, the tropospheric range-rate errors at 136 MHz and 1,500 MHz are the same because they are frequency independent.

Errors in range and range-rate measurements caused by propagation effects through the atmosphere are to some extent computable errors and, therefore, reducible errors. The extent to which the error is reducible depends on how accurately the tropo- and ionospheric characteristics are known over the region of interest. It is well known that seasonal day-to-day and diurnal variations in the integrated electron density occur, so that continuous monitoring would be required.

At the present, only the tropospheric refractivity profile is known with sufficient accuracy to permit adjustment of error data.

Models based on average daytime and nighttime ionospheric electron density profiles are useful in estimating average biasing effects which can be attributed to the ionosphere. However, correction procedures based on use of ionospheric profiles have not proved very accurate and may not lead to significant reductions in error[6]. The inability to predict the error encountered at a given time indicates that accurate systems must operate at frequencies high enough to reduce the initial values of ionospheric error to a tolerable value.

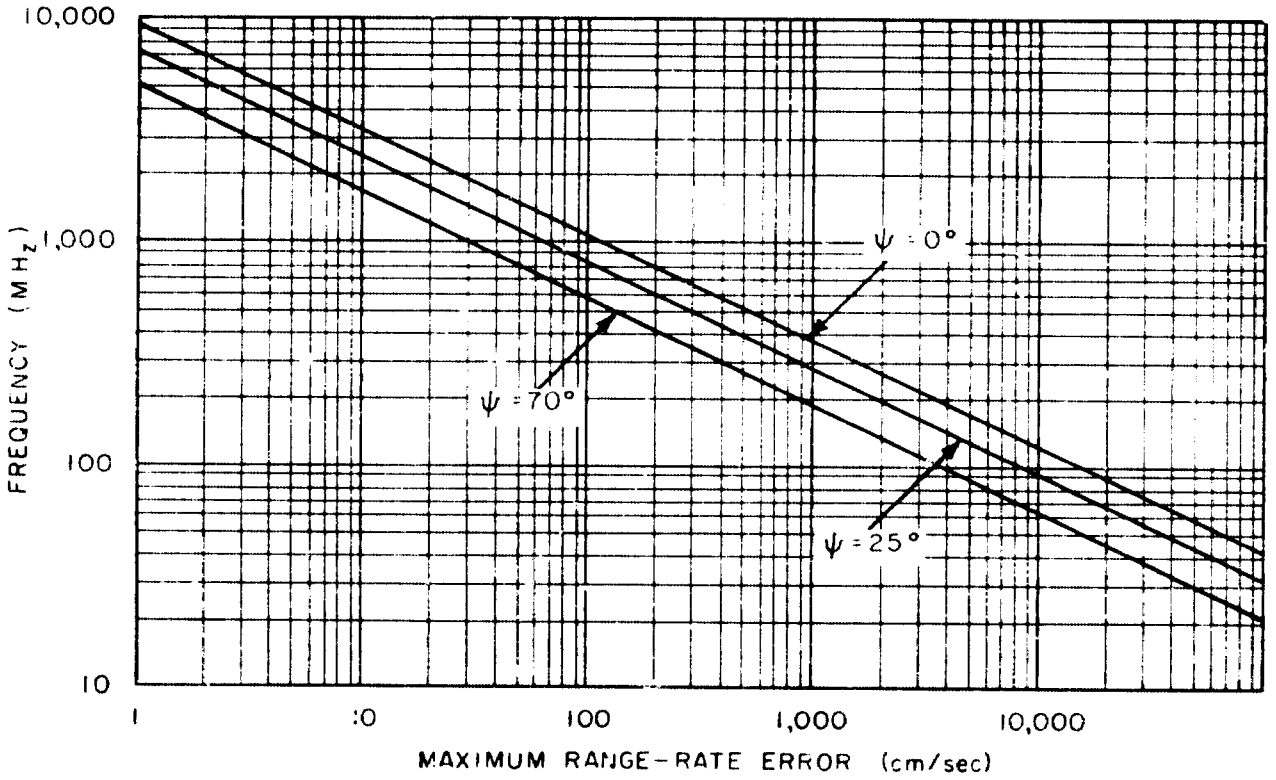

Figure A-4—Ionospheric Maximum Range-Rate Error for 0°, 25° & 70° Elevation Angle.

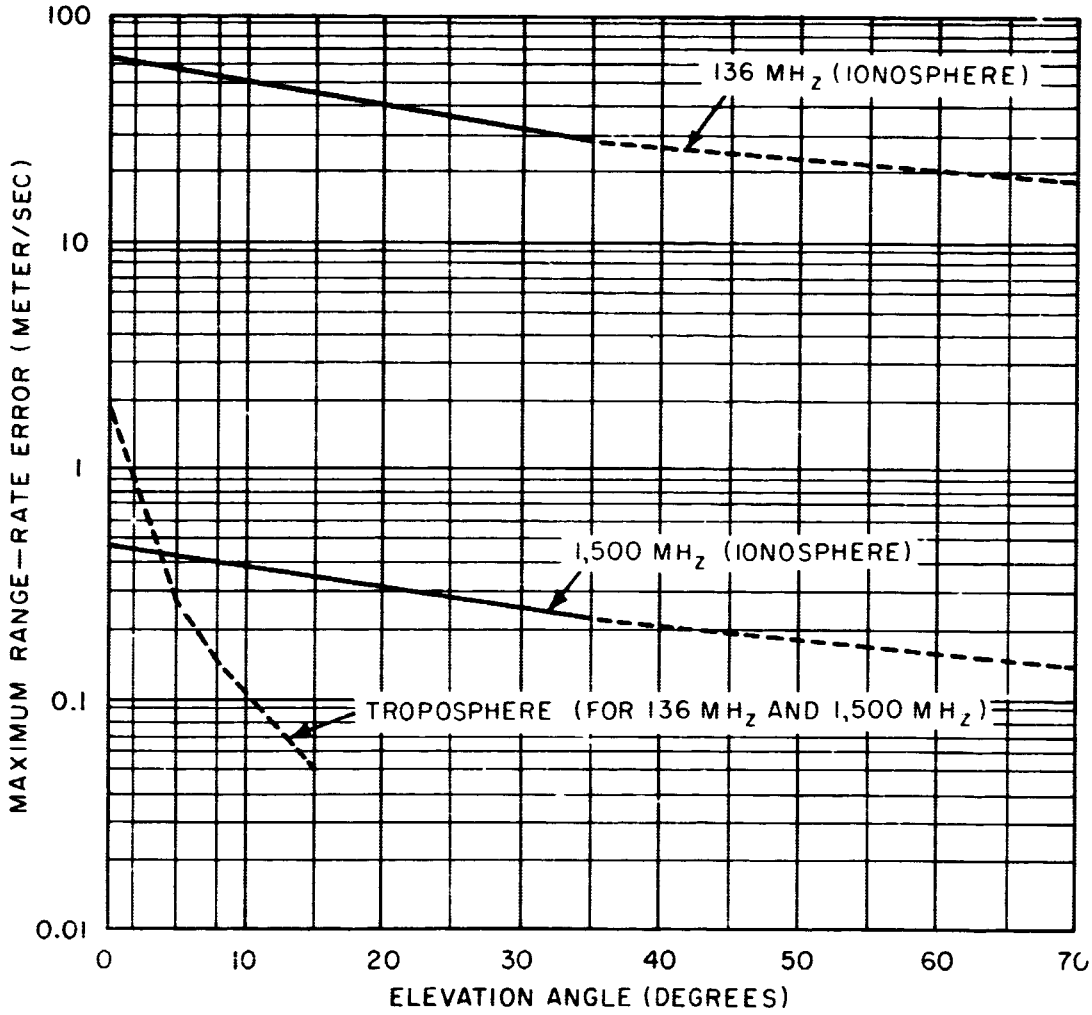

Figure A-5–Comparison of Tropospheric and Ionospheric Range-Rate Error Vs. Elevation Angle (at 136 MHz and 1,500 MHz).

REFERENCES

1. Anway, A. C., "Empirical Determination of Total Atmospheric Refraction at Centimeter Wave Lengths by Radiometric Means," NBS J. Res., Ser. D, 67 D(2):153-160, March-April, 1963.

2. Bean, B. R., and Thayer, G. D., "Comparison of Observed Atmospheric Radio Refraction Effects with Values Predicted Through Use of Surface Weather Observations," NBS J. Res. Ser. D, 67D(3):273-285, May-June 1963.

3. Bean, B. R., and Thayer, G. D, "CRPL Exponential Reference Atmosphere," NBS, Monograph, No. 4, October 29, 1959.

4. Smith, E. K., and Weintraub, S., "The Constants in the Equation for Atmosphere Refractive Index at Radio Frequencies," IRE Proc., 41, 1035-1037, 1953.

5. Bean, B. R., and Thayer, G. D., "A Model Radio Refractive Atmosphere," NBS, U.S., Rept. 5576 (Boulder Laboratories), June 9, 1958.

6. Schmid, P. E., "Atmospheric Tracking Errors at S- and C-Band Frequencies," NASA TN D-3470, August 1966.

7. Berkowitz, S. B., "Modern Radar," pp. 341-342, Fig. 1-12 and Fig. 1-13, John Wiley & Sons, Inc., N.Y., (1965).

8. Straiton, A. W., "Measurement of the Radio Refractive Index of the Atmosphere," in Advances in Radio Research, Vol. 1, ed. by J. A. Saxton, London: Academic Press 1964, pp. 2-50.

9. Lawrence, R. S., Little, C. G., and Chivers, H. J. A., "A Survey of Ionospheric Effects Upon Earth-Space Radio Propagation," IEEE Proc., Vol. 52, Jan. 1964, pp. 4-26.

10. Hughes Aircraft Company, Report R-73, Oct. 1958, "Technological Considerations Concerning Satellite Communication Systems."

11. Hame, T. G., and Stuart, W. D., "The Electron Content and Distribution in the Ionosphere," IRE Proc., Vol. 48, Mar. 1960, pp. 364-365.

12. Garriott, O. K., and Smith, F. L., "Observations of Ionospheric Electron Content Using a Geostationary Satellite" (Syncom III), Planet. Space Sci., 1965, Vol. 13, pp. 829-838, Pergamon Press, Ltd., Printed in North Ireland.

13. Garriott, O. K., "The Determination of Ionospheric Electron Content and Distribution from Satellite Observations," J. Geophys. Res., Vol. 65, 1960, pp. 1151-1157.

14. Hopfield, H. S., "The Effect of Tropospheric Refraction on the Doppler Shift of a Satellite Signal," Geophys. Res., Vol. 68, Sept. 15, 1963, pp. 5157-5168.

15. Willman, J. F., "Frequency-Dependent Ionospheric Refraction Effects on the Doppler Shift of Satellite Signals," IEEE Trans. on Aerospace and Electronic Systems, Dec. 1965, pp. 283-289.

16. Guier, W. H. and Weiffenbach, G. C., "A Satellite Doppler Navigation System," IRE Proc., Vol. 48, Apr. 1960, pp. 513, Table II.

17. Guier, W. H., "Ionospheric Contributions to the Doppler Shift at VHF from Near-Earth Satellites," IRE Proc., Vol. 49, Nov. 1961, pp. 1681, Table I.

APPENDIX B

COHERENT PHASE DEMODULATION

I. INTRODUCTION

A number of approaches exist to the reception of angle-modulated signals which are below the threshold of conventional demodulators. One approach to threshold-reduction is to construct signal-tracking demodulators using phase-locked loops. This technique partially eliminates the effect of the noise components whose frequencies differ from the instantaneous frequency of the signal by more than a predetermined amount. That is, the expected square error between the modulating signal and the signal-tracking demodulator estimate of the modulating signal is minimized.

The purpose of this paper is to consider the communication system which is illustrated in simplified form in Figure B-1. In either case shown, it is assumed that the modulated signal has been constructed so that a sufficient carrier component is present to permit adequate tracking of the carrier by the phase-locked demodulator. Also, the modulating spectrum is not allowed to have significant energy at very low frequencies so that the modulated spectrum does not extend into the equivalent tracking bandwidth about the carrier frequency. If the effective closed-loop bandwidth of the carrier-tracking loop is very small compared with the bandwidth of the received signal and noise, r (t), (shown in Figure B-2) will be an essentially noise-free copy of the received carrier both in frequency and in phase.

Under the above conditions, the system of Figure B-2(a) can be further simplified to that of Figure B-2(b) where the input signal is multiplied by the carrier coherent VCO output, r (t). Thus, the equivalent receiving system is simply a synchronous detector and if the power spectrum associated with y(t) is centered about the carrier frequency, f_c, the result is a linear translation and folding over of the received signal to zero frequency. If the received signal is perturbed by the presence of narrowband additive noise with a power spectrum centered at f_c, the noiseband will also be linearly translated to zero frequency and folded over. Therefore, the assumed receiving system produces an output signal-to-noise ratio (SNR) which is a linear function of the SNR at the input to the demodulator for all values of the latter so long as the conditions imposed on the carrier tracking loop are satisfied.

This being the case, it is at least heuristically evident that while the receiving system described above does not exhibit a threshold characteristic in

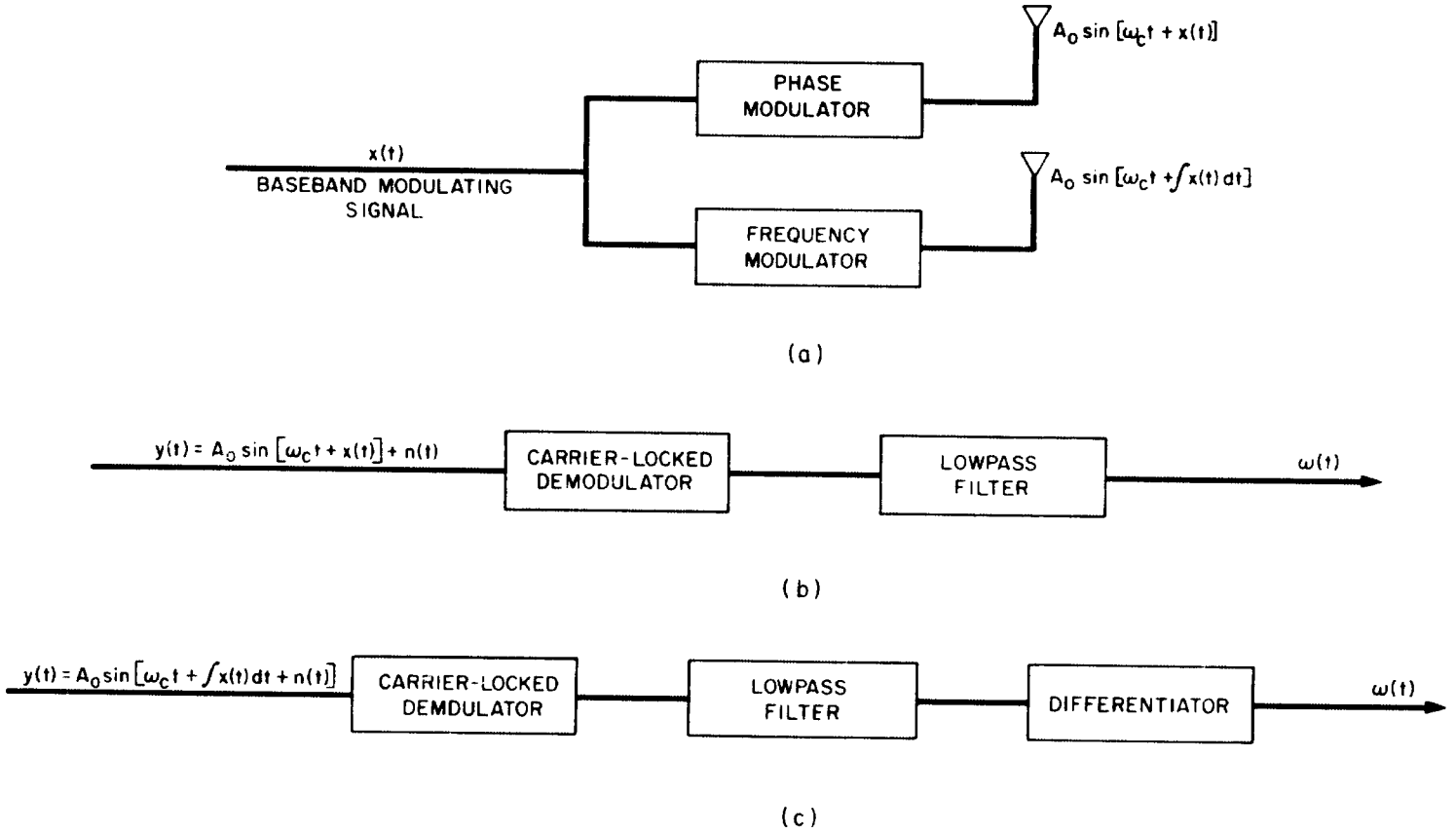

Figure B-1–Functional diagram of the communication system. (a) Modulators. (b) Phase demodulator. (c) Frequency demodulator.

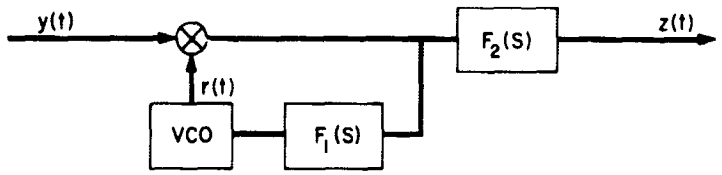

(a)

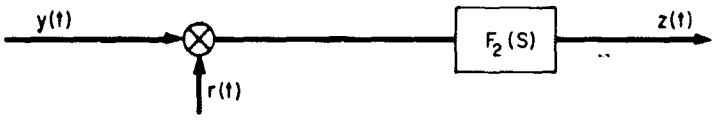

(b)

Figure B-2–(a) Functional diagram of the carrier-locked demodulator. (b) Simplified equivalent diagram.

the conventional sense, neither does it provide a demodulation improvement factor in the usual sense. That is, the possibility of obtaining an improved output SNR in exchange for channel bandwidth has been obviated and one must look elsewhere for any potential advantages that the system may hold.

It is well known that for small values of the mean square modulating signal, x(t), that the spectrum of y(t) approaches that of a sinusoid amplitude modulated by the same signal, x(t).[1] The applicability of the assumed receiving system under this condition is obvious and the relative performance of such a system compared with an equivalent amplitude-modulation system is easily calculated. However, as the amplitude of x(t) is increased, the modulating operation becomes an increasingly nonlinear one. If the resulting modulated spectrum can be represented by a series expansion containing a component which is linear with the modulating signal along with higher-ordered components, the most that one could hope to do with the linear receiving system described above is to recover the linear component and accept all the higher-ordered components as interference.

If this technique is to offer any advantage at all, then it will have to be as a result of the amount of power that can be packed into the first-order modulation

[1] See e.g. Stewart [1].

component compared with the higher-ordered components. Practical systems using these ideas have been demonstrated and Martin[2] has presented an analysis based on a deterministic modulating signal consisting of unmodulated subcarriers. Martin's analysis indicates that for a frequency-division-multiplex system (FDM), consisting of a limited number of subchannels, that a significant improvement may be obtained using phase modulation (FDM/PM) over a comparable amplitude-modulation system (FDM/AM). Unfortunately, his analysis does not consider a general case with random modulating signals and the effect of the higher-ordered interference components is completely neglected. However, Martin does provide a number of practical guidelines which he states have been experimentally verified and which are in agreement with the results presented here.

II. GENERAL ANALYSIS

In the analysis which follows, it is assumed that the power spectrum of the baseband modulating signal is a member of a Gaussian ensemble and hence that all its statistical properties are derivable from its second moments. We shall use both the auto-correlation function, $R_\zeta(\tau)$, of a sample from the time ensemble given by

$$R_\zeta(\tau) = \langle \zeta(t) \cdot \zeta(t+\tau) \rangle = \frac{1}{2\pi} \int_{-\infty}^{\infty} S_\zeta(f)\, e^{i\omega\tau}\, d\omega, \tag{1}$$

and its corresponding power spectrum as

$$S_\zeta(f) = \int_{-\infty}^{\infty} R_\zeta(\tau)\, e^{i\omega\tau}\, d\tau. \tag{2}$$

The power spectrum, being proportional to the mean square response of a filter of bandwidth df centered at f when $\zeta(t)$ is applied as an input, will be assumed to have limited total fluctuation so that $\zeta(t)$ is restricted to be free from both dc and sinusoidal components.

To begin, we write the received signal as

$$y(t) = A_0 \cos\,[\omega_c(t) - x(t)]. \tag{3}$$

Here, $\omega_c = 2\pi f_c$ is the fixed-carrier radian frequency, A_0 is the peak amplitude, and in the case of phase modulation, the angle of y (t) varies directly with the message x (t) while with frequency modulation, the message is the derivative of x (t) or $\dot{x}(t)$. We form z (t) by multiplying y (t) by the sinusoid r (t) = 2 sin $\omega_c t$. After expanding the product and selecting the video component by means of $F_2(s)$, there remains the remarkably simple result,

$$z(t) = A_0 \sin x(t). \tag{4}$$

The autocorrelation function corresponding to z (t) for a typical sample from the modulating ensemble is

$$R_z(\tau) = \langle z(t) \cdot z(t+\tau) \rangle$$

$$= \lim_{T\to\infty} \frac{A_0^2}{T} \int_{-T/2}^{T/2} \sin x(t) \sin x(t+\tau)\, dt. \tag{5}$$

By expanding (5) we obtain

$$R_z(\tau) = \frac{A_0^2}{2} \left\{ \langle \cos [x(t+\tau) - x(t)] \rangle - \langle \cos [x(t+\tau) + x(t)] \rangle \right\}$$

which is easier to handle in the following form.

$$R_z(\tau) = \frac{A_0^2}{2} \left\{ \mathrm{Re} \langle \exp i [x(t+\tau) - x(t)] \rangle - \mathrm{Re} \langle \exp i [x(t+\tau) + x(t)] \rangle \right\} \tag{6}$$

Since the random properties of the received signal derive from those of the message, our immediate goal is to reduce (6) to a form which relates the autocorrelation for z (t) to that of x (t). The steps necessary to accomplish this are rather lengthy and so they will not be done in detail here. However, the following outline of one approach to the problem is offered in the hope that it will provide some clarity to what follows.

Consider first the expectation in (6) given by

$$\langle \exp i\,(y_1 - y_2) \rangle \tag{7}$$

where y_1 has been written in place of $x(t + \tau)$ and y_2 in place of $x(t)$. Equation (7) can be compared directly with the definition of the bivariate joint characteristic function which is the two dimensional Fourier transform of the joint probability density function of the random variables* y_1 and y_2. That is,

$$M(v,u) = \langle \exp i\,(vy_1 + uy_2) \rangle$$

$$= \int_{-\infty}^{\infty} \int \exp i\,(vy_1 + uy_2)\, p(y_1, y_2)\, dy_1\, dy_2, \tag{8}$$

where

$$p(y_1, y_2) = \frac{1}{2\pi A} \exp\left[-\sigma_2^2\, y_1^2 + \sigma_1^2\, y_2^2 - 2\mu_{11}\, y_1\, y_2\right] / 2A^2. \tag{12}$$

In (12), A has been written for $\sigma_1^2\,\sigma_2^2 - \mu_{11}$ and μ_{11} is the convariance of y_1 with y_2.

We now note that (7) is the bivariate characteristic function evaluated at $v = 1$, $u = -1$. Thus,

$$M(1, -1) = \langle \exp i\,(y_1 - y_2) \rangle$$

$$= \exp\left[-\frac{1}{2}(\sigma_1^2 - 2\mu_{11} + \sigma_2^2)\right] \tag{13}$$

$$= \exp\left[-R_x(0) + R_x(\tau)\right]$$

*See e.g. [6], eqs. 8-12 and 8-23.

where the relations $\sigma_1^2 = \sigma_2^2 = R_x(0)$ and $\mu_{11} = R_x(\tau)$ have been used. In a completely analogous way, we can evaluate the second expectation in (6) to obtain

$$\langle \exp i (y_1 + y_2) \rangle = \exp [-R_x(0) - R_x(\tau)] . \tag{14}$$

Note that both (13) and (14) are entirely real which is a direct consequence of the assumptions that have been made regarding x (t). Now, (6) can be simplified to the following form by use of (13) and (14).

$$R_z(\tau) = \frac{A_0^2}{2} \exp [-R_x(0)] \left\{ \frac{\exp [R_x(\tau)] - \exp [-R_x(\tau)]}{2} \right\} \tag{15}$$

Using the identity,

$$\frac{e^z - e^{-z}}{2} = \sum_{n=1}^{\infty} \frac{z^{2n-1}}{(2n-1)!} ,$$

equation (15) becomes

$$R_z(\tau) = R_y(0) \exp [-R_x(0)] \sum_{n=1}^{\infty} \frac{[R_x(\tau)]^{2n-1}}{(2n-1)!} \tag{16}$$

where $R_y(0)$ has been written for $A_0^2/2$. The spectrum of z (t), $S_z(f)$ is found by substituting (16) into (2) and taking the term by term transform. The result is,

$$S_z(f) = R_y(0) \exp [-R_x(0)] \sum_{\substack{k=1 \\ (k \text{ odd})}}^{\infty} \frac{{}_kS_x(f)}{k!} , \tag{17}$$

where

$$ {}_kS_x(f) = \mathfrak{F}\left\{[R_x(\tau)]^k\right\} = \int_{-\infty}^{\infty} [R_x(\tau)]^k \cos \omega\tau \, d\tau. $$

III. MODULATION WITH A RECTANGULAR POWER SPECTRUM

To proceed further, we need a specific expression for the autocorrelation function of the modulating signal x (t). The rectangular power spectrum previously discussed and with parameters indicated in Figure B-3(a) permit us to write

$$ S_x(f) = \begin{cases} h & |f| < a \\ 0 & \text{otherwise} \end{cases} $$

$$ R_x(\tau) = h \int_{-a}^{a} e^{i2\pi f\tau} \, df = R_x(0) \frac{\sin u}{u} \qquad (18) $$

where the substitution $u = 2\pi a\tau$ has been made and the relationship $R_x(0) = 2ah$ has been used.

Examination of (16) and (17) shows that the detected signal is composed of a component which is linearly related to the modulating signal in addition to a sum of terms of higher orders. Equation (17) further shows that the higher-order terms involve multiple convolutions and therefore the total power associated with these terms is effectively interference noise. If we write the sum of these terms as

$$ I[f, R_x(0)] = R_y(0) \exp[-R_x(0)] \sum_{\substack{k=3 \\ (k \text{ odd})}}^{\infty} \frac{{}_kS_x(f)}{k!}, \qquad (19) $$

we can define a signal-to-interference power density ratio as

$$\frac{S}{I} = \frac{[S_z(f)]_{k=1}}{I[f, R_x(0)]} = \frac{S_x(f)}{\sum_{\substack{k=3 \\ (k\ \text{odd})}}^{\infty} \frac{{}_kS_x(f)}{k!}} \tag{20}$$

To make use of this definition, we must further evaluate (19). To this end, we write (19) as

$$I[f, R_x(0)] = Q \sum_{\substack{k=3 \\ (k\ \text{odd})}}^{\infty} \frac{\mathfrak{F}\{[R_x(\tau)]^k\}}{k!} \tag{21}$$

where Q has been substituted for $R_y(0) \exp[-R_x(0)]$ to reduce the notation. Using (18) in (21) and after some further manipulation we obtain

$$I[f/a, R_x(0)] = \frac{Q}{2\pi a} \sum_{\substack{k=3 \\ (k\ \text{odd})}}^{\infty} \frac{[R_x(0)]^k}{k!} \int_{-\infty}^{\infty} \left(\frac{\sin u}{u}\right)^k \cos(f/a)\, u\, du. \tag{22}$$

We will now evaluate the signal-to-interference power density ratio at the band limits by letting $f/a = 0$ and $f/a = 1$. To this end, we define

$$B_k = \int_{-\infty}^{\infty} \left(\frac{\sin u}{u}\right)^k du \tag{23}$$

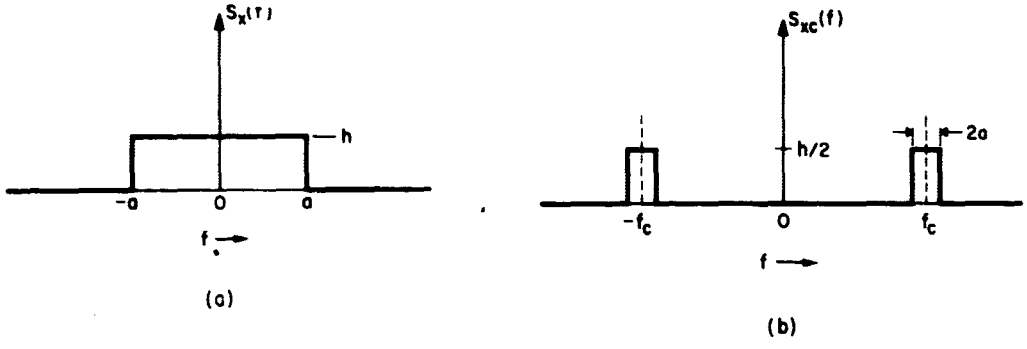

Figure B-3–Intensity spectra of the modulating signals. (a) Low pass case. (b) Narrow-band case.

and

$$C_k \equiv \int_{-\infty}^{\infty} \left(\frac{\sin u}{u}\right)^k \cos u \, du, \tag{24}$$

so that the interference power density at the band limits can be simplified to

$$I\,[0, R_x(0)] = \frac{Q}{2\pi a} \sum_{\substack{k=3 \\ (k \text{ odd})}}^{\infty} \frac{[R_x(0)]^k}{k!} B_k \tag{25}$$

and

$$I\,[1, R_x(0)] = \frac{Q}{2\pi a} \sum_{\substack{k=3 \\ (k \text{ odd})}}^{\infty} \frac{[R_x(0)]^k}{k!} C_k \tag{26}$$

As noted by Lewin[7], a very good approximation for B_k is

$$B_k \approx \frac{\pi k}{2(k-1)} . \tag{27}$$

Equation (27) is exact for k between 2 and 4 inclusive, and only becomes significantly in error for k = 8 and greater.

Now, by integrating (24) by parts, it is not difficult to show that

$$\int_{-\infty}^{\infty} \left(\frac{\sin x}{x}\right)^n \cos x \, dx = \left(\frac{n}{n+1}\right) \int_{-\infty}^{\infty} \left(\frac{\sin x}{x}\right)^{n+1} dx . \tag{28}$$

Therefore, a useful relation between B_k and C_k is found to be

$$C_k = \left(\frac{k}{k+1}\right) B_{k+1} \tag{29}$$

Substituting (27) into (25) and (29) into (26) provides the result that

$$I[0, R_x(0)] \approx \frac{Q}{4a} \sum_{\substack{k=3 \\ (k \text{ odd})}}^{\infty} \frac{k}{(k-1)\,k!} [R_x(0)]^k \tag{30}$$

and

$$I[1, R_x(0)] \approx \frac{Q}{4a} \sum_{\substack{k=3 \\ (k \text{ odd})}}^{\infty} \frac{[R_x(0)]^k}{k!} \tag{31}$$

Returning to Equation (20), we can substitute the pair of Equations (30) and (31) to obtain

$$\frac{S}{I} \approx \frac{2R_x(0)}{\sum_{\substack{k=3 \\ (k \text{ odd})}}^{\infty} \frac{k}{(k-1)k!} [R_x(0)]^k} \approx \frac{8}{R_x^2(0) + R_x^4(0)/24} \tag{32}$$

for frequencies near zero and

$$\frac{S}{I} \approx \frac{2R_x(0)}{\sum_{\substack{k=3 \\ (k \text{ odd})}}^{\infty} \frac{1}{k!} [R_x(0)]^k} \approx \frac{12}{R_x^2(0) + R_x^4(0)/20} \tag{33}$$

for frequencies near the upper band edge. The second approximation in the above two equations utilize only the first two terms of the series representing the interference. Keeping in mind that Equation (27) is exact for $k = 3$ and very nearly so for $k = 5$, it is easily verified that (32) and (33) are very good approximations for the range of $R_x(0)$ of interest as plotted in Fig. B-4. For small $R_x(0)$, (32) becomes $8/R_x(0)^2$ and (33) becomes $12/R_x(0)^2$ which establishes the lower asymptotes in Fig. 4.

IV. MODULATION WITH A NARROW-BAND RECTANGULAR POWER SPECTRUM

The parameters for the assumed narrowband Gaussian modulating signal are indicated in Fig. B-3(b) and in the following description of $S_{xc}(f)$.

$$S_{xc}(f) = \begin{cases} h/2 & |f - f_c| < 2a \\ 0 & \text{otherwise} \end{cases} \tag{34}$$

In (34) the extra subscript has been added to indicate that the spectrum of interest is now centered about some frequency f_c and further, it is required that the bandwidth 2a be small compared with f_c.

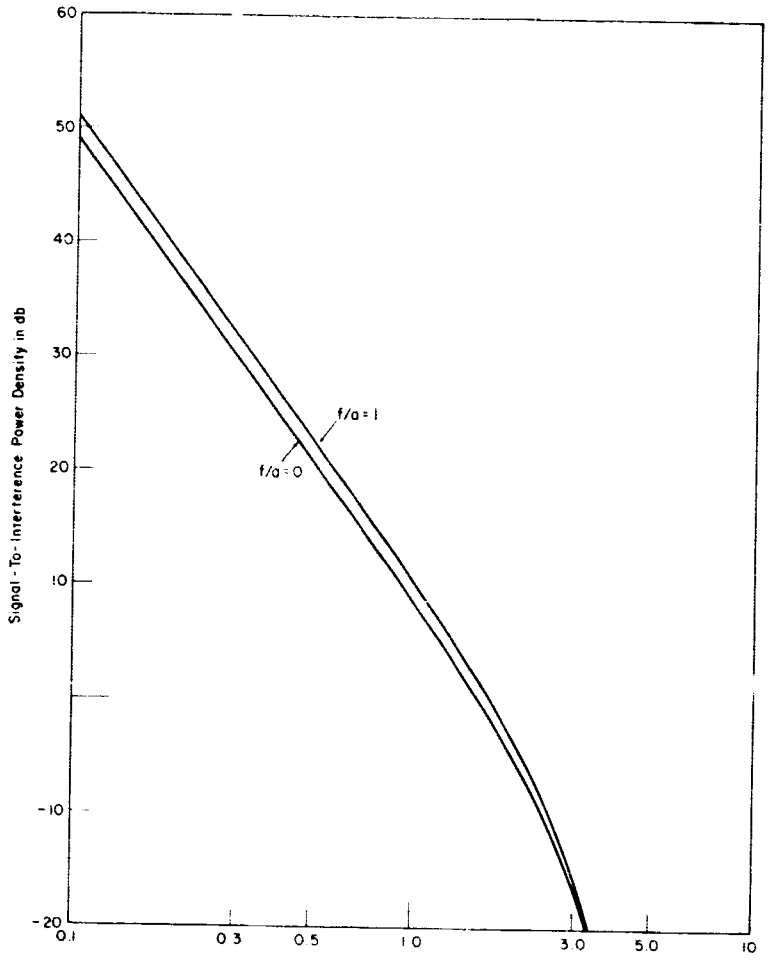

Figure B-4

In a straightforward manner, we can obtain $R_{xc}(\tau)$ as

$$R_{xc}(\tau) = \frac{h}{2} \int_{-\infty}^{\infty} e^{i\omega\tau} \, d\tau = R_x(\tau) \cos w_c \tau. \qquad (35)$$

Thus,

$$ {}_kS_{xc}(f) = \mathfrak{F}\{[R_{xc}(\tau)]^k\} = \mathfrak{F}\{[R_x(\tau)]^k\} * \mathfrak{F}\{[\cos w_c \tau]^k\} $$

$$ = {}_kS_x(f) * \left\{ \frac{1}{2^n} \sum_{i=0}^{n} \binom{n}{i} \delta[f - (n - 2i) f_c] \right\}. \tag{36} $$

and for the special case of $k = 2$, (36) reduces to

$$ {}_2S_{xc}(f) = \frac{1}{2} {}_2S_x(f) + \frac{1}{4} {}_2S_x(f - 2f_c) + \frac{1}{4} {}_2S_x(f + 2f_c) $$

which is sketched in Fig. B-5. The situation for $k = 3$, 4 and 5 are also sketched in Fig. 5.

For the assumed narrowband case, $F_2(s)$ can be selected to pass only components with frequencies near f_c and the factor within the braces in (36) can be reduced to

$$ \frac{1}{2^n} D_n [\delta(f + f_c) + \delta(f - f_c)] $$

where

$$ D_n = \begin{cases} \binom{n}{\frac{n-1}{2}} & \text{for n an odd positive integer} \\ 0 & \text{for n an even positive integer.} \end{cases} $$

Now, equations corresponding to (32) and (33) for the narrowband modulating signal can be written as below;

$$\frac{S}{I} \approx \frac{2R_x(0)}{\sum_{\substack{k=3 \\ (k\ \text{odd})}}^{\infty} \frac{1}{2^k} \frac{k}{(k-1)k!} \left(\frac{k}{\frac{k-1}{2}}\right) [R_x(0)]^k} \approx \frac{64/3}{R_x^2(0) + \frac{5}{144} R_x^4(0)} \tag{37}$$

for frequencies near the center of the modulating band and

$$\frac{S}{I} \approx \frac{2R_x(0)}{\sum_{\substack{k=3 \\ (k\ \text{odd})}}^{\infty} \frac{1}{2^k} \frac{1}{k!} \left(\frac{k}{\frac{k-1}{2}}\right) [R_x(0)]^k} \approx \frac{32}{R_x^2(0) + \frac{1}{24} R_x^4(0)} \tag{38}$$

for frequencies near the band edges. The right-hand approximations in (37) and (38) result from using the first two terms in the denominators of the middle expressions. Again it is easily verified that (38) and (39) are excellent approximations for the range of $R_x(0)$ of interest as plotted in Fig. B-6. The asymptotes for small $R_x(0)$ are $64/3R_x^2(0)$ for (37) and $32/R_x^2(0)$ for (38).

V. MODULATION WITH AN FDM SIGNAL

When the modulating signal is a frequency-division-multiplexed (FDM) signal comprised of more than one subchannel, a complete prediction of the performance that can be expected becomes difficult to obtain. However, it is possible to

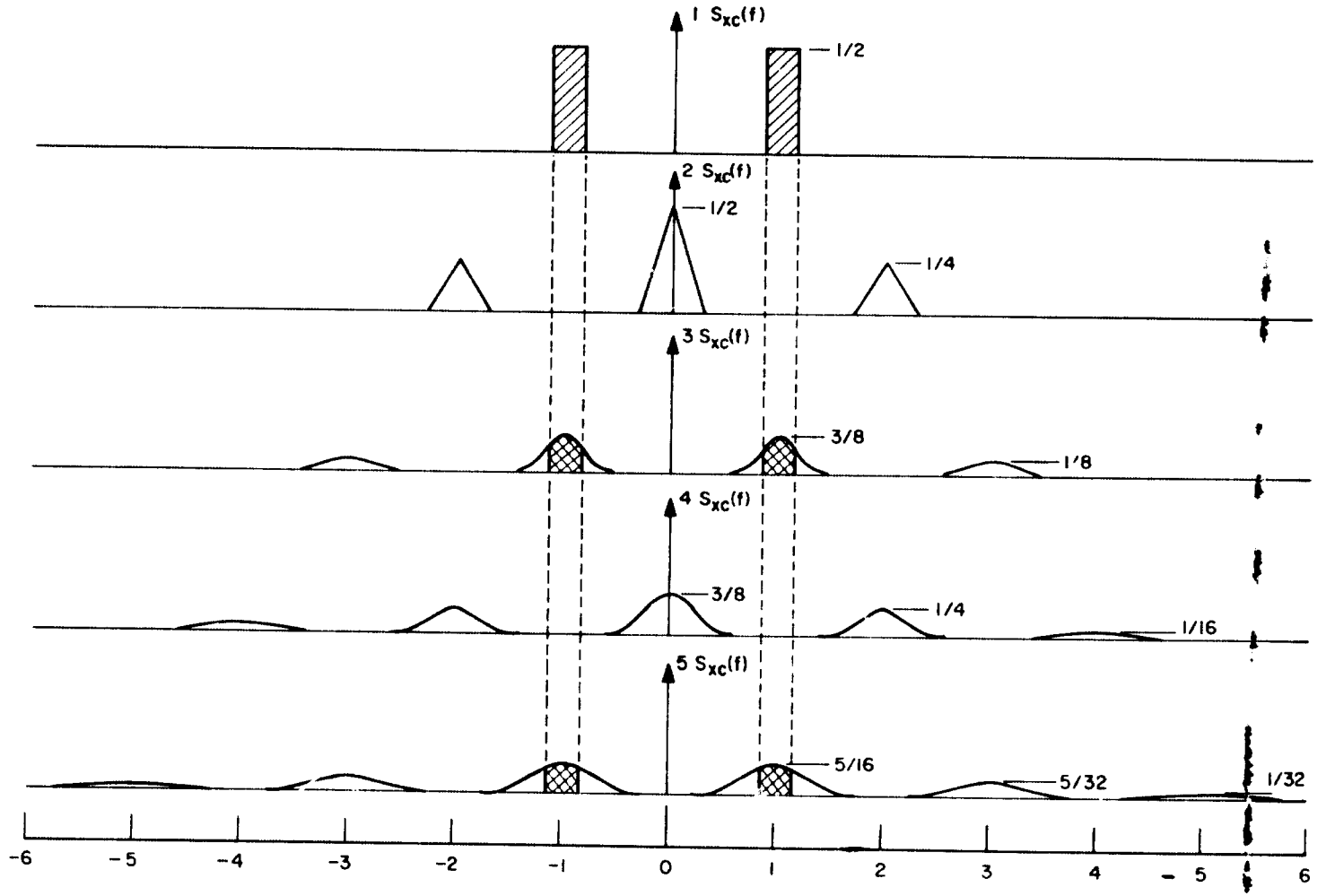

Figure B-5–Plots of the spectral intensities ${}_kS_{xc}$ leading to the determination of the D_n.

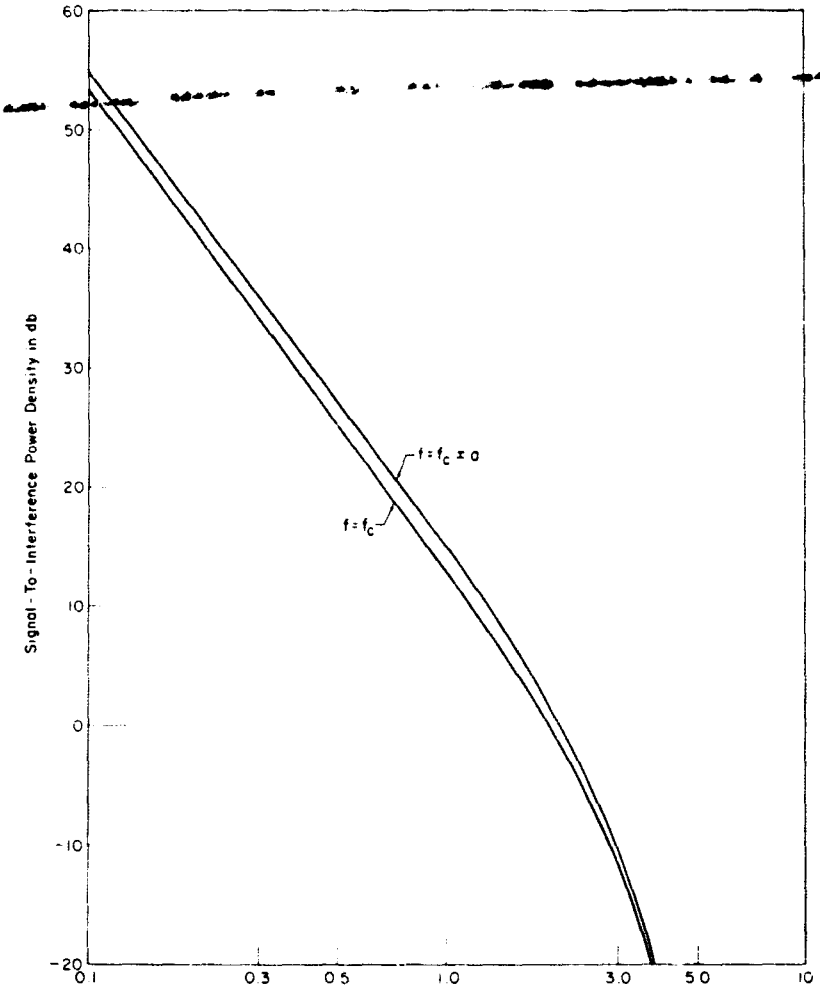

Figure B-6–S/I for a bandpass rectangular modulating spectrum.

establish some guidelines for design which are of value. Figure B-7 is a plot of the spectral densities for k S_{xc} (f) for k = 1 and 3 where no attempt has been made to indicate actual shapes. Two subchannels are assumed, each of which have bandwidths small compared to their center frequencies, and the center frequencies have been selected to prevent overlap of any of the resulting spectra. The situation for fifth-order products (k = 5) have not been included since in what follows, fifth-order products are relatively insignificant and do not alter the conclusions for the range of phase deviation of interest.

The reader should carefully consider how Figure B-7 is modified as the center frequencies, f_1 and f_2, are brought closer together. The shaded blocks

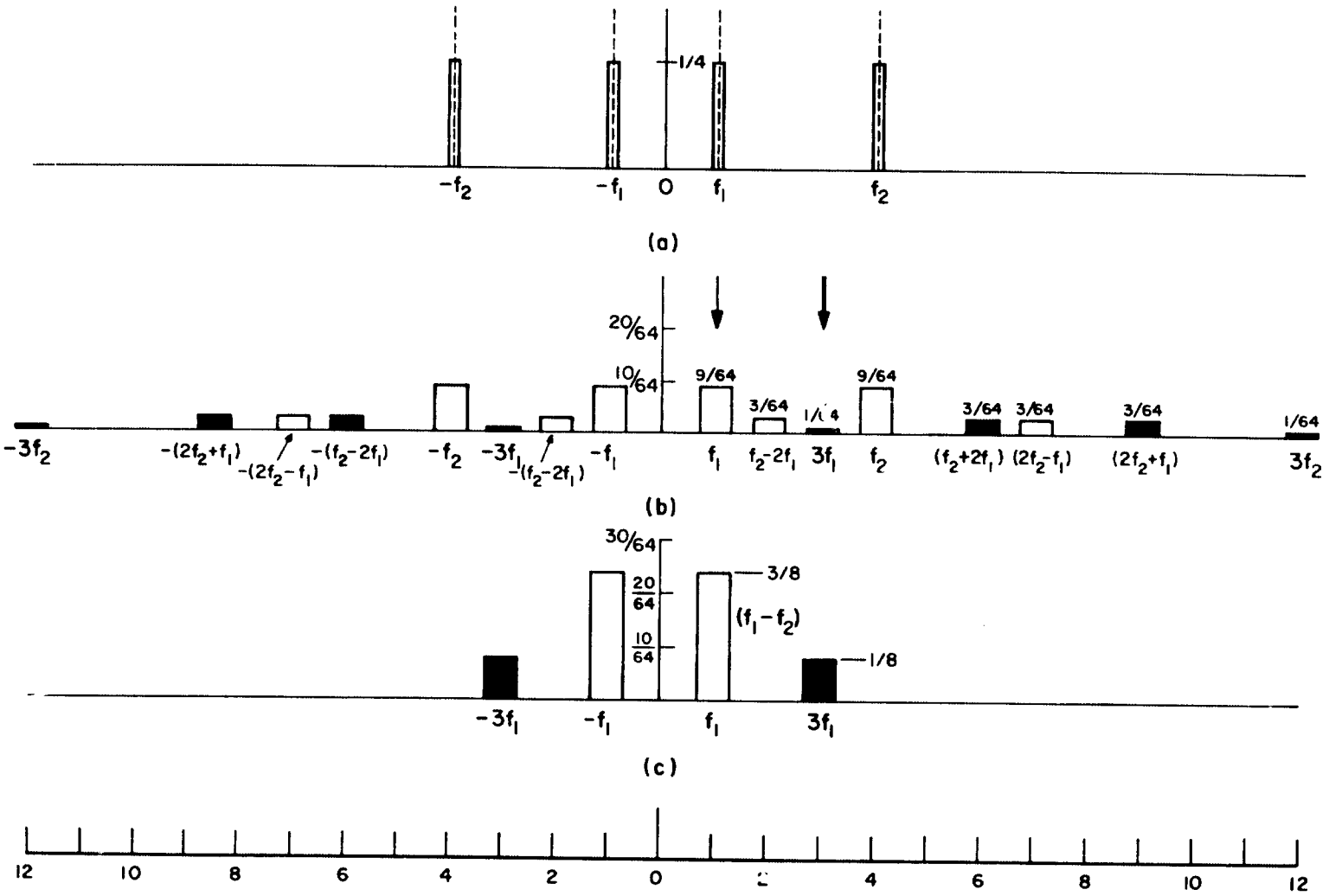

Figure B-7—Diagram pertaining to modulation with two subchannels.

converge to 3 f_1 while the unshaded blocks converge to f_1 as f_1 and f_2 are made to coincide as is shown in Fig. B-7(c). It should be noted that the spread of all the third-order products are three times the original subchannel bandwidths. Therefore, so long as f_1 and f_2 are separated by more than three times the subchannel bandwidths, the third-order products which are centered about f_1 and f_2 do not overlap the opposite subchannel. The individual subchannel filters can then entirely eliminate the most severe single third-order component due to the presence of the opposite channel. Since each channel alone must still contend with its own third-order component under any condition, the only additional interference produced by the existence of the opposite channel are the sum and difference components. However, all of the sum and difference components are smaller than those centered about f_1 and f_2 by at least the ratio of 9/64 to 3/64 or three-to-one as indicated in Fig. 7(b).

A similar argument when three subchannels are involved can be presented using the relative values given in Table B-1. To conserve space, the corresponding plot has not been included, but it is easy to deduce that the three-times bandwidth criteria for subchannel separation holds when there are any number of subchannels. The ratio of the components centered at f_1, f_2 and f_3 to the sum and difference components becomes approximately five to one. The following design guidelines have been established when more than one subchannel is involved.

(a) The plot of Fig. B-4 applies for any number of adjacent subchannels for which the combined signal is such that the assumptions of section III are appropriate.

(b) The plot of Fig. B-6 applies for any number of adjacent subchannels for which the bandwidth of the combined signal is less than one-third of the center frequency and for which the assumptions of section IV are appropriate.

(c) When two or more narrowband subchannels are involved for which the combined signal bandwidth is more than one-third of the center frequency, a channel spacing of three times the subchannel bandwidth is a necessary but not sufficient condition to minimize cross-channel interference. A complete minimization would require careful selection of center frequencies to minimize sum and difference inter-modulation products as well. If all third-order cross products can be made to fall outside of the desired subchannel bands, the performance per channel can be slightly better than that predicated by Fig. B-6.

Table B-1

Comparison With Three Subchannels
($m + n = 3$)

Location of Center Frequency	Relative Value
f_1, f_2 and f_3	19/216
$3f_1$, $3f_2$ and $3f_3$	1/216
$mf_1 \pm nf_2$	4/216
$mf_1 \pm nf_3$	4/216
$mf_2 \pm f_3$	4/216

VI. CONCLUSION

A phase-locked coherent receiver is a linear device which folds the received signal over about the carrier frequency and translates it to baseband. The resulting output signal-to-noise ratio is linearly related to the input signal-to-noise ratio for all values of the latter. That is, it does not exhibit a threshold characteristic in the conventional sense. With a $\pi/2$ shift in phase of the synchronous oscillator, all the desirable characteristics of a coherent receiver can be obtained in receiving an angle-modulated signal with a small phase deviation. As the phase deviation is increased, the nonlinear operation of angle modulation produces additional sidebands which, in a sense, are multiple copies of the modulating signal. The modulated signal can now be represented by a series of terms containing a component which is linearly related to the modulating signal along with higher-ordered components. The coherent receiver will still recover the modulating signal without threshold limitations. It cannot, however, take advantage of the multiple copies contained in the higher-ordered components to provide a signal-to-noise ratio improvement. Instead, it must accept these components as interference and any advantages of such a system must be looked for elsewhere.

In the analysis contained in this paper, it was found that only odd-ordered terms are present in the receiver output, as would be expected on heuristic grounds when the phase relationships of the sidebands are considered. Expressions for the received power spectrum are derived for the case of the lowpass and narrowband modulating signal with stationary Gaussian characteristics of nearly arbitrary power density. A signal-to-interference power density ratio was defined and modulating signals with rectangular power density were

assumed to derive explicit equations and curves predicting the performance of the assumed models. The results were extended to provide guidelines for the design of practical frequency-division-multiplexed (FDM) systems with a number of subchannels.

It is concluded that for digital transmission systems, the technique described is usable with rms phase deviations up to, or even slightly greater, than one radian. The method is particularly advantageous over channels with poor signal-to-noise ratios since a greater portion of the total transmitted power can be packed into the first-order sideband over that of a comparable amplitude modulation system. The distortion products which result are more easily tolerated if the channel signal-to-noise ratio is already relatively high. Since only odd-ordered distortion products are involved, a necessary criteria for minimizing adjacent-channel interference is to separate subchannels by three times their bandwidths in a multiple-channel system.

REFERENCES

1. J. Stewart, "The Power Spectrum of a Carrier Frequency Modulated by Gaussian Noise," Proc. IRE, Vol. 42, pp. 1539-1542; October 1954.

2. B. Martin, "The Pioneer IV Lunar Probe: A Minimum-Power FM/PM System Design," Jet Propulstion Laboratory Technical Report No. 32-215; March 15, 1962.

3. J. Muller and D. Middleton, "Limiting Forms of FM Noise Spectra," Proc. IRE, Vol. 45, pp. 874-877; June 1957.

4. N. Abramson, "Bandwidth and Spectra of Phase-and-Frequency Modulated Waves," IEEE Trans. on Communication Systems, Vol. CS-11, pp. 407-414; December 1963.

5. D. Middleton, "An Introduction to Statistical Communication Theory," McGraw-Hill Book Company, Inc., New York, N.Y.; 1960.

6. W. Davenport and W. Root, "An Introduction to the Theory of Random Signals and Noise," McGraw-Hill Book Company, Inc., New York, N.Y.; 1958.

7. L. Lewin, "Interference in Multichannel Circuits: Dependence on Harmonic Generation," Wireless Engineer, Vol. 27, p. 294; 1950.

8. W. Bennett, H. Curtis, and S. Rice, "Interchannel Interference in FM and PM Systems," Bell Sys. Tech. J., Vol. 34, pp. 601-636; May 1955.

APPENDIX C

SIND ERROR ANALYSIS

I. INTRODUCTION

The error analysis for the SIND system is summarized in Figure C-2 through Figure C-3. A general matrix relation describing the linearization and coordinate transformation between the output errors and the input measurement errors is shown in Figure C-2 where Λ is a coordinate transformation matrix derived from the geometry of the system. Figure C-2 presents three additional important relationships developed in the error analysis. The characterization of the input measurement errors is given by the covariance matrix of the input measurement errors, cov δm, in which all measurement errors are assumed to be independent. The output position and velocity errors are characterized by the covariance of the output error matrix, a 6 by 6 array, expressed in terms of the transformation matrix, Λ, and the covariance of the inverse of the input measurement error, cov $(\delta m)^{-1}$. The aircraft intrack, crosstrack, and altitude errors can be extracted from the position-velocity error matrix, cov δp, and are presented as the output errors in position which are located along the principal diagonal of the matrix, cov δR. The off-diagonal elements of this array are nonzero indicating the dependence between the error components which is specified by the correlation coefficient, ρ_{ij}.

The culmination of the error analysis is manifested in the geometrical interpretation of the error ellipsoid which is shown in Figure C-3. The distribution function of the position errors is given by the expression for $f(\delta R_{IT}, \delta R_{CT}, \delta R_h)$ where Σ is defined as cov (δR). The 1, 2, 3 axes shown in figure are in the direction of the eigenvectors of Σ and are the major and minor axes of the error ellipsoid. The quantities σ_1, σ_2, and σ_3 are the eigenvalues of Σ.

II. ANALYSIS

The analysis assumes that linearization is possible; i.e., differential correction can be employed. The equations which describe the latitude and longitude of the aircraft are not easily solved by direct means, but can easily be solved by differential correction. For differential correction, an estimated position is postulated. Then by taking the difference between the measured parameters associated with actual position and the postulated position, a second

1. LINEARIZATION AND COORDINATE TRANSFORMATION

$$\delta\vec{m} = \Lambda \quad \delta\vec{p}$$

Input Measurements — Geometry — Output Errors — GENERAL RELATION

WHERE

$$\delta\vec{m} = [m_i] = \begin{bmatrix} \delta R \\ \delta \dot{R} \\ \delta h \\ \delta \dot{X}_{A/C} \\ \delta \dot{Y}_{A/C} \\ \delta \dot{Z}_{A/C} \end{bmatrix}, \quad \delta\vec{p} = [p_j] = \begin{bmatrix} \delta R_{IT} \\ \delta R_{CT} \\ \delta R_h \\ \delta \dot{X}_{A/C} \\ \delta \dot{Y}_{A/C} \\ \delta \dot{Z}_{A/C} \end{bmatrix}$$

Λ IS A 6X6 MATRIX DETERMINED FROM SYSTEM GEOMETRY

$$\text{and } \Lambda = (\lambda_{ij}) = \left(\frac{\delta f_i}{\delta f_j}\right)$$

WHERE

$$m_i = f_i(\vec{p}) = f_i(p_3\ p_2 \cdots p_6)$$

Figure C-1–Linearization and Coordinate Transformation

2. MEASUREMENT ERROR CHARACTERIZATION

$$\text{cov}\,\delta\vec{m} = \begin{bmatrix} \sigma_R^2 & & & & & \\ & \sigma_{\dot{R}}^2 & & & (0) & \\ & & \sigma_h^2 & & & \\ & & & \sigma_{\dot{X}}^2 & & \\ & (0) & & & \sigma_{\dot{Y}}^2 & \\ & & & & & \sigma_{\dot{Z}}^2 \end{bmatrix}$$

COVARIANCE MATRIX OF THE INPUT (MEASUREMENT) ERRORS ASSUMES INDEPENDENCE OF ALL MEASUREMENT ERRORS.

3. OUTPUT ERROR RELATION – FOR POSITION & VELOCITY

$$\text{cov}\,\delta\vec{p} = \{\}_{6\times6} = \left(\Lambda^T \text{cov}\left(\delta\vec{m}\right)^{-1}\Lambda\right)^{-1} \quad \text{– GENERAL}$$

4. OUTPUT ERRORS IN POSITION

$$\text{cov}\,\delta\vec{R} = \{\}_{3\times3} = \begin{bmatrix} \sigma_{IT}^2 & \rho_{ic}\,\sigma_{IT}\,\sigma_{CT} & \rho_{ih}\,\sigma_{IT}\,\sigma_h \\ \rho_{ic}\,\sigma_{IT}\,\sigma_{CT} & \sigma_{CT}^2 & \rho_{ch}\,\sigma_{CT}\,\sigma_h \\ \rho_{ih}\,\sigma_{IT}\,\sigma_h & \rho_{ch}\,\sigma_{CT}\,\sigma_h & \sigma_h^2 \end{bmatrix}$$

ρ's ARE CORRELATION COEFFICIENTS WHICH SPECIFY THE INTERRELATION OF THE ERROR COMPONENTS.

Figure C-2–Error Characterization and Output Error

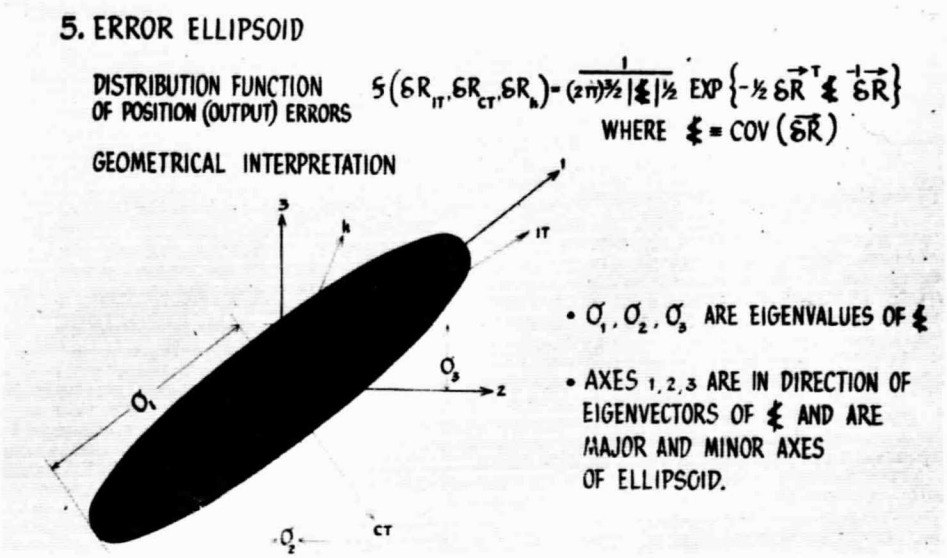

Figure C-3–Error Ellipsoid

postulated position is obtained. Successive iterations by the technique of linear differentials pinpoint the location of the aircraft. It can be shown when $|V_t| > 10\ \sigma_V$, that the estimates are essentially unbiased and the only significant errors can be determined from the covariance (error) matrices.

The covariances of a set of random variables with themselves can be expressed conveniently in matrix form. Let $\bar{x}$ be an n-dimensional column vector. Then $\overline{xx}^T$ is an n by n symmetric matrix whose ij^{th} element is $x_i x_j$. Further, let us define the expected value of a matrix as the matrix of the expected values of the elements. Then $E(\overline{xx}^T)$ is the covariance matrix for x. It is seen that the diagonal elements of $E(\overline{xx}^T)$ are simply the $\sigma^2_{x_i}$.

One theorem is required for the development of the linear model. If A is an n by n matrix of constants and $B = \overline{xx}^T$, then

$$E(AB) = AE(B)$$

This follows from the fact that the E-operator is a linear operator and matrix multiplication is a linear operation.

For the problem at hand we have

$$y = \Lambda x \tag{1}$$

and we seek the covariance matrix of x. First, we define the n by n matrix Σ whose ij^{th} element is $\sigma_i \sigma_j \delta_{ij}$, where δ_{ij} is the Kronecker delta. The Σ is in fact the covariance matrix of y follows from the assumption of independence of measurements. $E(y_i y_j) = 0$ $i \neq j$. From Equation (1),

$$\overline{yy}^T = \Lambda x (\Lambda x)^T$$

$$= \Lambda x x^T \Lambda^T$$

whence,

$$xx^T = \Lambda^{-1} yy^T \Lambda^{T^{-1}}$$

$$E(xx^T) = \Lambda^{-1} E(yy^T) \Lambda^{T^{-1}} \tag{2}$$

$$= \Lambda^{-1} \Sigma \Lambda^{T^{-1}}$$

Although this completes the theoretical derivation of $E(xx^T)$, we note that this does not provide a good computational scheme. Equation (2) requires two matrix inversions, which are computational procedures that often introduce significant round-off error in the final result. To avoid this pitfall (although, we cannot completely circumvent it) we proceed as follows.

Define $\Sigma^{1/2}$ as a matrix which when multiplied by itself yields Σ. In the case where Σ is a diagnonal matrix, $\Sigma^{1/2}$ is simply that matrix whose x-y element is $\sigma_i \delta_{ij}$. Furthermore, let $\Sigma^{-1/2}$ be the inverse of $\Sigma^{1/2}$, which in this case is the matrix whose ij^{th} element is δ_{ij}/σ_i.

Now we rewrite Equation (2) as

$$E(xx^T) = \Lambda^{-1} (\Sigma^{1/2} \Sigma^{1/2}) \Lambda^{T^{-1}}$$

$$= \Lambda^{-1} (\Sigma^{-1/2})^{-1} (\Sigma^{-1/2})^{-1} \Lambda^{T^{-1}}$$

$$= \Lambda^{-1} (\Sigma^{-1/2})^{-1} (\Sigma^{-1/2})^{-1} \Lambda^{T^{-1}}$$

$$= (\Sigma^{-1/2} \Lambda)^{-1} (\Lambda^T \Sigma^{-1/2})^{-1}$$

Defining $\Lambda_\sigma = \Sigma^{-1/2} \Lambda$ and noting that $\Sigma^{-1/2} = \Sigma^{-1/2 T}$ we have

$$E(xx^T) = \Lambda_\sigma^{-1} (\Lambda_\sigma^T)^{-1}$$

$$= (\Lambda_\sigma^T \Lambda_\sigma)^{-1} = p^{-1}$$

We have thus reduced the computation to only one matrix inversion.

There still remains an additional computational problem concerning the inversion of the P-matrix. P may be ill-conditioned, which means that the determinant of P may be close to zero though a true inverse may exist. To avoid this difficulty, we introduce the matrix S, where $S_{ij} = \delta_{ij} \sqrt{p_{ij}}$ and where p_{ij} is the element of the P matrix. S^{-1} is then $\delta_{ij} / \sqrt{p_{ij}}$. Let $Q = S^{-1} P S^{-1}{}_{ij}$, where Q is related to P by a scaling or normalization process. This procedure makes Q less ill-conditioned than P.

Now:

$$P = SS^{-1} P S^{-1} S$$

$$= S Q S$$

and

$$P^{-1} = S^{-1} Q^{-1} S^{-1}$$

In other words we scale, invert and rescale. This concludes the development of the computational technique used in the computer program.

Measurements are taken of six quantities: aircraft altitude, range, range rate and the velocity components. From these measurements, six quantities are to be determined: three components of position (in spherical coordinates) and three components of velocity. In reality, we are primarily interested in position determination from range, range rate and altitude. Let us define the M-space as the 6-dimensional vector space, in which the components of the vector are the measurements. Similarly the P-space is the space of position-velocity vectors (six-dimensional). Since we know the covariance matrix of a vector in M-space, and we wish to calculate the covariance matrix for a related vector in P-space, we seek a linear transformation between the two spaces.

To start, we write down six equations relating M quantities to P-V quantities:

$$m_1 = f_1(p_1, p_2, \cdots p_6)$$

$$m_2 = f_2(p_1, p_2, \cdots p_6)$$

$$m_6 = f_6(p_1, p_2, \cdots p_6)$$

or, in vector form, $\bar{m} = f(\bar{p})$. Let $\bar{p}^*$ be a fixed point in P space and let $\bar{m}^* = f(\bar{p}^*)$. If we expand f_1 in a Taylor series about the point p^*, we obtain

$$m_1 = f_1(p^*) + \sum_{k=1}^{6} \frac{\partial f_1}{\partial p_k} (p_k - p_k^*) + \text{higher order partials} \qquad \text{(a)}$$

It can be seen that if the higher order partials are considered to be negligible, Equation (a) reduces to a linear relationship between m and p. In particular, defining

$$\Delta m_1 = m_1 - f_1(p^*) = m_1 - m_1^* \qquad \text{and}$$

$$\Delta p_k = p_k - p_k^*$$

we have

$$\Delta m_i = \sum_{k=1}^{6} \frac{\partial p_i}{\partial p_k} \Delta p_k$$

Similarly,

$$\Delta m_j = \sum_{k=1}^{6} \frac{\partial p_j}{\partial p_n} \Delta p_n \qquad j = 1, 2, \cdots 6$$

In vector form,

$$\Delta \bar{m} = \Lambda \Delta \bar{p}$$

where

$$\Lambda_{ij} = \frac{\partial f_i}{\partial p_j}$$

This is the linear model for the position-velocity determination problem. In it, we assume that the $\Delta \bar{m}_j$ are independently, normally distributed with mean $\bar{0}$ and given covariance matrix Σ.

Let $x, y, z, \dot{x}, \dot{y}, \dot{z}$ be coordinates of position and velocity, respectively. Also, let θ and $\emptyset$ be latitude and longitude of plane, R_e be plane distance from geocenter, R_s be satellite distance from geocenter. We shall assume that the satellite is in an equatorial, circular stationary orbit with longitude zero.

Now in spherical coordinates:

$$x = R_e \cos\theta \cos\emptyset$$

$$y = R_e \cos\theta \sin\emptyset$$

$$z = R_e \sin\theta$$

Since the satellite is at $x = R_s$, the equation for range becomes:

$$R^2 = (x - R_s)^2 + y^2 + z^2 = R_e^2 + R_s^2 - 2R_e R_s \cos\theta \cos\phi \qquad \text{(b)}$$

To find range rate (dR/dt) we differentiate both sides of Equation (b):

$$2R\dot{R} = 2(x - R_s)\dot{x} + 2y\dot{y} + 2z\dot{z}$$

or

$$\dot{R} = \frac{(x - R_s)\dot{x} + y\dot{y} + z\dot{z}}{R}$$

The six f functions relating $\bar{m}$ to $\bar{p}$ become

1. Altitude

$$R_e = R_e$$

2. Range

$$R = \left[R_e^2 + R_s^2 - 2R_e R_s \cos\theta \cos\phi\right]^{1/2}$$

3. Range Rate

$$\dot{R} = \frac{(R_e \cos\theta \cos\phi - R_s)\dot{x} + (R_e \cos\theta \sin\phi)\dot{y} + (R_e \sin\theta)\dot{z}}{R}$$

4. Velocity - x $\dot{x} = \dot{x}$

5. Velocity - y $\dot{y} = \dot{y}$

6. Velocity - z $\dot{z} = \dot{z}$

It is clear that the problem reduces to determining μ and θ, given measurements of R and $\dot{R}$.

Since we have assumed the y_i to be jointly normally distributed, it follows that the x_i's ($\bar{x} = \Lambda^{-1} \bar{y}$) are also jointly normally distributed. The joint normal probability density function may be written as:

$$f(x_1, x_2, \cdots x_n) = \frac{1}{(2\pi)^{n/2} |P|^{1/2}} \exp\left[-1/2 (\bar{x} - \bar{u})^T P^{-1} (\bar{x} - \bar{u})\right] \qquad (3)$$

where μ is the vector of means and where $P = \Lambda^{-1} \Sigma (\Lambda^T)^{-1}$ is the covariance matrix. In the problem at hand $\mu = 0$. Since the expression in the exponent:

$$\bar{x}^T \bar{P}^{-1} x = \text{constant}$$

is the equation of an ellipsoid in n-dimensions, it is natural to ask probability questions in terms of the probability that a point lies in a certain ellipsoid. This entails integrating Equation (3).

It is obvious that the integration would be easier to perform if $[x^T \Sigma^{-1} x]$ did not involve crossproducts. To eliminate cross-terms, one can change variables in such a way that the resulting coordinate variables lie along the axes of the ellipsoid that they define. That this change of variables can always be done is the Principal Axis Theorem.

In terms of matrices, the resulting variables will lie in the direction of the eigenvectors of Σ and the coefficient of x_i in the quadratic form will be the i^{th} eigenvalue. Let us assume that this change of variables has been done. Then the quadratic in the exponent of (3) has the form:

$$\sum_{i=1}^{n} \lambda_i x_i^2$$

and

$$I = \prod_{i=1}^{n} \int \frac{\sqrt{\lambda i}}{\sqrt{2\pi}} \exp\left(-1/2\,\lambda_i\, x_i^2\right) dx_i$$

Now let $z_i = \sqrt{\lambda_i}\, x_i$ $i = 1, 2, \ldots n$ which leads to

$$I = \prod_{i=1}^{n} \int \frac{1}{\sqrt{2\pi}} \exp\left(-1/2 Z_i^2\right) dx_i \qquad (4)$$

It can be shown, with some manipulation, that the integral of (3) reduces to an expression in terms of only the error function and its integral.

For the problem at hand, we deal with the covariance matrix of R and $\dot{R}$. This is merely a submatrix of the total 6-6 covariance matrix. In general, this 2 by 2 matrix may be written as

$$\sum = \begin{bmatrix} \sigma_R^2 & \rho\,\sigma_R\,\sigma_{\dot{R}} \\ \sigma_R\,\sigma_{\dot{R}} & \sigma_{\dot{R}}^2 \end{bmatrix}$$

The solutions are:

$$\lambda = \frac{\sigma_R^2 + \sigma_{\dot{R}}^2 \pm \sqrt{\sigma_R^4 + \sigma_{\dot{R}}^4 - 2(1 - 2\rho^2)\,\sigma_R^2\,\sigma_{\dot{R}}^2}}{2}$$

If relatively accurate measurements of range and altitude are assumed, then almost all of the system error occurs in the measurement of range rate and the aircraft velocity vector. As will be seen later, the actual operational situation closely approximates these assumptions.

Similarly, the measured aircraft velocity vector, $\bar{V}_m$, may be expressed as:

$$\begin{bmatrix} V'_{mt} \\ V'_{mr} \\ V'_{mr} \end{bmatrix} = \begin{bmatrix} 1 & \epsilon \cos\theta & -\epsilon \sin\theta \\ -\epsilon \cos\theta & 1 & 0 \\ +\epsilon \sin\theta & 0 & 1 \end{bmatrix} \begin{bmatrix} V_{mt} \\ V_{mn} \\ V_{mr} \end{bmatrix} \tag{3}$$

The case of interest affecting the position fix accuracy occurs when the measured component of aircraft velocity between the satellite and aircraft, V'_{mr}, is equal to the measured Doppler, $\dot{r}_m$, or $V'_{mr} = \dot{r}_m$. If the actual velocity, V_{ar}, is equal to the actual Doppler, $\dot{r}_{ar}$, $V_{ar} = \dot{r}_{ar}$, such that ϵ represents a positional error on the circle of position then:

$$V'_{mr} = r_{ar} + e_r \tag{4}$$

Also, from the matrix relationships (3):

$$\begin{aligned} V'_{mr} &= \epsilon \sin\theta V_{mt} + V_{mr} \\ V'_{mr} &= \epsilon \sin\theta V_{at} + e_t + V_{ar} + e_r \end{aligned} \tag{5}$$

Equating V'_{mr} from Equations (4) and (5):

$$r_{ar} + e_r = \epsilon \sin\theta V_{at} e_t + V_{ar} + e_r \tag{6}$$

If $V_{at} >> e_t$, an assumption which will be discussed in detail later and, since $\dot{r}_{ar} = V_{ar}$, equation (6) simplifies to:

$$\epsilon \approx \frac{-e_r + e_r}{V_{at} \sin\theta}$$

Thus, if

$$-\epsilon_r + \epsilon_t \neq 0$$

the positional error on the circle of position is described by the angle ϵ, which corresponds to a linear distance error, d, on the circle of position equal to the product of the small ange, ϵ, and the normal distance from the aircraft, r_{ss}, to the satellite to center of earth range vector.

$$d = \epsilon\, r_{ss}$$

where

$$r_{ss} = r_s \sin\theta$$

and

$$d = \epsilon\, r_s \sin\theta$$

Therefore

$$\sigma_d = \frac{r_s}{V_t}\sqrt{\sigma_v^2 + \sigma_t^2}$$

This formula approximates all the important error characteristics of the system.

There will be a linear solution for our problem as long as $\ddot{V}_t \geq 10\,\sigma_V$. The projection of the velocity vector onto the satellite direction has been shown to be a monotonic function as long as the projection of the velocity vector onto the ring is not zero. This justifies the concept of sliding the proposed position along the ring until the projection in the direction of the satellite is equal to the Doppler.

If the inequality in V_t is not satisfied, then $V_t \simeq 0$. This means that the aircraft is flying directly away from the subsatellite point. The position can still be determined, but the linearization used in the analysis is not valid for this specialized situation.

III. DISCUSSION

In discussing the properties of the system, the position and velocity time histories of the aircraft have not been considered. Only the capability of obtaining the instantaneous fix has been discussed. It must be noted, however, that any actual realization of the system will utilize such time histories.

From the preceeding discussion, it can be seen that the linear model is not valid for $|V_t| < 10\sigma_v$, i.e., if the tangential projection of the aircraft's velocity on the circle of position is zero. This indicates that the aircraft heading is normal to the "ring" direction. Viewed in this light, the system presents no difficulties when the velocity projection in the ring direction is zero. It is noted that this situation exists only for the linear analysis presented here. There is a quadratic solution which has not been considered because of mathematical difficulties and the time allowed for this report.

If over ocean flight patterns are considered, particularly over the North Atlantic, a large velocity component will always exist tangent to the circle of position, or position ring. In fact, a satellite can be in positions such that the velocity vector very roughly parallels the ring over all flight paths. Aircraft almost never fly directly away from the mid-ocean subsatellite point in crossing the ocean. Therefore, although the case for $V_t \approx 0$ was not studied, this report essentially applies to all over-water air traffic control situations. The error analysis has shown that the error ellipsoid for the SIND system is cigar-shaped while the error ellipsoids for other techniques are generally "football"-shaped. In both cases, the minor axes are in tens of meters for the current state-of-the-art. The length or major axis of the cigar ellipsoid will normally be of the order of kilometers. The major axis of the cigar ellipsoid points in the tangential direction of the ranging line-of-position ring and therefore tends to be pointed in the direction of flight for typical North Atlantic great circle routing. The SIND system can accurately monitor the separation of air traffic lanes while the accuracy for monitoring in-lane separation of aircraft is somewhat less. From an operational point of view, when not using time histories, this characteristic is not serious as the relative speed between aircraft within an air traffic lane is small. Aircraft today often have weather radars, so the chance of one aircraft overtaking another is generally small. However, the closure speed between aircraft traversing lanes in the opposite direction will soon be as high as 4000 knots. It is therefore critical that lane separation be maintained. The SIND technique can do this.

The system is less accurate for the slower moving aircraft, but again the need for better position fixing increases as the aircraft speed increases. The SIND technique has the desirable property of increasing its accuracy when

more accuracy is needed. The accuracy of SIND is basically limited by the accuracy with which the velocity vector and Doppler can be determined. The SIND technique using onboard inertial data should be better than an independent inertial system using the same data. This assumes that the SIND implementation would have available moderately accurate altitude, range and range rate measurements.

If two communication satellites were available in the North Atlantic region, the SIND approach could be employed reliably in that one satellite could serve as a backup system and prevent navigation service outages due to the failure of a single communications satellite.

In the above discussions, the existence of some sort of gyro-accelerometer platform aboard the aircraft has been assumed. Future aircraft may not have this equipment. Such aircraft must, however, have some sort of real time dead-reckoning capability. With almost continuous updating that could be developed from satellite systems, the dead-reckoning system could be very crude, but some real time dead-reckoning system is needed.

If the dead-reckoning system did not contain acceleromaters, the SIND system could obtain crude velocity vector information from the Doppler radar and compass heading of the aircraft. Under these conditions, the major axis, or length of the cigar-shaped error ellipse, would be of the order of tens of kilometers. The system still could probably maintain adequate lane separations and provide operational "back-up" to the other navigation systems utilized.